Models and Gene Therapy for GM1-Gangliosidosis and Morquio Syndrome Type B

A DISSERTATION SUBMITTED TO THE FACULTY OF
THE UNIVERSITY OF MINNESOTA
BY

Michael John Przybilla

IN PARTIAL FULFILLMENT OF THE REQUIREMENTS
FOR THE DEGREE OF
DOCTOR OF PHILOSOPHY

Chester B. Whitley, Ph.D., M.D., Advisor

December 2018
MOLECULAR, CELLULAR, DEVELOPMENTAL BIOLOGY
& GENETICS GRADUATE PROGRAM

DEDICATION

I would like to dedicate this thesis to my wife, Kristen, and son, Lincoln, in addition to my family and friends. Each of you have provided me with continuous support over the last four years that I will always appreciate. If you choose to read this, I hope that many of the blank expressions I saw when you asked what I was working on will become more clear expressions of, “Oh, I get it now.”

More importantly, I would like to dedicate this thesis to the patients suffering from these debilitating diseases and their loving families that I’ve met, but also those I haven’t. The hope that each of you have to find a treatment for your children/grandchildren has been, and will continue to be, the motivation for my work.

ACKNOWLEDGEMENTS

I would first like to thank my graduate advisor, Dr. Chester Whitley, for introducing me to and sharing his passion for lysosomal diseases with me. Additionally, I would like to thank Dr. Whitley for providing me with the advice, guidance and opportunities during my tenure in his laboratory to succeed and to reach this milestone. His tutelage throughout this period has provided me with many new skills and perspectives that I will continue to use as my career continues.

I would also like to thank my colleague and friend Dr. Li Ou, who has continued to provide a breadth of knowledge and insight at every turn of my research. I am thankful that Dr. Ou has tolerated being inundated with my questions over the years. His prior experiences in this program and the field of lysosomal diseases has been helpful for forging my own path. I would also like to thank Dr. Jeanine Jarnes for providing her expertise and passion for GM1-gangliosidosis with me. Additionally, I would like to thank the members of the Whitley lab and administrative team that have helped me throughout my time in the lab, including Renee Cooksley, David Erickson, Brenda Diethelm-Okita, Sarah Kim, Evelyn Redtree, and Ashley Schneider.

Further, I would like to thank the other members of my graduate committee, Dr. Nikunj Somia, Dr. R. Scott McIvor, Dr. Walter Low, and Dr. Thomas Neufeld who have provided their scientific insights and helpful suggestions that have helped guide and shape my research.

I would also like to thank the members of neighboring labs and collaborators that have contributed to the success of the work that is presented here: Brenda Koniar, Kelly Podetz-Pedersen, Dr. M. Gerard O'Sullivan, Dr. Alexandru-Flaviu Tăbăran, Dr. Shunji Tomatsu, Dr. Dale Cowley, Dr. Xuntian Jiang, and Dr. Daniel Ory.

Finally, I want to thank my wife, Kristen, for being patient and understanding when things became stressful over the years. I want to thank you for always being willing to sit and talk with me about my research, and providing encouragement and unwavering support.

THESIS ABSTRACT

GM1-gangliosidosis and Morquio syndrome type B are lysosomal diseases caused by deficiencies in the lysosomal enzyme β-galactosidase (β-gal). β-gal is responsible for catabolizing the terminal β-linked galactose residues in GM1 and GA1 ganglioside, keratan sulfate, and oligosaccharides. If β-gal enzyme activity is deficient, these macromolecules accumulate within the lysosomes, resulting in either severe neurodegeneration in GM1-gangliosidosis or severe skeletal dysplasia in Morquio syndrome type B. Sadly, no therapies for these debilitating diseases exist, so the development of novel treatments is of the utmost importance; however, to be able to test these new treatments, animal models are necessary. Previous murine models of GM1-gangliosidosis were generated using an inefficient method to disrupt the *Glb1* gene by introducing foreign DNA into the coding sequence. While useful, these mutations do not recapitulate those that could be found in patients with GM1-gangliosidosis. Utilizing CRISPR-Cas9 genome editing, the mouse β-gal encoding gene was targeted to generate mutations that resulted in two novel mouse models of β-gal deficiencies (Chapter II). In one line, a 20 bp deletion was generated to remove the catalytic nucleophile of the β-gal enzyme, resulting in a mouse devoid of β-gal enzyme activity (β-gal$^{-/-}$). This resulted in ganglioside accumulation and severe cellular vacuolation throughout the central nervous system (CNS). β-gal$^{-/-}$ mice also displayed severe neuromotor and neurocognitive dysfunction, and as the disease progressed, the mice became emaciated and succumbed to the disease by 10 months of age (Chapter III). Overall, this model phenotypically

resembles a patient with infantile GM1-gangliosidosis. In the second model, a missense mutation commonly found in patients with Morquio syndrome type B, *GLB1*^{W273L}, was introduced into the mouse *Glb1* gene (*Glb1*^{W274L}). Mice harboring this mutation showed a significant reduction in β-gal enzyme activity (8.4-13.3% of wildtype) but displayed no marked phenotype after one year of observation (Chapter IV). This is the first description of using CRISPR-Cas9 genome editing to generate mouse models of a lysosomal disease. With these models in hand, preliminary experiments were conducted to test the functionality of a novel gene therapy to treat these diseases (Chapter V). Previous studies in lysosomal diseases have shown that tissue-specific expression of lysosomal enzyme ameliorates the disease pathology, including improvement of neurocognitive function. Here, a gene therapy system was designed to integrate the human *GLB1* cDNA into the albumin locus by creating a double-strand break in the DNA by an AAV8-encoded nuclease. Theoretically, this integration of *GLB1* cDNA would be achieved by co-injecting a second AAV8 vector encoding the transgene that is flanked by homologous sequence to the albumin locus, allowing for homology directed repair to incorporate the sequence. 30 days post treatment, plasma enzyme activity was 4.8-fold higher than heterozygous levels. However, by four months post-treatment, β-gal enzyme activity in plasma from treated β-gal$^{-/-}$ mice decreased to heterozygous levels. Four months following injection, β-gal enzyme activity in a subset of treated β-gal$^{-/-}$ mice was observed in the liver and spleen. Motor function testing on the rotarod showed that the amount of enzyme being produced does not prevent the neurological symptoms

of the disease. This preliminary data shows that this gene therapy system can produce functional β-gal enzyme that is secreted into the plasma and is capable of being taken up into peripheral tissue. Future studies focused on optimizing the dose of AAV to provide a higher enzyme level will be important for the success of this therapy for β-galactosidase deficiencies.

TABLE OF CONTENTS

LIST OF TABLES

LIST OF FIGURES

LIST OF MULTIMEDIA FILES

Movie 1. Presence of ambulatory dysfunction in a female β-gal$^{-/-}$ mouse at 6 months of age.

Movie 2. Initial ambulatory dysfunction in a male β-gal$^{-/-}$ mouse at 6 months of age.

Movie 3. At 9 months of age, neurological dysfunction has progressed significantly in female β-gal$^{-/-}$ mice and slowed their ability to ambulate normally.

Movie 4. Severe neurological decline in male β-gal$^{-/-}$ mice at 9 months of age, resulting in limited mobility.

LIST OF ABBREVIATIONS

4-MU	4-methylumbelliferone
4-MUGal	4-methylumbelliferyl-β-D-galactopyranoside
aa	Amino acid
AAV	Adeno-associated virus
Ad	Adenovirus
BBB	Blood-brain barrier
Ca^{2+}	Calcium
CHAPS	3-[(3-cholamidopropyl)-dimethylammonio]-1-propanesulfonate
CNS	Central nervous system
Cas	CRISPR associated protein
CRISPR	Clustered interspaced short palindromic repeats
crRNA	CRISPR RNA
DGJ	1-deoxygalactonojirimycin
DSB	Double-strand break
dsDNA	Double-stranded DNA
EBP	Elastin binding protein
ECM	Extracellular matrix
ER	Endoplasmic reticulum
ERT	Enzyme replacement therapy
ES cells	Embryonic stem cells
ESS	English Springer Spaniel
GAG	Glycosaminoglycan
GALNS	Galactosamine-6-sulfate sulfatase
GEM	Glycosphingolipid-enriched microdomain
GLB1	Gene encoding β-galactosidase (human)
Glb1	Gene encoding β-galactosidase (mouse)
GlcCer	Glucosylceramide
GM2A	GM2-activator protein
H&E	Hematoxylin and eosin
HCG	Human chorionic gonadotropin
HDR	Homology directed repair
HIV	Human immunodeficiency virus
HPLC	High performance liquid chromatography
HPLC-MS/MS	High performance liquid chromatography, tandem mass spectrometry
HR	Homologous recombination
IDS	Iduronate-2-sulfatase
IDUA	α-L-iduronidase
IL-1β	Interleukin-1 beta
ITR	Inverted terminal repeats
KS	Keratan sulfate

LFB	Luxol fast blue
LTR	Long-terminal repeat
LV	Lentivirus
M6P	Mannose-6-phosphate
M6PR	Mannose-6-phosphate receptor
MAMs	Mitochondria-associated ER membranes
MHC II	Major histocompatibility complex class II
MPS	Mucopolysaccharidosis
mRNA	Messenger ribonucleic acid
NANA	*N*-acetyl-α-neuraminidate
*N*B-DGJ	*N*-(*n*-butyl)-deoxygalactonojirimycin
N-B-DNJ	*N*-butyldeoxynojirimycin
NBF	Neutral buffered formalin
NEU1	Neuraminidase 1
NEU3	Neuraminidase 3
NHEJ	Non-homologous end joining
NO	Nitric oxide
NOEV	*N*-octyl-4-epi-valienamine
PAM	Protospacer adjacent motif
PAS	Periodic acid-Schiff
PCR	Polymerase chain reaction
PMSG	Pregnant mare's serum gonadotropin
PPCA	Protective protein/cathepsin A
PWD	Portuguese Water Dog
QC	Quality control
RV	Retrovirus
RTB	Ricin toxin B-subunit
RT-qPCR	Reverse transcription quantitative PCR
sgRNA	Single guide RNA
SRT	Substrate reduction therapy
ssDNA	Single-stranded DNA
ssRNA	Single-stranded RNA
TALEN	Transcriptional activator-like effector nuclease
TNFα	Tumor necrosis factor α
TNF-R1	Tumor necrosis factor receptor type 1
tracrRNA	Trans-activating RNA
UPR	Unfolded protein response
ZFN	Zinc finger nuclease
β-gal	β-galactosidase

CHAPTER I

Background and Significance

Overview

GM1-gangliosidosis (MIM #230500, 230600, 230650) and Morquio syndrome type B (MIM #253010) are two rare metabolic disorders that are classified as lysosomal diseases. Lysosomal diseases are a group of over 70 inherited metabolic diseases caused by deficiencies in lysosomal hydrolases, their activator proteins, or transporters, affecting nearly 1 in 5,000 live births [1]. These deficiencies result in accumulation of the complex macromolecules within the lysosome, leading to lysosomal dysfunction and alterations to cellular homeostasis and subsequently cell death [2]. β-galactosidase (β-gal), the enzyme that is deficient in GM1-gangliosidosis and Morquio syndrome type B, is responsible for the catabolism of terminal β-linked galactose residues found in GM1 and GA1 ganglioside, the glycosaminoglycan (GAG) keratan sulfate, and oligosaccharides; thus, when mutated, these substrates accumulate within the lysosome of the cell. Clinically, patients suffering from GM1-gangliosidosis, primarily a disease of the central nervous system (CNS), will present with severe developmental regression, hepatosplenomegaly, ataxia, a cherry-red spot in the eye, and potentially some skeletal abnormalities [3]. In Morquio syndrome type B (mucopolysaccharidosis type IV B, MPS IVB), primarily a skeletal disease, patients will present with short stature, corneal clouding, protruding sternum, and kyphosis of the thoracic and lumbar vertebrae in addition to other skeletal abnormalities [3]. Patients with severe GM1-gangliosidosis (infantile onset) will develop symptoms within the first 6 months of life and succumb to the disease by

the age of 2 without disease intervention [3]. Currently, the only available therapy for β-gal deficiencies is palliative measures, which only provide relief of symptoms and do not slow the progression of the disease. Thus, the development of novel treatments is pivotal. Developing model organisms to test these treatments is crucial. Currently, there are no available models of Morquio syndrome type B and the two mouse models of GM1-gangliosidosis were developed by integrating foreign DNA into the *Glb1* gene. Thus, the focus of this thesis was to generate and characterize novel models of these diseases that harbored mutations in *Glb1* that could be observed in the human population. Additionally, preliminary data from a novel gene therapy approach for these diseases is described.

Proteins Encoded by the *GLB1* Gene

The human *GLB1* gene is comprised of 16 exons, is approximately 100.6 kb in length, and is located on chromosome 3 at 3p21.33 [4, 5]. Following transcription, the *GLB1* mRNA can be alternatively spliced into two transcripts: one that encodes the lysosomal hydrolase β-galactosidase (β-gal, EC 3.2.1.23) and another that encodes elastin binding protein (EBP). The EBP-encoding transcript is processed from the alternative splicing of the *GLB1* pre-mRNA, skipping exon 3, 4 and 6, and using an alternative reading frame of exon 5. This yields a 2.2 kb transcript that is translated into a 546 aa, 67 kD protein. The alternate reading frame possesses a unique 32 aa sequence that contains the elastin binding site. Unlike β-gal, EBP is catalytically inactive [5, 6], is primarily

localized to the plasma membrane, and is categorized as a β-galactoside lectin protein [7]. EBP has been shown to form the elastin receptor complex with two membrane-associated proteins, neuraminidase 1 (NEU1) and protective protein/cathepsin A (PPCA) [8]. This complex plays a major role in elastogenesis [9]. EBP acts as a chaperone to tropoelastin (the precursor to elastin), protecting it from premature degradation by elastases and self-aggregation [10]. The EBP-tropoelastin complex is directed to the plasma membrane, where it is secreted. Following secretion, galactose sugars bind to the galactolectin-binding site in EBP, causing the release of tropoelastin and recycling of the EBP protein [11]. Following release from EBP, tropoelastin is incorporated with other tropoelastin molecules to form the mature elastin structure, a primary component of connective tissue [12]. In addition to elastogenesis, the elastin receptor complex has been shown to be involved in transducing cellular signals [13, 14].

The second transcript encoded by the *GLB1* gene is a 2.6 kb mRNA that is translated to the catalytically active lysosomal hydrolase β-gal, which catabolizes terminal β-linked galactose residues found in GM1 ganglioside, its asialo derivative GA1 ganglioside, the GAG keratan sulfate, and oligosaccharides. The β-gal-encoding mRNA transcript is translated into a 677 aa, 88 kDa prepropeptide, which subsequently has the 23 aa signal sequence [15] removed upon entry into the endoplasmic reticulum (ER), resulting in a 654 aa propeptide [16]. Following glycosylation, a mannose-6-phosphate (M6P) is covalently linked to the 84 kDa β-gal propeptide [17] and is sorted to the lysosomal compartment. Following sorting, the 88 kDa propeptide (now including

M6P), is proteolytically processed at its C-terminus to a mature, catalytically active, 64 kDa β-gal enzyme. Interestingly, the cleaved 20 kDa C-terminal fragment is an essential component of the mature β-gal enzyme [18] and is necessary for proper folding in the ER and Golgi, but is not required for catalytic activity [19, 20]. β-gal is sorted to the lysosomal compartment in complex with PPCA [21] to protect β-gal from intralysosomal degradation by proteases. Once in the lysosome, this β-gal/PPCA heterodimer forms a catalytically active complex with NEU1 [22], however, it has been shown that the 88 kDa propeptide is catalytically active as a monomer [17]. Importantly, in 1997, McCarter *et al.* [23] elucidated that the glutamic acid at position 268 (*GLB1*^{Glu268}; *Glb1*^{Glu269} in mice) is the catalytic nucleophile responsible for the hydrolysis reaction to remove β-galactose residues. This was further confirmed by Ohto *et al.* [24], who determined the crystal structure of the human β-gal protein.

Mutations in the *GLB1* gene that alter the ability of β-gal to catabolize the terminal β-galactose moiety lead to the accumulation of the complex macromolecules within the lysosomes of the cell. In most lysosomal diseases, a deficiency in one enzyme will result in one disease or differing severities of the same disease. In the case of β-gal deficiency, there are two distinct diseases that can arise: 1) GM1-gangliosidosis, a neurodegenerative disease, or 2) Morquio syndrome type B, a skeletal disease. The phenotype that arises is dependent upon the mutation, level of β-gal enzyme activity, and which macromolecules accumulate in the lysosome. There are over 223 reported mutations in the Human Gene Mutation Database (v. 2018.3) in the *GLB1* gene [25], but because

of the extensive heterogeneity of phenotypes in GM1-gangliosidosis and Morquio syndrome type B patients, a relationship between the GLB1 mutations and which disease arises is still relatively unclear. However, there are mutations that have been shown to correlate to specific disease pathologies, including I51T in Japanese patients with adult GM1-gangliosidosis [26, 27], R201C in patients with juvenile GM1-gangliosidosis [26, 28], R208C in Puerto Rican patients with infantile GM1-gangliosidosis [29] and R482H in Italian patients with infantile GM1-gangliosidosis [30]. In patients with Morquio syndrome type B, a few common mutations have been observed in different populations. In Japanese patients, the mutations Y83H and R482C [31] are prevalent, where in the Caucasian population, W273L [32] and W509C [32] mutations are prevalent. Ohto *et al.* [24] discuss how these mutations may cause their respective phenotypes. Additionally, our group has recently utilized bioinformatic tools to investigate how specific mutations in the *GLB1* gene could affect the structure of the β-gal enzyme to cause very distinct phenotypes [33]. Interestingly, patients who suffer from GM1-gangliosidosis or Morquio syndrome type B with mutations found in the coding sequences of both β-gal and EBP have impaired elastogenesis [34, 35].

Diseases Resulting from Deficiencies in β-Galactosidase

GM1-Gangliosidosis: A Neurodegenerative Disease

History and Clinical Characteristics

GM1-gangliosidosis is a neurodegenerative lysosomal disease caused by mutations in the *GLB1* gene, which encodes the lysosomal enzyme β-gal. GM1-gangliosidosis was first described in 1959 as "Tay-Sachs disease with visceral involvement" [36]. In 1964, eight similar cases were described [37], but it wasn't until the following year that O'Brien *et al*. determined that the storage material in this disease was structurally different than that which accumulates in Tay-Sachs disease [38]. Finally, in 1968, it was determined by Okada and O'Brien that a deficiency in β-gal was the underlying cause of the ganglioside accumulation [39]. In this disease, GM1 ganglioside and its asialo derivative, GA1 ganglioside, are the primary accumulating macromolecules within the lysosomes of cells of the central and peripheral nervous system. GA1 ganglioside is GM1 ganglioside that has its sialic acid residue removed when in the presence of the GM2-activator protein (GM2A) and the membrane protein neuraminidase 3 (NEU3) [40]. Additionally, accumulation of keratan sulfate in the liver of GM1-gangliosidosis patients has also been observed [41].

Clinically, there are three classifications of GM1-gangliosidosis: infantile, late-infantile/juvenile, and late-onset/adult. Categorization into a group is dependent upon the patient's symptoms, time of disease onset, and residual β-gal enzyme activity. In the case of GM1-gangliosidosis, the severity of the disease is correlated to the amount of residual enzyme activity (Figure 1). Infantile GM1-gangliosidosis patients usually have 0.07-1.3% of normal levels of β-gal enzyme activity [42]. Symptoms can present at birth, however, by 6 months of age the child typically displays developmental regression. This is followed by

progressive neurological deterioration displayed as loss of neurocognitive and neuromuscular function. Additionally, these children will have enlarged spleens and livers (hepatosplenomegaly), macular cherry-red spots (50% of cases), corneal clouding, and skeletal dysplasia [3]. Typically, children with infantile GM1-gangliosidosis will succumb to the disease before the age of 2 due to complications from viral or bacterial-induced respiratory illnesses. In juvenile, or late-infantile, GM1-gangliosidosis, β-gal enzyme activity is between 0.3-4.8% of normal values [42], and the disease onset is around 7 months – 3 years of age. Many of the symptoms of infantile GM1-gangliosidosis are still present in juvenile patients, however, the onset of these symptoms is delayed. Patients in many cases of juvenile GM1-gangliosidosis will become epileptic and show severe spasticity, in addition to ataxia and hypotonia. Life expectancy is still reduced, with death typically occurring between mid-childhood and early adulthood. The mildest form of GM1-gangliosidosis, known as late-onset or adult onset, is typically more difficult to diagnose. Residual β-gal enzyme activity is approximately 4 to 10% of normal levels. Disease onset is variable, ranging from age 3 to 30 years. Clinical presentation is also extremely variable, potentially including ataxia, muscle weakness, dystonia, declining neurocognitive function, and some mild skeletal abnormalities.

The incidence of GM1-gangliosidosis is presumed to be between 1:100,000 to 1:200,000 live births. However, in some instances, higher frequencies are found in certain populations, including southern Brazil (1:17,000) [43], the Rudari sub-isolate (1:10,000) [44], and the Maltese Islands (1:3,700)

[45]. Therapies have been tested, including bone marrow transplant [46] and substrate reduction therapy [47], however, neither have proved to be efficacious for the treatment of GM1-gangliosidosis.

GM1 Ganglioside: Normal Function and Role in Neurological Diseases

As stated above, GM1 ganglioside is the primary accumulating substrate in patients with GM1-gangliosidosis. GM1 ganglioside is an amphipathic macromolecule that contains a ceramide tail covalently attached to a head chain composed of several carbohydrate moieties, including β-D-glucose, β-D-galactose, and *N*-acetyl-β-D-galactosamine (Figure 2). Additionally, a sialic acid residue, *N*-acetyl-α-neuraminic acid, is hydroxylation-linked to the β-D-galactose residue (Figure 2). If in the presence of NEU3 and GM2A, the sialic acid residue can be catalytically removed from GM1, resulting in GA1 ganglioside accumulation [40].

While gangliosides can be found throughout the body, the highest concentration are found in the plasma membrane of cells in the nervous system [48], typically localized into microdomains known as lipid rafts [49, 50]. Overall, gangliosides make up over 10% of the total lipid mass in the brain [49, 51]. During neural development *in utero* and following birth, as the neural functions become more intricate and elaborate, there is a coinciding increase in the number and complexity of gangliosides, too. This is an observation that has been described in both mice [52] and in humans [53, 54]. Specifically, in mice, relatively simple gangliosides GD3 and GM3 are the predominant gangliosides

present at embryonic day 14 (E14.0) [52]. However, after E16.0, the concentration of more complex gangliosides, such as GD1a, increases [52]. Similarly, in humans, between fetal week 10 and 5 years of age, GM1 and GD1a ganglioside levels increase 12-15-fold [53]. These results depict how gangliosides are functionally important in the neurodevelopment.

However, the function of gangliosides is not limited to neuronal development. Gangliosides have also been shown to be involved in ion transport [55], apoptosis during neuronal differentiation [56], nerve regeneration [57], neuroprotection [58], and synaptogenesis [59]. When looking specifically at the functions of GM1 ganglioside, it has been shown to be involved in many cellular processes including cell signaling, modulating calcium transport, neuronal development, neuroprotection, and modulating G-protein couple receptors [49, 60-62]. Unfortunately, GM1 ganglioside also plays a significant role in disease. Cholera toxin, a bacterial protein infection secreted by *Vibrio cholerae*, can utilize GM1 ganglioside as a docking point on the cell surface prior to endocytosis into the cell [63]. Additionally, the proteins β-amyloid and α-synuclein, which are proteins shown to be involved in the pathogenesis of Alzheimer's and Parkinson's diseases, respectively, have domains capable of binding GM1 ganglioside [64, 65]. In Alzheimer's disease, the formation of β-amyloid aggregates in neurons is central to the development of pathogenesis. It has been shown that GM1 ganglioside in lipid rafts in the cell membrane aggregate β-amyloid monomers, and form toxic β-amyloid β-sheets [66]. Similarly, α-synuclein, a protein implicated in Parkinson's disease, has a high affinity for

binding to GM1 ganglioside in lipid rafts [67]. However, it seems that GM1 ganglioside plays a role in maintaining α-synuclein homeostasis, as mice deficient in GM1 ganglioside aggregate α-synuclein and have impaired motor function, a common symptom observed in patients with Parkinson's disease [68].

Conversely, GM1 ganglioside has been shown to be beneficial for several neurological disorders, including spinal cord injury [69, 70], traumatic brain injury [71], Parkinson's disease [72-76], Alzheimer's disease [77], and Huntington's disease [78].

The Pathology of GM1-Gangliosidosis

In humans, the pathological mechanisms of GM1-gangliosidosis have not been elucidated to date. However, the pathology of the disease has been studied in mouse models of GM1-gangliosidosis, which show how the accumulation of GM1 ganglioside leads to disease pathogenesis. In one study, CNS inflammation in β-gal$^{-/-}$ mice was studied [79]. Histologically, β-gal$^{-/-}$ mice displayed microglial activation, macrophage infiltration, and astrogliosis in all regions of the β-gal$^{-/-}$ brain. As the GM1-gangliosidosis disease progressed, major histocompatibility complex class II (MHC class II) staining in the brain increased. Interestingly, CNS inflammation was observed as early as 2 months of age in β-gal$^{-/-}$ mice, which is before disease symptoms arise. Brains from β-gal$^{-/-}$ mice also stained positively for tumor necrosis factor receptor type 1 (TNF-R1), which is a mediator of apoptosis. In addition to histological analysis, inflammatory cytokine levels were measured in brain homogenates of β-gal$^{-/-}$ mice. Not only were tumor necrosis

factor α (TNFα) and interleukin 1 β (IL1β) levels increased, their levels continued to increase as the disease progressed. Further, nitrotyrosine staining was present in macrophage and neurons, suggesting nitric oxide (NO) was present. While NO has been shown to be involved in normal neurological functions such as neurotransmission, memory, and synaptic plasticity, it can also be toxic in high concentrations [80, 81]. Research into the role of NO in other neurodegenerative diseases, including Parkinson's [82] and Alzheimer's [83] diseases, suggests it may play a significant part in disease pathology. A similar pathological mechanism including NO may also play a role in GM1-gangliosidosis.

In another study, it was shown that progressive accumulation of GM1 ganglioside in neurons causes prolonged stress on the ER, leading to depletion of calcium (Ca^{2+}) stores [84]. The depletion of Ca^{2+} results in activation of the unfolded protein response (UPR) [85], leading to neuronal apoptosis. The UPR then triggers an apoptotic pathway through upregulation of C/EBP-homologous transcription factor and activation of c-Jun N-terminal kinase 2. This then leads to cleavage of the UPR-specific cysteine protease, caspace-12, contributing to neuronal cell death. Later, the same group showed that GM1 ganglioside accumulation could also cause mitochondria-mediated apoptosis [86]. This is due to GM1-ganglioside accumulating in the glycosphingolipid-enriched microdomain (GEM) fraction of the mitochondria-associated ER membranes (MAMs), which control Ca^{2+} homeostasis. When Ca^{2+} ions are suddenly released because of the stress on the ER, they are rapidly taken up by the mitochondria. This induces

mitochondrial membrane permeabilization, opening the permeability transition pore and activating the mitochondrial apoptotic pathway.

Additionally, Takamura *et al.* [87] studied the role of autophagy and mitochondrial dysfunction in neurodegeneration observed in GM1-gangliosidosis. They showed that the brains of β-gal deficient mice had an increase in the amount of LC3-II protein (microtubule-associated protein 1 light chain 3), a standard marker of autophagy, and beclin-1 protein, which is involved in autophagosome formation [88]. Additionally, increased levels of LC3-II protein were found in cells that accumulate GM1 ganglioside. Autophagy has been shown to be involved in many neurodegenerative disorders, including Parkinson's [89], Alzheimer's [90], and Huntington's disease [91], in addition to many lysosomal diseases [92-94]. Further, Takamura *et al.* [87] observed that mitochondria isolated from the brains of β-gal deficient mice were morphologically abnormal. They suggest that these changes could potentially lead to cellular degeneration and disease progression in GM1-gangliosidosis.

Morquio Syndrome Type B: A Skeletal Disease

History and Clinical Characteristics

Typically, when a lysosomal hydrolase is defective, a single lysosomal disease arises. However, in the case of β-gal, mutations in the encoding gene, *GLB1*, can result in two lysosomal diseases: GM1-gangliosidosis, the neurodegenerative disease described above, and Morquio syndrome type B, a skeletal disease. While GM1 ganglioside is the primary accumulating substrate in

GM1-gangliosidosis, the GAG keratan sulfate (KS) accumulates in Morquio syndrome type B. The discovery of Morquio syndrome type B was made in 1976 by O'Brien *et al*. [95], who reported about a 14-year-old female who had multiple skeletal deformities, including spondyloepiphyseal dysplasia, flat vertebral bodies and femoral heads. This patient also exhibited corneal clouding and β-gal enzyme activity less than 5% of normal [95]. The intriguing discovery, though, was that there were no neurological abnormalities. In 1977, Arbisser *et al.* [96] described another 14-year-old patient who presented with similar skeletal abnormalities, including short stature, corneal clouding, abnormal gait, and increased urinary KS levels. At that time, an increase in KS suggested a deficiency in the enzyme galactosamine-6-sulfate sulfatase (GALNS), which is indicative of Morquio syndrome type A. However, the patients in the case report had normal GALNS enzyme activity. Thus, the group suggested designating the new disease as Morquio syndrome type B.

Clinically, more is known about this disease now compared to 40 years ago. Typically, development progresses normally in infancy and early childhood. After early childhood, growth begins to become delayed. Patients then develop progressive physical abnormalities, including a short trunk, sternal protrusions, kyphosis, platyspondylia (flattening of vertebrae in spine), swelling of distal ends of long bones, thickening of wrist and interphalangeal joints, and corneal clouding [95-98]. Diagnosis of Morquio syndrome type B is typically based upon residual β-gal enzyme activity (1.3-11.9% of normal activity [32, 99-102]) and symptoms.

Additionally, urinalysis shows an increase in KS and oligosaccharides secretions [97, 103].

To date, the incidence of Morquio syndrome type B is too rare to be calculated. In four natural history studies of patients with MPS diseases [104-107], only 2 cases of Morquio syndrome type B were reported in Germany out of 474 reported to have an MPS disease [107]. As reported in The Metabolic and Molecular Bases of Inherited Diseases, as of 1997, only 16 cases were ever described [31, 95-98, 103, 108-110]. Since then, a few additional patients have been described [99, 111, 112], however, the incidence still remains extremely low.

Function of Keratan Sulfate and its Potential Role in Morquio Syndrome Type B

Keratan sulfate (KS) (Figure 3) is the primary macromolecule that accumulates in patients with Morquio syndrome type B. It is a large glycosaminoglycan that is composed of repeating disaccharides composed of galactose and N-acetylglucosamine. KS exists as a carbohydrate bound to a core protein, forming a proteoglycan. These core proteins are typically found in the extracellular matrix (ECM) covalently attached to a core protein or on the cell surface. While there are many functions of KS [113, 114], the role it potentially has in the pathology of Morquio syndrome type B are discussed below.

The highest abundance of KS in the body is found in the cornea, which contains keratocytes that synthesize KS [115]. Within the cornea, KS plays a

crucial role in maintaining tissue hydration that is essential for the corneal transparency. This is due to KS-linked proteoglycans in the cornea having water-binding properties [116]. If catabolism of KS is deficient, the result is accumulation in the tissue. This accumulation could be the cause of the corneal clouding that is present in patients with Morquio syndrome type B.

Furthermore, KS is also found in bones and cartilage. Specifically, it is covalently attached to core proteins such as osteoadherin. The pathological mechanism of how deficiencies in KS catabolism results in skeletal abnormalities has not been elucidated, but hypotheses can be made based on the location of KS. Osteoadherin is a protein that is has been shown to be involved in regulating bone homeostasis and development [117, 118]. Dysregulation of KS homeostasis could cause disruption of the normal function of osteoadherin or other proteoglycans, resulting in the abnormal bone development observed in Morquio syndrome type B patients.

Additionally, Morquio syndrome type B patients will have abnormalities in the connective tissue that makes up the cartilage. In the ECM, chondrocytes are responsible for the synthesis and secretion of KS into the ECM [119]. Another KS proteoglycan, aggrecan, is important for the proper formation of the compressive properties of cartilage [120]. Aggrecan can help tissues withstand compressive forces due to its ability to fill the space and absorb water in the cartilaginous tissues [121]. The degradation of KS is impaired in patients with Morquio syndrome type B. The limited mobility and range of motion due to joint stiffness

seen in patients with Morquio syndrome type B could be caused by dysregulation of a KS proteoglycan such as aggrecan.

Animal Models of β-galactosidase Deficiencies

Animal models are a critical component for studying and developing novel therapies for human diseases. This is especially true with rare diseases such as GM1-gangliosidosis and Morquio syndrome type B. Currently, the only models of β-gal deficiencies in existence are those that recapitulate GM1-gangliosidosis. To date, no animal models of Morquio syndrome type B have been described. Aside from mice, the models of GM1-gangliosidosis that have been described are naturally occurring. These models include black bear, cattle, sheep, dogs, and cats. Each of these models will be described briefly.

Black Bear, Bovine, and Ovine Models

In the black bear population, a naturally occurring mutation (Y348H) was discovered [122] in a subset of animals that resulted in the presentation of many GM1-gangliosidosis symptoms. These bears have a reduced lifespan, succumbing to the disease around 2 years of age, compared to wild black bears which live 32-36 years. Additionally, these diseased bears have reduced β-gal enzyme activity, between 1.2-2.3% of normal, and a significant accumulation of GM1 and GA1 gangliosides. Histological analysis showed the presence of severe vacuolation in mononuclear cells, chondrocytes, and in the CNS. Additionally, the

bear had skeletal abnormalities similar to those in some humans with GM1-gangliosidosis.

GM1-gangliosidosis was also observed in inbred Holstein Friesian cattle [123, 124]. The symptoms of GM1-gangliosidosis, including labored movement and ataxia, appeared within the first month of life. Further, their lifespan was reduced to 6-9 months of age, compared to a normal cow that can live approximately 20 years. Histological analysis of the CNS showed that neurons had a swollen, foamy, and vacuolated morphology. Ganglioside quantification in these calves showed significant increases compared to normal calves.

In sheep, multiple naturally occurring models exist. In one model [125, 126], disease symptoms present around 4-6 months, including severe ataxia and the inability to stand. Histological analysis showed severe lesions in the CNS, including swollen neurons with foamy or vacuolated cytoplasm. Enzyme activity was less than 5% of normal levels in the brain and kidney. Ganglioside accumulation was also seen in affected sheep. In a second model, three lambs presented with a more severe and aggressive β-gal deficiency. These lambs presented with neurological impairments around 1 month of age and by 4 months had either died or required euthanasia [127]. Pathological analysis showed that neurons were ballooned and had cytoplasmic inclusions. Enzyme activity was approximately 10% of normal levels. A possible third model of ovine GM1-gangliosidosis was published by Ryder and Simmons [128], who found histopathological abnormalities in the brains of three adult Romney sheep that were comparable to those observed in late-onset GM1-gangliosidosis. These

sheep had an isolated disease pathology, only present within the corpus striatum. Within the neurons of the basal nuclei, they observed granulated occlusions, and positive Luxol fast blue (LFB) and Periodic acid-Schiff (PAS) staining. However, no other biochemical analysis was conducted, so the diagnosis of GM1-gangliosidosis is only speculative.

Overall, while these large animals could be useful for future studies of therapies for GM1-gangliosidosis, the cost of generating and maintaining a colony and the genetic heterogeneity make their use for developing treatments unattractive and impractical.

Canine Models

GM1-gangliosidosis has been described in many breeds of canines, including mixed-breed beagles [129, 130], English Springer Spaniels (ESS) [131, 132], Portuguese Water Dogs (PWD) [132-134], Alaskan Huskies [135-137], and Shiba Inu [138-141].

In mixed-breed beagles, an initial animal was described to present with GM1-gangliosidosis symptoms [129]. The animal was observed for 4 months, where it displayed progressive motor dysfunction including head tremors and impaired coordination. The animal also had progressive vision loss, hyperactivity, and became uncoordinated as it aged [129]. At 9 months of age, the animal was unable to stand and was euthanized. Histological analysis revealed that neurons in the brain, spinal cord, and retina were enlarged and vacuolated. The storage material within the vacuoles stained positive with Sudan black and LFB. Further,

vacuolation was also observed in hepatocytes, spleen, and kidney [129]. Ganglioside levels were elevated in the brain, spleen, and liver of affected animals. β-gal enzyme activity in the gray matter of the brain was significantly reduced below 6% of normal levels [129]. Further studies were conducted on beagles from the same pedigree described above [130]. Affected animals developed normally until approximately 3 months of age, when their eyes began to become crossed. Further neurological impairments presented around 6 months, when affected animals started developing hind-limb ataxia [130]. Around 7-9 months, diseased dogs displayed severe neuromotor dysfunction, including ataxia, weakness in their limbs, and head tremors [130]. Similar to the dog discussed in [129], by 9-10 months of age, diseased animals became paralyzed and were euthanized [130]. Histological observations were similar to the dog described by Read *et. al.* [129], with distended and vacuolated neurons in the brain and spinal cord [130]. Biochemical analysis revealed that ganglioside levels were significantly increased and β-gal enzyme activity was 4% of normal levels in diseased dogs.

In English Springer Spaniels (ESS) [131], diseased puppies are dwarfed compared to their littermates. Around 4 months of age, diseased ESS puppies displayed neurological impairments, including ataxia. By 8 months of age, the animal was completely ataxic and had nystagmus and decreased neural response to stimulation [131]. In affected ESS puppies, disease progression occurred quickly, where most animals required euthanasia by 10 months of age. Histological analysis revealed cellular vacuolation in the neurons in the brain,

spinal cord, and retina, in addition to the pancreas, kidneys, and chondrocytes [131]. Interestingly, one diseased ESS dog at 8 months of age displayed skeletal abnormalities at necropsy, including thickened intervertebral disk spaces and deformed femoral heads. Biochemical analysis revealed that GM1 ganglioside levels in the brain and oligosaccharide levels in the brain, liver, urine, and cartilage were increased in diseased ESS dogs. Further, enzyme assays showed that β-gal enzyme activity was significantly reduced in affected animals [131].

A few years later, another canine model presenting with GM1-gangliosidosis symptoms was described in the Portuguese Water Dog (PWD) [133]. Examination of PWD at 6 months of age revealed significant neurological deterioration. Symptoms of affected animals included generalized ataxia, head tremors, and nystagmus. By 7 months of age, diseased PWD dogs were euthanized due to disease severity. Histological analysis revealed vacuolation in the neurons of the brain, spinal cord, and retina, which stained positive with LFB and toluidine blue. Vacuolation was also present in non-neuronal tissue, including the liver, kidneys, spleen, pancreas, and lung. Biochemical analysis revealed β-gal enzyme activity in the liver was less than 10% of normal, and that there was a significant accumulation of GM1 ganglioside in the brain. Further characterization and comparisons of diseased PWD to affected ESS dogs was done by Alroy *et. al.* [132]. They described that both ESS and PWD puppies had skeletal abnormalities as young as 2 months of age. Histological studies showed again that the neurons in brains, spinal cord, and retina were severely vacuolated and the cytoplasmic inclusions stained positively with LFB. Biochemically, they

saw that ganglioside levels in both models were significantly elevated and β-gal enzyme activity was approximately 6.2% and 1.5-8.8% of normal levels in ESS and PWD, respectively. The group also noted that while these two models of GM1-gangliosidosis had similar disease pathology and progression, only affected ESS animals were dwarfed and developed coarse facial features.

Another naturally occurring model of canine GM1-gangliosidosis was described in Alaskan Huskies [135-137]. Initial observations [135] of diseased Huskies showed that they were dwarfed compared to littermates and had neurological impairments that arose around 4 months of age. The neurological impairment progressively worsened until 7 months of age, at which time the animals were euthanized. Histological analysis revealed a vacuolated pathology in neurons, macrophages, and lymphocytes. Enzymatic analysis showed that β-gal enzyme activity was 4.0-11.3% of normal levels in lymphocytes and 4.2%, 6.3%, 1.9%, and 2.1% of normal levels in the liver, kidney, spleen, and brain, respectively. Additionally, ganglioside levels were significantly elevated. Further studies [136] on Huskies from the same pedigree showed that the disease symptoms are first noticeable around 6-8 weeks of age, including weight loss, abnormal gait, and a slight head tremor. At 7 months of age, diseased Huskies were still dwarfed compared to littermates and displayed symptoms of cerebellar dysfunction including impaired coordination of their hindlimbs, in addition to a more severe head tremor. A similar skeletal phenotype was observed in Huskies to that described in ESS and PWD dogs, including widening of the intervertebral disc space and delayed ossification of the lumbar vertebra. Again, neurons if the

brain, spinal cord, and peripheral ganglia were severely vacuolated in diseased Huskies. The storage material in these vacuolates stained positive with both PAS and LFB.

More recently, a naturally occurring Shiba Inu canine model of GM1-gangliosidosis has been described and studied [138-141]. The first description of this model [138] discussed a Shiba dog that had progressive motor dysfunction beginning at 5 months of age. This dysfunction displayed a similar cerebellar disorder described above for the other canine models, including ataxia, head tremors, and the inability to maintain its balance. By 8 months of age, the affected Shiba was unable to stand and while it was able to respond to stimulus (e.g. sound or touch), the response was delayed. At 10 months of age, corneal clouding and loss of vision was observed. Pathological analysis showed that the liver and spleen of the affected animal were slightly enlarged and that neurons throughout the CNS were vacuolated. Ganglioside quantification revealed that GM1 ganglioside levels were more than 20-fold normal levels in the cerebral cortex and 10-fold normal levels in the cerebral medulla. Additionally, β-gal enzyme activity was less than 2% of normal in the liver and leukocytes of affected animals. In the same paper, Yamato *et. al.* [138] describe a second case of GM1-gangliosidosis in a Shiba puppy that died shortly after birth. While ganglioside levels were not elevated, β-gal enzyme activity in the cerebrum, cerebellum, liver, spleen, and kidney were 1%, 0.6%, 2.1%, 1.2%, and 5.2% of normal, respectively. Yamato *et. al.* [139] followed this initial description with a longitudinal study on the Shibas model of GM1-gangliosidosis that further

characterized the behavioral and clinical features of these animals. Unlike affected ESS puppies [131] which are dwarfed at birth, diseased Shiba puppies are normal. Interestingly, they observed that around 10 months of age, affected animals started to become aggressive and bark. Further, while their food intake does not change, affected Shibas begin to lose weight around 10 months of age. This decrease in weight coincides with the diseased animals increase in mortality. Beginning around 13 months of age, diseased Shiba become completely lethargic, and by 15 months require humane euthanasia due to the severity of the disease.

Overall, these canine models recapitulate many of the clinical symptoms and disease pathology of GM1-gangliosidosis and could be important models for testing potential therapies in a larger model of the disease. However, the high cost of maintaining canine models hinders their use.

Feline Models

In felines, many cases of GM1-gangliosidosis phenotypes have been described. At 4 months of age, a Siamese cat [142, 143] started showing weakness and incoordination in its hind legs, and progressive ataxia, until the animal became completely incapacitated at 6 months of age and required euthanasia. Histological analysis showed that the neurons of the CNS and retina were enlarged and vacuolated. This vacuolation was also present in the spleen, where vacuolated macrophages were observed. Biochemical analysis revealed

that ganglioside content was 2-fold of normal levels and β-gal enzyme activity was 15% and 20% of normal levels in the brain and kidney, respectively.

In an isolated case, a 7-month-old Korat cat [144] was reported to have delayed growth, hindlimb tremors, labored breathing and seizures. The affected cat also displayed other neurological symptoms, including mental deterioration, ataxia, and impaired ability to complete the wheelbarrow behavior test. Following euthanasia at 21 months of age, histological analysis showed severe neuronal vacuolation throughout the brain, spinal cord, and peripheral ganglia. Vacuolation was also present throughout the visceral organs, including the liver, kidney, bronchi, and esophagus. Biochemical analysis of the affected cat revealed β-gal enzyme activity was significantly reduced (19% of normal in brain; 33% of normal in liver). Ganglioside quantification revealed that this decrease in enzyme activity resulted in a 3-fold and 1.7-fold increase in total gangliosides levels in the brain and liver, respectively.

Other cases of felines with GM1-gangliosidosis have also been described in non-purebred domestic cats found in the United Kingdom [145-147], Japan [148, 149], and Bangladesh [150]. In these cases, similarities in symptoms to human GM1-gangliosidosis were observed.

Similar to canine models, felines with GM1-gangliosidosis could provide a feasible larger model for studying therapies for this disease. However, the use of feline models poses similar challenges as all the previously described animal models, which is the high cost. This highlights the need for a more practical and cost-efficient model.

Murine Models

In comparison to the naturally occurring models of GM1-gangliosidosis in larger animal models described above, genetic engineering was utilized to generate murine models of the disease. Prior to this dissertation, two mouse models of GM1-gangliosidosis had been developed [151, 152]. Both of these models were generated by inserting an exogenous neomycin resistance gene cassette into the reading frame of the *Glb1* gene through homologous recombination in embryonic stem (ES) cells [153]. In one line developed by Hahn *et al.* [151], the *Glb1* gene was disrupted by targeting exon 6, while Matsuda *et. al*. [152] targeted exon 15. Both of these mutations resulted in a significant loss of β-gal enzyme activity. In the Matsuda mouse, β-gal enzyme activity in tail snips was 6.8% of wildtype levels and enzyme activity in the brain, spleen, liver, kidney, and testes was extremely low compared to wildtype levels [152]. Similarly, in the Hahn mouse, enzyme activity was 7.4%, 3.9%, 2.3%, and 1.1% of wildtype levels in the kidney, brain, liver, and spleen, respectively [151]. The groups attributed this residual enzyme activity levels to the presence of a second β-galactosidase, galactocerebrosidase, which is capable of cleaving the synthetic substrate utilized in enzyme assays [154]. The loss of β-gal enzyme activity led to the accumulation of GM1 ganglioside in the CNS of both murine models. Ganglioside quantification showed that the Matsuda *et. al* mouse showed a 20-fold increase in GM1 ganglioside levels in the brain and that GA1 ganglioside levels were increased [152]. Similarly, Hahn *et. al.* observed an increase in ganglioside levels, beginning as early as 3 weeks of age [151]. Between this time

point and 3.5 months of age, GM1 ganglioside levels increased from 2.2-fold of normal levels to 4.8-fold of normal levels. Histological analysis revealed that this loss of β-gal enzyme activity and subsequent ganglioside accumulation resulted in the presence of neuronal vacuolation in the brain that stained positive with PAS as early as 3 weeks of age. By 5 weeks, the severity of neuronal vacuolation increased significantly and was observed in nearly all regions of the brain, which again stained positive with PAS.

In both cases, β-gal deficient animals were reported to be behaviorally and phenotypically normal at birth compared to littermates. However, around 4 months of age, as the disease progressed and neuronal ganglioside content and vacuolation increased, neurological symptoms including body tremors, ataxia, and abnormal gait became apparent. As the animals aged, the severity of the disease worsened. As animals started to become paralyzed and completely emaciated, they finally succumbed to the disease around 10 months of age [151, 152]. Initial neurological impairment was described by Matsuda *et. al*. [155], who observed that affected mice at 8 months old displayed a limb-clasping behavior when hung by their tail, pulling their limbs in close to their body. In contrast, a neurologically normal mouse will extend their limbs outwards to balance. This limb-clasping behavior is a common observation in mice with neurodegeneration [156]. Further behavior analysis in β-gal deficient mice showed that their motor function was significantly impaired [157-160]. However, no cognitive testing has been conducted on these animals.

Overall, mice are a useful model organism for testing therapeutics because they are genetically identical, increasing the reproducibility of experiments. The low cost and frequent breeding of mice make them more practical and accessible than larger animal models. Furthermore, most experiments for biochemical analyses and behavior tests have been developed. However, the mechanism by which these previous models were made is completely synthetic and does not recapitulate *GLB1* mutations in human patients with β-gal deficiencies. Additionally, the models that are published do not synthesize any function β-gal enzyme, limiting the approaches that can be tested in these animals. The near absent level of β-gal enzyme activity also prevents testing therapies for patients who have missense mutations in the *GLB1* gene, resulting in residual enzyme activity, such as patients who have juvenile or late-onset GM1-gangliosidosis. Therefore, we created two models of β-gal deficiency, one completely devoid of β-gal activity, in addition to the first β-gal deficient mouse with residual enzyme activity, using CRISPR-Cas9 genome editing. These are the first mouse models of lysosomal diseases to be generated utilizing this technology.

CRISPR-Cas9 Genome Editing to Create Genetically Modified Mouse Models

CRISPR, or clustered regularly interspaced short palindromic repeats, are present in the adaptive immune system of archaea and bacteria to counter infections by viruses [161]. When a virus infects bacteria, the bacterial response

is to incorporate a piece of this viral DNA into its own genome. Bacteria then use this incorporated DNA as an adaptive immune response to subsequent infections by transcribing a small RNA, approximately 20 nucleotides in length (CRISPR RNA, crRNA; also known as the protospacer sequence), which guides an effector endonuclease to the invading viral DNA and binds to the complementary strand [162]. One of these endonucleases that has been adapted for genome editing is the CRISPR-associated (Cas) protein, Cas9. To create a site-specific double-strand DNA break (DSB), Cas9 must form a complex with a crRNA and a trans-activating RNA (tracrRNA) that partially complements the crRNA. For gene editing, these two RNA sequences are combined to form a single guide RNA (sgRNA). One requirement of Cas9 DNA cleavage is the presence of a 3 bp DNA sequence known as the protospacer adjacent motif (PAM), which needs to be positioned directly 3' to the crRNA complementary sequence [163, 164].

Following a DSB, the cell undergoes double-strand DNA repair following one of two paths, either homology directed repair (HDR) or non-homologous end joining (NHEJ) [165-167]. These pathways can be exploited with the CRISPR-Cas9 system to generate mouse models in the following ways. A specific mutation can be created through HDR by providing a DNA template containing a specific mutation that is flanked by a sequence homologous to the targeted region of DNA. In contrast, insertions or deletions (indels) can be created by a second method of DSB repair known as NHEJ. This approach can yield mutations resulting in the creation of a gene knockout model in mice.

Current Clinical Therapies for β-galactosidase Deficiencies

Clinically, there are no treatments for the β-galactosidase deficiencies GM1-gangliosidisis and Morquio syndrome type B. Because the number of Morquio syndrome type B patients is so low, most approaches taken to date have been for GM1-gangliosidosis, which will be the sole focus of discussion on therapies in this section.

Substrate Reduction Therapy

One method of alleviating the devastating pathology of GM1-gangliosidosis is by substrate reduction therapy (SRT) with a drug called miglustat, also known as *N*-butyldeoxynojirimycin (*N*-B-DNJ) or Zavesca®. It was shown that this iminosugar is capable of inhibiting glucosylceramide synthase, which is responsible for the formation of glucosylceramide (GlcCer), a major component of most glycosphingolipids including GM1 ganglioside. Miglustat has been shown to reduce ganglioside content in mice with gangliosidoses [168, 169]. By inhibiting the ability to form new gangliosides, miglustat reduces the number of accumulating gangliosides. This therapy has been implemented for use in patients who suffer with either GM1-gangliosidosis or GM2-gangliosidoses. However, while this treatment temporarily helps with symptoms, it does not slow down the progression of the disease [170-174].

A combination of miglustat with a ketogenic diet, which is a diet that contains higher amounts of fats and lower amounts of carbohydrates, is currently in clinical trials (ClinicalTrials.gov Identifier: NCT02030015). The rationale behind

this combination therapy is that by reducing the carbohydrates content, there will be a synergistic effect with miglustat. Whether this has any effect on therapy or disease progression is still unknown as the trial is ongoing.

Hematopoietic Stem Cell Transplant

In 2005, Shield *et. al*. [46] published a case report of a patient with juvenile GM1-gangliosidosis who had undergone a successful bone marrow transplant at 7 months of age. Cells were isolated from her older sister whose β-gal enzyme activity was 240 nmol/hr/mg protein. At the time of transplantation, her development and neurological pathology were normal compared to other children her age. At 14-months of age, she was able to walk and had normal speech skills. However, around 20 months of age, she began progressively losing speech and motor skills. At 29 months of age, MRI scans showed both myelin dysfunction and loss of myelination, and her EEG showed she had cerebral dysfunction. Sadly, by the time she was 5 years old, she was severely ataxic, had limited motor function, and lost her ability to communicate. At 7 years of age, she was completely wheelchair bound and suffering from seizures. Interestingly, at 7 years post-transplant, the patient's β-gal enzyme activity was 246 nmol/hr/mg protein in white blood cells. Overall, this outcome suggests that, even though there were high levels of β-gal enzyme present, stem cell transplantation is not sufficiently treating the neurodegeneration in this debilitating disease.

Pre-clinical Studies for Treating β-galactosidase Deficiencies

Rationale for Treating Lysosomal Diseases

The rationale for nearly all approaches for treating lysosomal diseases such as GM1-gangliosidosis is based upon the phenomenon known as metabolic cross-correction. Cross-correction was first shown in 1968 by Dr. Elizabeth Nuefeld and her group, where they observed that by culturing fibroblasts from patients with two different lysosomal diseases (one from MPS I, another from MPS II), degradation of GAG occurred normally [175]. However, when the fibroblasts were cultured separately, GAG accumulated. Later experiments showed that most lysosomal enzymes are post-translationally modified by the covalent attachment of mannose 6-phosphate (M6P) [176] and sorted to the Golgi by binding to the M6P receptors (M6PR) [177, 178]. The lysosomal enzyme and M6PR complex is then sorted to the lysosomal compartment, where the acidic pH dissociates the enzyme from the M6PR [179].

However, 5-20% of the enzyme follows another pathway and is trafficked to the cell surface and released into the extracellular space [180]. The secreted lysosomal enzymes are able to interact with the M6PR or mannose residues on the surface of nearby cells and be internalized and trafficked to the lysosome, where they can be used to degrade macromolecules. This is what is known as metabolic cross-correction and is the basis for most clinical and pre-clinical research in the treatment of many lysosomal diseases.

Molecular Chaperone Therapy

For GM1-gangliosidosis, a couple of molecular chaperones have been studied that could increase the activity of defective β-gal. *In vitro* studies conducted on fibroblasts from GM1-gangliosidosis patients treated with derivatives of galactonojirimycin showed restoration of β-gal activity [181]. Previously, 1-deoxygalactonojirimycin, or DGJ, had been shown to increase the activity of mutated α-galactosidase, which is the deficient enzyme in the lysosomal disease Fabry disease [182]. This increase in activity was shown to be a result of accelerated transport and maturation of the mutated protein [182]. In mutant fibroblasts, the use of low concentrations of DGJ and *N*-(*n*-butyl)-deoxygalactonojirimycin (NB-DGJ) elevated β-gal enzyme activity 3-fold and 7-fold in cells with I51T and R201C mutations, respectively. However, cells from patients with other mutations, including patients with Morquio syndrome type B, showed minimal increase in enzyme activity.

In another study by Matsuda *et. al.* [183], a galactose derivative, *N*-octyl-4-epi-β-valienamine (NOEV), was tested to determine if β-gal enzyme could be stabilized or have an increase in activity. To test this, they randomly inserted a transgene expressing the human *GLB1*^{R201C} mutation found in patients with GM1-gangliosidosis into their β-gal-deficient mouse model [183]. *In vitro* and *in vivo* testing of NOEV showed a marked increase in β-gal enzyme activity. Additionally, the group showed that NOEV could reduce the levels of GM1 ganglioside in the brain. This showed that NOEV could cross the blood-brain barrier (BBB), which is the significant limitation of enzyme replacement therapy in

lysosomal diseases with neurological involvement. However, this approach has not been applied clinically.

Enzyme Replacement Therapy

While enzyme replacement therapy (ERT) has been approved for use in multiple lysosomal diseases [184], it has not been tested *in vivo*, nor approved, for use in GM1-gangliosidosis clinically. However, recombinant proteins have been synthesized from felines [185, 186] and from humans [187]. In one of these studies [185], purified feline β-gal in liposomes reduced ganglioside levels in β-gal deficient fibroblasts.

Recently, a group tested a β-gal fusion protein that included the human *GLB1* sequence fused to the ricin toxin B-subunit (RTB), which is known to bind carbohydrates and mediate transport into cells [188-191]. The rationale for this fusion construct was that RTB can bind to the cells of the BBB, be transcytosed, and treat the neurological component of GM1-gangliosidosis. *In vitro*, this fusion construct showed uptake into fibroblasts from GM1-gangliosidosis patients and had functional β-gal activity. To date, *in vivo* testing of this enzyme has yet to be published. However, a similar system has been tested in a mouse model of the lysosomal disease MPS I (Hurler syndrome) [192] and was shown to reduce GAG levels and improve neurocognitive function of diseased animals.

Another ERT approach in MPS I mice showed that by providing a high dose (20-fold clinical dose) of recombinant enzyme intravenously, neurocognitive function was improved [193]. This result was important, because it shows that if a

therapy can provide large and continuous amounts of enzyme, there is a possibility that neurological function can be improved.

Gene Therapy

Over the last few decades, gene therapy has emerged as the next revolutionary approach to treating genetic conditions such as lysosomal diseases. To date, many pre-clinical gene therapy studies have been conducted in lysosomal diseases. These approaches include the use of liposomes, polymers, minicircles, and Sleeping Beauty transposons for non-viral therapy, and retroviruses (RV), lentiviruses (LV), adenoviruses (Ad), and adeno-associated viruses (AAV) for viral therapies.

Non-viral systems provide many advantages, including reduced pathogenicity, reduced risk of insertional mutagenesis, relatively cheap to develop, and easy manufacturing. However, they are inefficient at entering cells and expressing enough transgene to have a therapeutic effect. Many non-viral approaches have been used for gene therapy in lysosomal diseases [194], however, viral approaches will be the focus of this dissertation.

The field of gene therapy has also utilized the capacity of different viruses to infect cells and express a specific transgene. Which viral vector is used is dependent upon many factors, including the size of the transgene, types of cells being targeted, delivery method (*ex* vivo or *in vivo*), and whether DNA integration is necessary.

Retroviruses

The first virus used in clinical trials were retroviruses (RVs). RVs are single-stranded RNA (ssRNA) containing enveloped viruses. The proteins necessary for viral infection and reproduction are encoded by three RV genes, *gag*, *pol*, and *env*. These three RV genes are flanked by long-terminal repeat (LTR) sequences that are required for proper viral DNA reverse transcription and integration into the host genome. Following infection, reverse transcriptase, encoding by the *pol* gene, reverse transcribes the viral genome to produce a single strand of DNA, which is converted to double-stranded DNA through multiple steps [195]. Following double-strand synthesis, the DNA is transported to the nucleus and is integrated into the host cell's DNA by the virally-encoded integrase protein. For gene therapy purposes, researchers remove the *gag*, *pol*, and *env* sequences and replace them with an exogenous promotor to drive the expression of a transgene of interest. The capacity of the RV is approximately 8 kb, so the coding sequences for most lysosomal enzymes could be used. While powerful and capable of providing a permanent transgene expression, RVs have limitations. One of these limitations is the inability of RVs to transduce non-dividing cells, which makes them an unlikely candidate for transducing neurons and treating neurological diseases.

For GM1-gangliosidosis, preclinical studies have been done *in vitro* and *ex vivo* utilizing RVs. *In vitro* studies in human fibroblasts from GM1-gangliosidosis patients transduced with RVs encoding either human or mouse β-galactosidase resulted in the restoration of β-gal enzyme activity [196]. This experiment also

showed that mouse β-gal enzyme was secreted more efficiently than human β-gal, and that it also had a higher enzyme activity [196]. In a second study [157], normal (expressing endogenous mouse *Glb1*) bone marrow cells were transduced with RVs encoding human *GLB1* and transplanted into β-gal deficient mice. Treated mice displayed increased β-gal enzyme activity in the brain, resulting in improvement of neuronal pathology and reduction in GM1 ganglioside accumulation. Treated mice also had improved neuromotor function in the rotarod test.

Lentiviruses

The human immunodeficiency virus (HIV)-1-based lentivirus (LV) has been adapted for use in gene therapy and is capable of transducing both dividing and non-dividing cells [197, 198]. LVs have been utilized in many preclinical studies in lysosomal diseases [199, 200], however, have never been applied to treating GM1-gangliosidosis. LV approaches have been utilized to transduce hematopoietic stem cells *ex vivo* for the treatment of diseases such as β-thalassemia [201], Wiskott-Aldrich syndrome [202] and X-linked adrenoleukodystrophy [203] with great success. While these therapies have been promising, LVs also have their limitations. LV integration has been shown to be semi-random [204, 205], leading to safety concerns regarding insertional mutagenesis. This observation led to the development of LV vectors that are incapable of integrating into the genome, also called non-integration LV vectors

[206]. However, there are other viruses that are non-integrating that are capable of transducing both dividing and non-dividing cells.

Adenoviruses

One of the non-integrating viruses are adenoviruses (Ads), which have a double-stranded DNA (dsDNA) genome that is approximately 36 kb in length, encoding over 50 polypeptides [207]. Following infection and subsequent loss of the viral capsid, the viral DNA is released and transported to the nucleus [208]. Once in the nucleus, transcription and translation of viral DNA occurs by utilizing host and viral DNA. Gene expression in Ads is broken into two phases, early and late. Genes expressed in the early phase encode for proteins involved in initiation and regulation of cellular functions that allow for DNA replication, where late genes encode structural proteins required for encapsidation of the newly replicated DNA [207, 209]. Currently, there are 57 human adenovirus serotypes classified into seven different species, however only two (Ad2 and Ad5) are commonly used for gene therapy [210]. Ads were attractive vectors for gene therapy because of their large capacity for transgenes (~36 kb), ability to transduce dividing and non-dividing cells, and are non-integrating. For GM1-gangliosidosis, the use of Ads has been limited to testing in β-gal deficient mice [211]. This study showed that a single intravenous injection of an Ad encoding the mouse β-gal enzyme into a neonatal β-gal deficient mouse had beneficial outcomes for disease pathology. This included an increase in β-gal enzyme activity in tissue and decrease in GM1 ganglioside content in animals that were

treated with the β-gal-encoding Ad. However, by 60 days post-treatment, GM1 ganglioside content was increased compared to day 30, as if the amount of β-gal enzyme was not sufficient to keep up with the rate of accumulation [211].

One of the potential limitations of naturally-found Ads is that most humans have been exposed to them. They are responsible for causing respiratory and gastrointestinal symptoms such as colds, sore throats, pneumonia, and diarrhea. Moreover, Ads are very immunogenic. However, this has not hindered their use in clinical trials, as over 500 gene therapy trials have been or are being conducted using human Ad vectors [212].

Adeno-associated viruses

Another non-integrating virus is the adeno-associated virus (AAV), so named because it is a dependovirus and requires co-transfection of another virus, adenovirus or herpes simplex virus, to complete its viral lifecycle [213-215]. AAVs are small, non-enveloped viruses that have a single-stranded DNA (ssDNA) genome consisting of approximately 4.7 kb. The AAV genome contains two open reading frames, *rep* and *cap*, that are flanked by two inverted terminal repeat (ITR) sequences required for genome replication and packaging. *Rep*, short for replication, encodes four overlapping genes responsible for viral replication. *Cap,* short for capsid, contains three overlapping sequences that encode the capsid proteins VP1, VP2, and VP3 which form the icosahedral viral capsid [216, 217]. To enter the cell, the capsid of the AAV interacts with glycan moieties for initial attachment to the cell surface [218] and is then endocytosed

into the cell by clathrin-coated vesicles [219, 220]. The cell-type that is transduced by the AAV depends on the serotype of the AAV capsid. To date, there have been over 100 different variants of AAV identified in human or nonhuman primate tissues [221-225], however, 11 different serotypes have been described (AAV1-AAV11, respectively). Each of these variants, with the exception of AAV10 and AAV11, have been well studied and shown to have various tropisms, or preferences for specific cell-types. AAV2, though, has been the most widely used and studied AAV serotype [226-230].

For use as a gene therapy vector, the AAV genes *rep* and *cap* are removed and replaced with the therapeutic gene, and in most cases, a promotor to drive transgene expression. With the removal of the wildtype AAV genes, three plasmids to produce AAV are required. One of these plasmids encodes the transgene flanked by the ITRs from AAV2. The second plasmid encodes the *rep* and *cap* genes that were removed, which are required for viral replication and capsid formation. To be able to specify which cells are transduced, AAV tropism is selected by replacing the *cap* genes from a specific AAV. For this study, the AAV8 capsid was utilized for its ability to effectively transduce hepatocytes [231]. The third plasmid encodes helper genes from adenovirus (Ad), E4orf6, E2a, and VA RNA. These three plasmids are then transfected into producer HEK293 cells, which express two additional Ad helper genes, E1a and E1b55k, from which active virus can be isolated from cell lysates [232, 233].

AAV has become an attractive virus for use in gene therapy because it can transduce dividing and non-dividing cell types, and is not known to cause

any pathogenic conditions in humans. Additionally, where wildtype AAV is capable of integrating into the AAVS1 site on chromosome 19 [234, 235], AAVs have had the *rep* gene removed, removing their capacity to integrate [236]. However, some of these benefits are also limitations of AAV. Over time, many cells that have been transfected with AAV will die off, or divide, leading to a loss or reduction of transgene expression. This problem is further exacerbated by the inability to administer another dose of AAV due to the formation of neutralizing antibodies and T-cell responses [237-239]. Further, the ability to produce high titers (concentrations) of AAV is limited and costly. The ability to produce these high titers also becomes more difficult as the size of the transgene increases, which is a problem, because the capacity of AAV is only 4.7 kb.

These potential pitfalls, though, have not limited the use of AAV vectors in clinical trials. As of August 2018, AAV has been utilized in 227 gene therapy clinical trials, which is approximately 8.1% of all gene therapy trials [212]. From these clinical trials, many have been successful at treating their respective disease, including spinal muscular atrophy 1 [240], α-1-antitrypsin deficiency [241], hemophilia B [242-244], childhood-onset blindness [245], and macular degeneration [246, 247]. Further, two AAV-based gene therapies have successfully cleared experimental trials and have been approved for clinical use. The first ever approved gene therapy, known as Glybera®, developed for patients with lipoprotein lipase deficiency, was successfully approved for use in Europe in 2012 [248]. However, due to the cost of the treatment (>$1,000,000 per treatment) and the limited number of patients available (prevalence of 1 in

1,000,000 people), the development and use of the drug was discontinued. In December of 2017, the U.S. Food and Drug Administration approved the use of Luxturna™, an AAV gene therapy developed by Spark Therapeutics to treat patients with a rare inherited form of vision loss that can result in blindness [249]. The approval of these drugs shows the vitality and strength of AAV vectors for use in gene therapy.

While the approved gene therapies utilize episomal expression of the unmutated transgene, there are at least two current clinical trials for lysosomal diseases that are circumventing the potential dilution or loss of AAV expression over time. Our group, in collaboration with Sangamo Therapeutics, utilized three AAV vectors to incorporate the deficient lysosomal enzyme into the albumin locus to provide permanent expression of the transgene. Two of these AAV vectors encode zinc-finger nucleases that generate a DSB in the albumin locus, and a third AAV vector that encodes the deficient lysosomal enzyme, either α-L-iduronidase (IDUA) [250] or iduronate-2-sulfatase (IDS) [251]. Each of these transgenes is flanked by DNA sequence that is homologous to the region targeted in the albumin locus, which promotes homology directed repair of the DSB. This allowed for stable integration of the missing enzyme, meaning that AAV dilution should not occur following cell division, as the daughter cells will also have the incorporated sequence.

Thesis Statement

The introduction above has laid out the current models of the β-gal deficiencies, including GM1-gangliosidosis and Morquio syndrome type B, and the limitations in clinical care of patients with these debilitating diseases. In the following chapters, the development of novel models of β-gal deficiencies and the application of a novel gene therapy approach for GM1-gangliosidosis will be discussed. Chapter II discusses how CRISPR-Cas9 genome editing was used to introduce two novel mutations into the β-gal encoding gene. Chapter III describes the comprehensive assessment of one these mutations that completely abolishes β-gal enzyme activity, resulting in a mouse model of GM1-gangliosidosis. In Chapter IV, the mouse containing the second mutation that reduces β-gal enzyme activity is discussed. Chapter V will discuss preliminary data from a proprietary gene therapy approach that utilizes the endogenous albumin promotor drive the expression of the human *GLB1* cDNA. Overall, these studies advance the development of a treatment for β-galactosidase deficiencies.

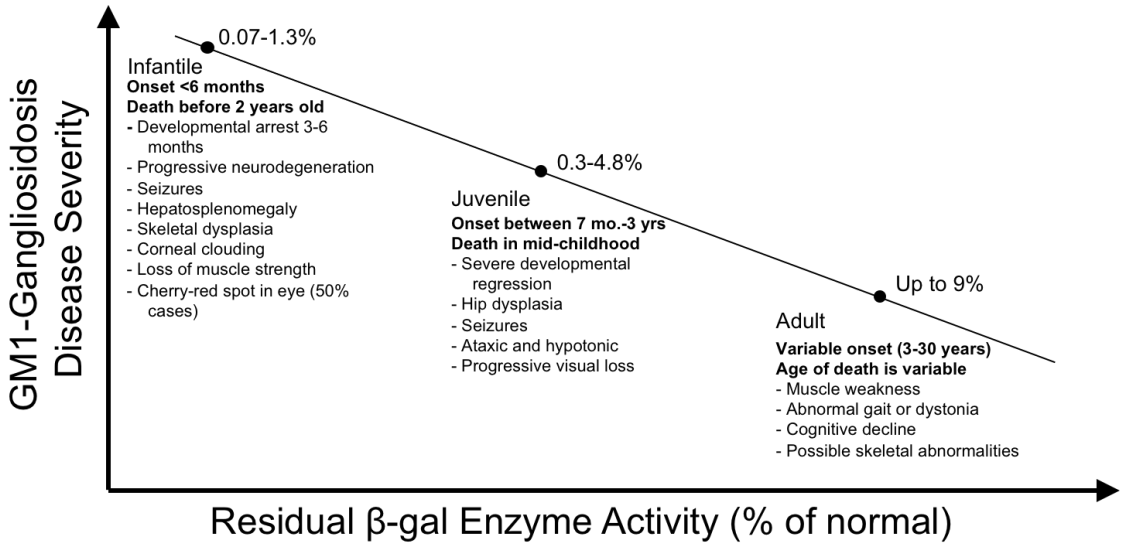

Figure 1. Severity of GM1-gangliosidosis increases as residual β-galactosidase enzyme activity decreases. Derived from [3, 42].

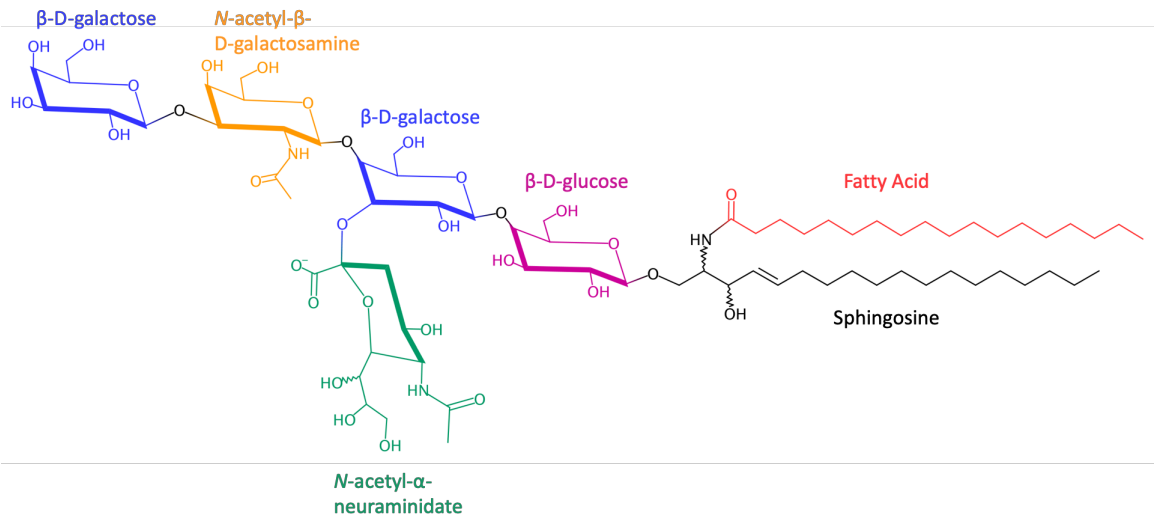

Figure 2. Chemical structure of GM1 ganglioside. GM1 ganglioside is synthesized in the Golgi apparatus through the sequential addition of carbohydrate moieties to a ceramide group. Red, fatty acid; Black, sphingosine; Red and Black, ceramide; Purple, glucose; Blue, galactose; Yellow, *N*-acteyl-β-D-galactosamine; Green, *N*-acetyl-α-neuraminidate (NANA).

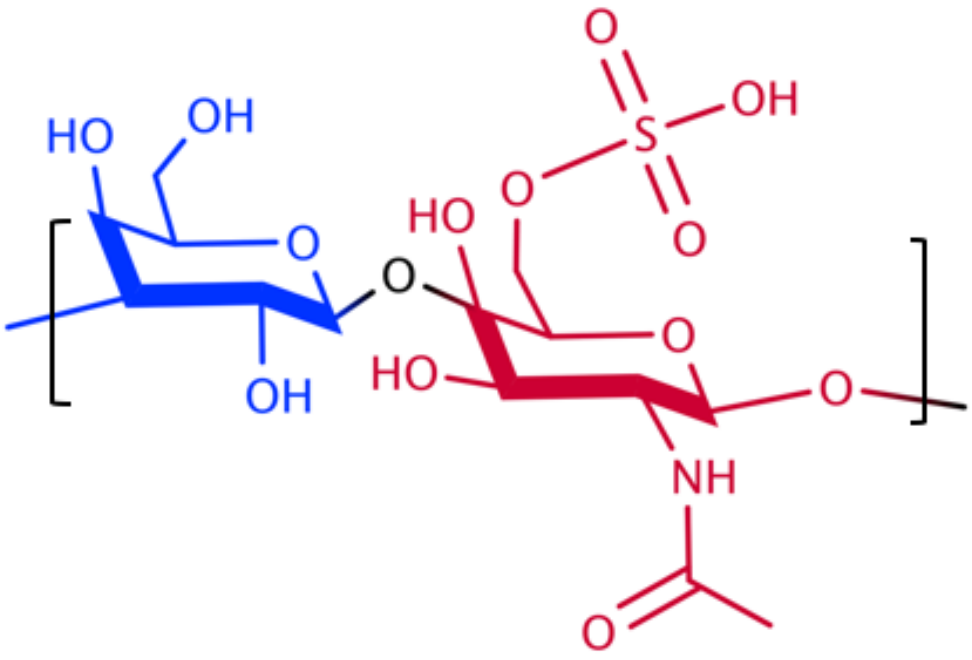

Figure 3. Chemical structure of the repeating disaccharide in keratan sulfate. Keratan sulfate is composed of repeating disaccharides containing β-D-galactose (Blue) and *N*-acetyl-D-glucosamine-6-sulfate (Red).

CHAPTER II

Utilizing CRISPR-Cas9 Genome Editing to Introduce Mutations into the Murine *Glb1* Gene

Introduction

Animal models are key for the development of novel therapies. Mice have become a cornerstone for pre-clinical drug development for many reasons: 1) mice share approximately 85% genetic similarity to humans in protein-coding genes, 2) they are capable of being genetically manipulated, 3) they can be inbred to minimize genetic variations, allowing for more accurate and repeatable experiments, 4) they have an accelerated lifespan (~2.5 years), and 5) the age of reproduction is approximately 6 weeks, and they can reproduce quickly (~every 21 days). In the past, there were two techniques used for creating mouse models, including pronuclear injection and embryonic stem (ES) cell manipulation, which are time consuming. Further, pronuclear injection relies upon random integration of the transgene, which could result in inactivation of necessary genes or integration into a region that activates an oncogene. With ES cell manipulation, targeted mutagenesis via homologous recombination (HR) was possible; however, the efficiency of desired HR is extremely low (<0.01%) [153] and the experimental timeframe is extensive and costly. Thus, new technologies were needed that allow for site-specific mutagenesis, in addition to accelerating the process and be more economical. It was shown that by introducing a DSB in the DNA, the efficiency of HR increased by approximately 5000-fold [252]. Utilizing this knowledge, and recent discoveries of programable DNA binding proteins, new technologies were developed, including synthetic zinc finger nucleases (ZFNs) [253] and transcriptional activator-like effector nucleases (TALENs) [254], both of which are able to create targeted DNA breaks and

circumventing the need for ES cells. However, these systems can be expensive and designing constructs that target a region of interest is time-consuming. In the last few years, CRISPR-Cas9 has become the frontrunner as the technology to use in targeted gene modifications, as it is relatively straightforward and inexpensive. This system utilizes a short oligonucleotide sgRNA that is complementary to the sequence to be modified. This sgRNA forms a complex with Cas9, a nuclease, and "guides" the complex to the complementary sequence in the genome, causing Cas9 to generate a DSB in the DNA. Following a DSB, the cell has two primary mechanisms of repairing the break, either by NHEJ or HDR. NHEJ typically creates in small insertions and deletions, which could be utilized to create knockout mutations. However, HDR can be promoted by providing a donor sequence that contains a sequence of interest flanked by homologous sequence to the targeted region of the genome. Here, we exploited this knowledge to create novel models of two lysosomal diseases.

Typically, when a lysosomal hydrolase is defective, a single lysosomal disease arises; however, in the case of the enzyme β-gal, mutations in the encoding gene, *GLB1*, can result in two lysosomal diseases: GM1-gangliosidosis, a neurodegenerative disease, and Morquio syndrome type B, a skeletal disease. β-gal is responsible for catabolizing the terminal galactose residue in GM1 ganglioside, its asialo derivative GA1, and the glycosaminoglycan keratan sulfate [38, 255]. The primary substrates that accumulate in GM1 gangliosidosis are GM1 and GA1 gangliosides, while in Morquio syndrome type B, keratan sulfate accumulates. Clinically, GM1-

gangliosidosis patients are categorized into one of three disease severities, 1) infantile, 2) late infantile/juvenile, and 3) adult, depending upon symptoms and residual β-gal enzyme activity. Those with the most severe infantile form have minimal or no residual enzyme activity. Patients usually present with severe neurocognitive regression around 6 months of age, hypotonia, macular cherry-red spot, hepatosplenomegaly, skeletal dysplasia, and typically succumb to the disease by 2 years of age [3]. In Morquio syndrome type B, patients have residual β-gal enzyme activity (1.3-11.9% of normal [32, 99-101]). Morquio syndrome type B patients present with normal intellect, but suffer from progressive skeletal dysplasia, short stature, in addition to odontoid hypoplasia and corneal clouding [256]. Besides palliative approaches, there are no available treatments for either of these debilitating diseases.

Previous mouse models of GM1-gangliosidosis were developed utilizing ES cell gene targeting to insert the exogenous neomycin resistance gene into the *Glb1* locus; where the model developed by Hahn *et al.* [151] disrupted the gene by inserting the cassette in exon 6 and Matsuda *et al.* [152] targeted exon 15. To create more natural models of β-gal enzyme deficiency for use in the development of novel therapies, we employed CRISPR-Cas9 genome editing to introduce either a deletion in the mouse *Glb1* gene or a missense mutation commonly found in Morquio syndrome type B patients. These mutations resulted in a loss of (β-gal$^{-/-}$) or a significant reduction (*GLB1*^{W273L}) of β-gal enzyme activity. See Chapters III and IV, respectively, for how the loss or reduction of β-

gal enzyme activity affects the phenotype of these mice. Both of these models will be important for use in therapeutic testing.

Materials and Methods

Mice

All animal care and experimental procedures were conducted under the approval of the Institute Animal Care and Use Committee (IACUC) of the University of Minnesota. All animals were housed in specific pathogen-free conditions and genotyped by polymerase chain reaction (PCR). C57BL/6J (000664) animals were purchased from The Jackson Laboratory.

Generation of β-gal$^{-/-}$ and Glb1^{W274L} Mice by CRISPR-Cas9 Embryo Micro-injection

To develop two models of β-galactosidase deficiency in a single experiment, CRISPR-Cas9 genome editing was employed to target the *Glb1* gene. Candidate CRISPR-Cas9 sgRNA targeting exon 8 of the mouse *Glb1* gene were designed utilizing Benchling® software (Benchling, Inc, San Francisco, CA) based on a system established previously by Mali *et al.* [257]. To increase specificity and reduce the potential of off-target Cas9 cleavage, truncated 17 bp sgRNAs were designed, as suggested by Fu *et al.* [258]. sgRNAs were produced by T7 *in vitro* transcription and validated *in vitro* by incubating a sgRNA, Cas9 protein, and PCR amplified target site, followed by gel electrophoresis to determine the extent of *in vitro* cleavage activity. The most efficient candidate

sgRNA (5'-CTGAGTTCTATACTGGC-3') was chosen for *in vivo* use in zygote microinjections.

Zygotes for microinjection were produced by super-ovulating C57BL/6J females by injection of pregnant mare's serum gonadotropin (PMSG) and human chorionic gonadotropin (HCG) and then mated with C57BL/6J stud males. 114 one-celled embryos were collected from the ampulla oviducts the morning after mating and microinjected with 400 nM of Cas9 protein, 50 ng/ul sgRNA targeting exon 8 of *Glb1*, and 50 ng/ul of donor oligonucleotide. For this experiment, Cas9 protein was utilized for microinjections to increase on-target efficiency of DNA cutting [259, 260] and to circumvent the issues with using Cas9 mRNA, including mosaicism at the target site [261]. The donor oligonucleotide was designed as a template for homologous recombination to introduce a 2 bp mutation resulting in a tryptophan to leucine substitution at position 274 (*Glb1*^{W274L}), commonly found in Morquio syndrome type B patients. Of the 114 injected zygotes, 106 were transferred into 4 pseudopregnant mothers, yielding 24 neonates.

Sequencing of Potential Founder Mice

Toe or tail samples were obtained from each of the potential founder neonates and DNA was isolated using the HotSHOT DNA preparation [262]. Briefly, 100 µl of Solution A is added to the biopsy tube (Solution A: 25 mM NaOH, 0.2 mM EDTA (pH ~12.0). The tubes are then incubated at 95ºC for 30 minutes. 100 µl of Solution B is then added (Solution B: 40 mM Tris-HCl in ddH_2O (pH ~5.0)), and the samples are vortexed. Tubes are then spun down for

1-5 minutes at max speed. DNA from each potential founder was PCR amplified at the sgRNA target site within exon 8 of *Glb1*. The amplified PCR product was then subjected to Sanger sequencing. Primer sequences for PCR and sequencing are listed in Table 1. Of the 24 live offspring, three had mutations within the target site of the sgRNA. Two founders had undergone HDR and were heterozygous for the 2 bp mutation that results in the W274L amino acid substitution of interest (*Glb1*^{W274L}), while the third founder had undergone NHEJ and harbored a 20 bp deletion of the targeted region (β-gal$^{-/-}$).

Sequencing of Potential Off-Target Sites

Potential off-target cutting by Cas9 was assessed in founder animals. To predict these sites of off-target Cas9 DNA cleavage, the CCTOP algorithm [263] was used. Sites of interest were determined by sgRNA sequence homology near a potential PAM sequence. Ten loci were sequenced, 5 containing the NGG protospacer adjacent motif (PAM) sequence and 5 with a NAG PAM sequence. Each of the founder mice were bred to C57BL/6J wildtype mice for germline transmission of the mutant allele. Genotyping of the offspring (N1 generation) was conducted similar to that described above for founder mice. Heterozygous N1 animals were bred to obtain wildtype, heterozygous, and homozygous mutant animals used in these studies.

Genotyping of β-gal$^{-/-}$ and *Glb1*^{W274L} Mice

Genotyping was conducted by amplifying the targeted mutation site with PCR by using the Glb1-ScF1 (forward) and Glb1-ScR1 (reverse) primers (Table 1). In *Glb1*^{W274L} mice, PCR products were digested using *Hae*III (Promega, Madison, WI), which differentially cleaves wildtype and mutant *Glb1* alleles. Wildtype mice have bands at 288 and 160 bp, where mutant alleles contain bands of 202, 160, and 86 bp in length. Undigested DNA is found at 448 bp. For β-gal$^{-/-}$ mice, PCR amplification utilizes the same primer sequences as *Glb1*^{W274L} mice. However, to distinguish mutant and wildtype mice, the PCR amplified product is treated with *Xba*I. Wildtype animals have a single band at 448 bp, where homozygous mutant β-gal$^{-/-}$ mice have bands of 242 and 186 bp. Heterozygous mice have all three bands.

Polymerase Chain Reaction (PCR)

PCR reactions of 25 µL total volume were set up with the following reagents: 12.5 µL 2X Pfu DNA Polymerase Mastermix (2X, Cat. #786-817, G-Biosciences, St. Louis, MO), 6.5 µL nuclease-free water, 2.0 µL of each 10 µM PCR primer, and 2 µL of template DNA. All PCR reactions were performed using the following cycling conditions: [1] 98ºC, 30 seconds; [2] 98ºC, 10s; [3] 58ºC, 30s; [4] 72ºC, 30s; [5] repeat steps 2-4 for 35 cycles; [6] 72ºC, 5 minutes, [7] 10ºC, infinite hold.

Restriction Enzyme Digest

Restriction enzyme digestions of the PCR products were done using the following 24 µL reaction: *Glb1*^{W274L}: 2.4 µL of 10X Buffer C (Promega), 0.24 µL of 10 mg/mL BSA, 12.36 µL of nuclease-free water, 1 µL of *Hae*III, and 8 µL of PCR amplified product. β-gal$^{-/-}$: 2.4 µL of 10X Multi-Core Buffer (Promega), 0.24 µL of 10 mg/mL BSA, 12.36 µL of nuclease-free water, 1 µL of *Xba*I, and 8 µL of PCR amplified product. The reaction was incubated at 37ºC for 2-4 hours.

Agarose Gel Electrophoresis

NuSieve™ GTG™ Agarose (Cat. #50080, Lonza, Basel, Switzerland) or LE Agarose (Cat. #E-3120-500, VWR International, Radnor, PA) solutions for separation of DNA fragments was conducted in 1X TAE (diluted from 50X made with 141 g Tris free base, 28.55 mL of Glacial acetic acid, 9.3 g ethylenediaminetetraacetic acid [EDTA], made up to 500 mL with ddH_2O). Ethidium bromide was added to allow for DNA visualization under ultraviolet (UV) light in the gel documentation system. Restriction enzyme-digested samples were loaded (10 µL) onto the cast gel, along with 5 µL of Invitrogen™ 1 kb Plus DNA ladder (Cat. #10787, Thermo Fisher Scientific, Waltham, MA) in a separate well, and the gel was run at 120 volts for 60-100 minutes, or until DNA fragments were sufficiently separated. Visualization and image capturing were done under UV light using the EpiChemi^3 Darkroom (UVP BioImaging Systems, Upland CA) system with QCapture software (V2.9.13, Quantitative Imaging Corporation, Surrey, British Columbia, Canada).

Results

Introduction of Mutations into the *Glb1* Locus Using CRISPR-Cas9 Genome Editing

To develop two models of β-gal deficiency, one with residual β-gal activity, and another completely devoid of enzyme activity, CRISPR-Cas9 genome editing was utilized. A sgRNA was designed to target exon 8 of the *Glb1* gene. To generate a model of β-gal deficiency with residual enzyme activity, a donor oligonucleotide was developed to promote HDR to incorporate a 2 bp mutation commonly found in Morquio syndrome type B patients. The donor oligonucleotide, along with Cas9 protein, and the sgRNA was injected into 114 one-cell-stage zygotes isolated from C57BL/6J mice. Of the 114 injected zygotes, 106 were transferred into 4 pseudopregnant females, which yielded 24 live pups (Figure 4A). PCR amplification and sequencing of the sgRNA targeted site showed that three of the 24 pups contained potential mutations of interest (Figure 4B). Two of the potential founders had undergone HDR, resulting in a 2 bp missense mutation at position 274 (*Glb1*^{W274L}, Figure 4C). Additionally, one mouse had undergone non-homologous end joining, which resulted in a 20 bp deletion within exon 8, yielding 3 premature stop codons, in addition to deleting the catalytic nucleophile of β-gal, *Glb1*^{Glu268} (*GLB1*^{Glu269} in humans) (β-gal$^{-/-}$$\Delta$20, Figure 4C). All three heterozygous mice were bred to wildtype C57BL/6J mice, resulting in N1 heterozygous offspring. Heterozygous mice were then bred to obtain homozygous mutant *Glb1*^{W274L} and β-gal$^{-/-}$ mice, in addition to heterozygous and wildtype control animals. PCR amplification and Sanger

sequencing of *Glb1*^{W274L} and β-gal$^{-/-}$ mice at the sgRNA target site confirmed homozygosity of the mutations (Figure 5).

No Off-target Cleavage by Cas9 in β-gal$^{-/-}$ and *Glb1*^{W274L} Mice

One potential pitfall of CRISPR-Cas9 genome editing is off-target cutting by the Cas9 nuclease. To predict potential off-target sites of Cas9 DNA cleavage, the CCTOP algorithm [263] was used. Sites of interest were determined by sgRNA sequence homology near a potential protospacer adjacent motif (PAM) sequence. Ten loci were sequenced in all three founder mice, 5 with an NGG PAM sequence and 5 containing a NAG PAM sequence (Table 2). Sanger sequencing of these sites showed that the potential off-target sites were unedited.

Genotyping *Glb1*^{W274L} and β-gal$^{-/-}$ Mice

Sequence analysis of *Glb1*^{W274L} and β-gal$^{-/-}$ mice showed that each mutation in exon 8 of *Glb1* introduced novel restriction enzyme sites that could be utilized for genotyping via restriction fragment length polymorphism (RFLP) analysis. In *Glb1*^{W274L} mice, a novel *Hae*III restriction site is introduced. PCR amplification results in 448 bp band in both mutant *Glb1*$^{W274L/W274L}$ and control animals. Following treatment with *Hae*III, mutant *Glb1*$^{W274L/W274L}$ mice have DNA bands at 86, 160, and 202 bp, whereas wildtype mice have bands at 160 and 288 bp (Figure 6A). While β-gal$^{-/-}$ mice are missing 20 bp, which is detectible via sensitive PCR amplification and gel electrophoresis, the presence of a novel

*Xba*I site allows for a more definitive confirmation of the mutation. Following treatment of the PCR amplified product with *Xba*I, mutant β-gal$^{-/-}$ mice have DNA bands present at 186 and 242 bp, and wildtype mice have a single band at 448 bp (Figure 6B). Heterozygous mice display bands present in both homozygous mutant and wildtype mice.

Discussion

In the present study, CRISPR-Cas9 genome editing was utilized to successfully introduce a 2 bp mutation into the *Glb1* gene, in addition to creating a 20 bp deletion in the same gene of another mouse. The results of these experiments demonstrate the power, precision, and convenience of the CRISPR-Cas9 genome editing system. By utilizing this tool, it was possible to knock-in a desired two base pair mutation into the *Glb1* locus of one mouse, and also generate another containing a 20 bp deletion, in a single step. This allowed for the development of two mouse models for the cost of generating a single model. Additionally, by using CRISPR-Cas9, the time and expenditures were significantly reduced compared to traditional gene editing techniques like ES cell manipulation.

The development of novel gene targeting strategies, including ZFNs, TALENs, and CRISPR-Cas9, has opened the door for investigators to manipulate the genome of many organisms. These methods utilize the ability of nuclease enzymes to generate a targeted double-stranded break in DNA, inducing the cell's DNA repair mechanisms that include non-homologous end

joining and homology directed repair, allowing for targeted gene editing. In the last few years, CRISPR-Cas9 has pulled ahead of the other technologies due to its simplicity and ease of use. This is shown by the numerous publications utilizing this technology, not only to generate mouse models, but to study diseases such as cancer [264, 265]. However, to date, this methodology has not been utilized to generate a mouse model of lysosomal diseases.

Similar to other novel technologies, this system has its limitations. One of these is the off-target effects. The main requirement for Cas9 cleavage is the presence of the protospacer adjacent motif (PAM), which is typically NGG [163, 266, 267]. To effectively guide the Cas9 protein to the region to be cleaved, a 20-nucleotide guide RNA sequence that is complementary to the target region is necessary. Initially, this was thought to be specific enough, however, it has been shown that DNA with three to five nucleotides that are mismatched to the sgRNA are still capable of being cleaved by Cas9 [268-271]. One way this was minimized was by utilizing a shorter (17 nt) sgRNA, which has been shown to increase specificity [258]. Sequencing of 10 potential off-target sites with 2 or fewer mismatches showed that founders were not edited.

Another limitation of this system is the possibilities of mosaic founder mice caused by DNA cleavage after the first cell division [261, 272]. To limit the possibility of this, Cas9 protein was injected into zygotes instead of alternative methods including a plasmid or mRNA encoding Cas9, bypassing the need for transcription or translation events. By minimizing the time necessary to have an active protein and with Cas9 having a short half-life, the number of potential DNA

cleavage events is significantly reduced [273, 274]. Sequencing of N1 offspring of each founder mouse confirmed that this was not an issue.

In summary, CRISPR-Cas9 is an effective technology that can be utilized to generate mouse models via targeted DNA breaks. Here, we describe the first instance of creating a mouse model of lysosomal diseases using CRISPR-Cas9 genome editing. The resulting mutations created two potential mouse models of β-galactosidase deficiencies by introducing a 2 bp mutation in one mouse line, and creating a 20 bp deletion in another. In the following chapters, the characterization of these mice will be discussed.

Primer	Length	Sequence	Application
Glb1-SqF1	25	5’-GAAATGTCACTATTGGTGGACACTC-3’	Sequencing
Glb1-SqR1	26	5’-GGTCCCACCTATAAACATGTACCTAC-3’	Sequencing
Glb1-ScF1	29	5’-GGTTGACTGTAGTTGTAGTATGTAAGATG-3’	PCR
Glb1-ScR1	19	5’-ACCAATGGATGTGAAACGG-3’	PCR

Table 1. Primers used for sequencing and PCR amplification of targeted region of *Glb1*.

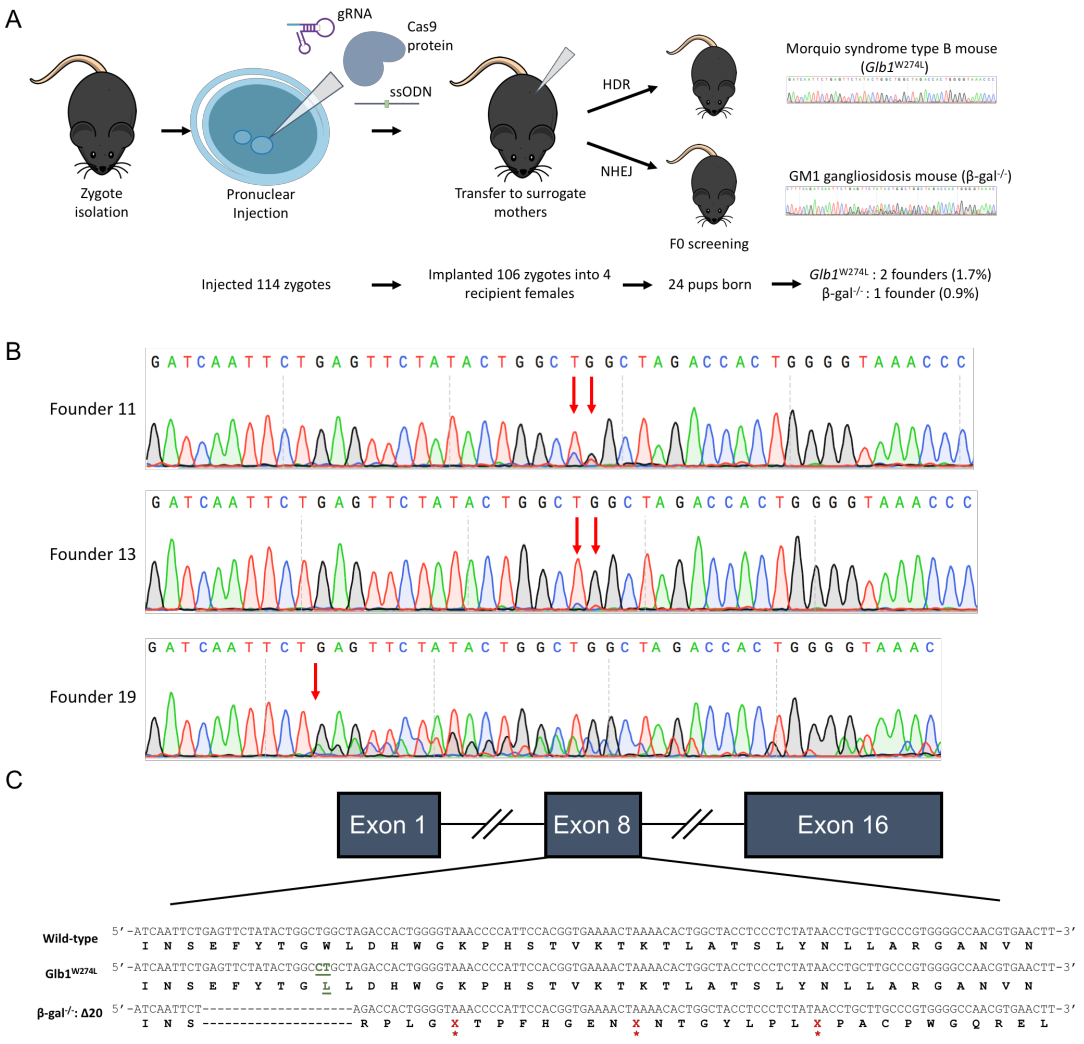

Figure 4. Introducing mutations into the β-galactosidase encoding gene, *Glb1* utilizing CRISPR-Cas9 genome editing. (A) Experimental schematic to introduce two mutations into the *Glb1* gene in a single experiment using CRISPR-Cas9 genome editing. (B) Sequencing of founder mice showed three mice (11, 13, and 19) contained mutations at the target site in *Glb1*. Red arrows indicate location of mutation in each line. (C) Founder animal mutations in exon 8 of β-galactosidase encoding gene *Glb1*. Two mice had 2 bp mutation resulting in tryptophan to leucine substitution commonly found in Morquio syndrome type B ($Glb1^{W274L}$, green underlined sequence). Another founder contained a 20 bp deletion (β-gal-/- Δ20; red asterisks denote stop codons introduced by the deletion).

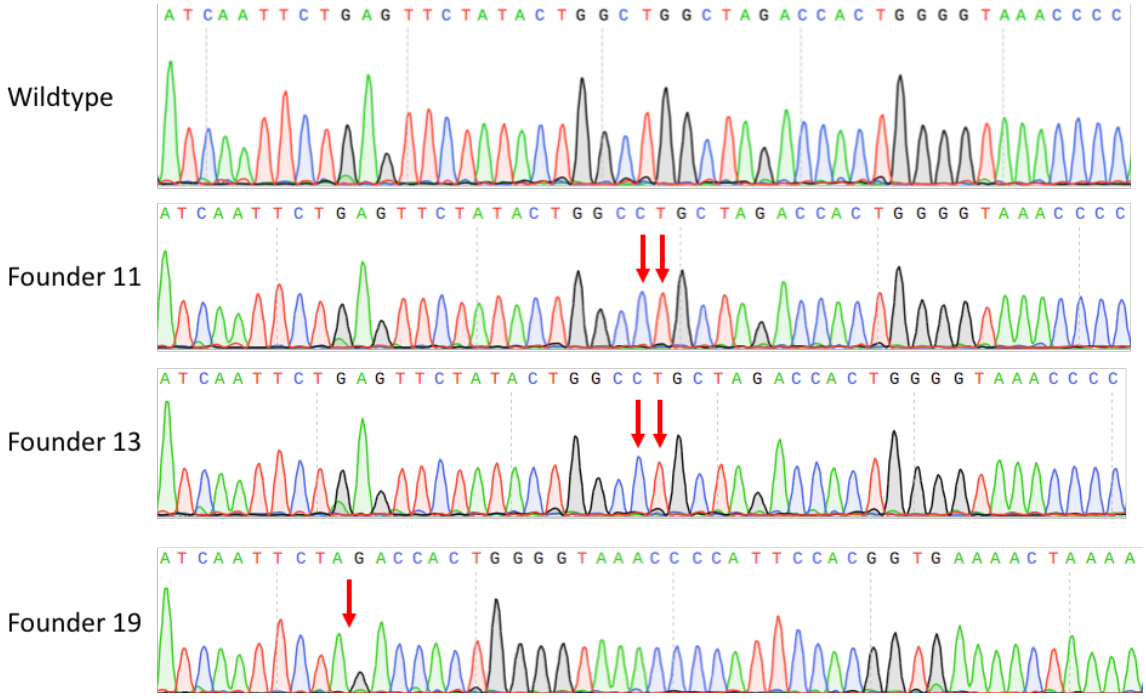

Figure 5. Confirmation of homozygosity in offspring derived from founder mice. Amplification and sequencing at the Cas9 targeted site in *Glb1* in homozygous offspring derived from founder mice confirmed the presence of the *Glb1*^{W274L} and β-gal$^{-/-}$ mutations. Red arrows indicate site of mutation.

Site	Gene Name	Chromosome	Sequence	PAM	MM	Off-target cleavage?
Target	Glb1	9	[CTGAGTTCTATACTGGC]	TGG	-	-
OT1	intergenic	10	[TTGAGTTCTGTACTGGC]	TGG	2	No
OT2	Nek10 (intron)	14	[CTTAGTTCTGTACTGGC]	TGG	2	No
OT3	Ccne1	7	[CTGACTTCTTTACTGGC]	AGG	2	No
OT4	Slc44a1 (intron)	4	[CTGAGTTACATACTGGC]	TGG	2	No
OT5	Zcwpw2 (intron)	9	[CTGAGTTTCATACTGGC]	GGG	2	No
OT6	Pias2 (intron)	18	[CTGTGTTCTATACTGGC]	AAG	1	No
OT7	Rasgrp2	19	[GTGAGTTCTATCCTGGC]	TAG	2	No
OT8	Spata6	4	[CTGAGTTCTATACAGGC]	TAG	1	No
OT9	Serbp1	6	[CTGAGTCCTATACTTGC]	TAG	2	No
OT10	G630016G05Rik	2	[CTGGGTTCTATACTGCC]	AAG	2	No

Table 2. Ten potential off-target cleavage sites of Cas9 enzyme. Off-target sequencing sites determined by CCTop algorithm. 5 contained an NGG PAM sequence and 5 contained a NAG PAM sequence. OT, off-target; Chrom., chromosome; PAM, protospacer adjacent motif; MM, number of mismatches. Black underlined nucleotide signifies the base that is mismatched compared to the target sequence of the sgRNA.

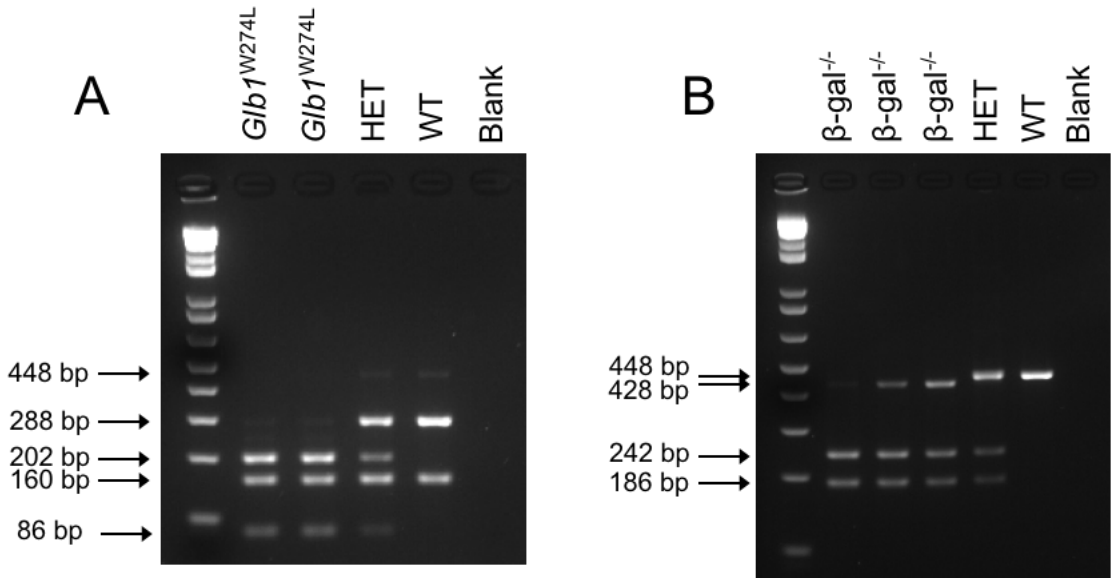

Figure 6. Genotyping β-gal$^{-/-}$ and *Glb1*^{W274L} mice. (A) PCR products from *Glb1*^{W274L} mice amplified with *Glb1*-ScF1 and *Glb1*-ScR1 after digestion with *Hae*III restriction digest. Three *Glb1*^{W274L} bands at 86, 160, 202 bp; two wildtype (WT) bands at 160 and 288 bp; and heterozygous (HET) had all four bands at 86, 160, 202, and 288 bp. Undigested DNA bands were at 448 bp. (B) PCR products from β-gal$^{-/-}$ mice amplified with *Glb1*-ScF1 and *Glb1*-ScR1 after digestion with *Xba*I restriction digest. Two β-gal$^{-/-}$ bands at 186 and 242 bp; one WT band at 448 bp; HET had all three bands. Undigested DNA bands were at 448 for WT and HET, and 428 and 448 in β-gal$^{-/-}$. Samples were run on a 3% agarose gel at 120V for 45 minutes.

CHAPTER III

Comprehensive Behavioral and Biochemical Outcomes of a Novel Murine Model of GM1-Gangliosidosis

Introduction

GM1-gangliosidosis is an autosomal recessive lysosomal disease caused by mutations in the *GLB1* gene, which encodes the lysosomal hydrolase β-galactosidase (β-gal; EC 3.2.1.23). β-gal is responsible for catabolizing the terminal β-galactose residue from many macromolecules, including GM1 ganglioside, its asialo derivative GA1 ganglioside, keratan sulfate, and oligonucleotides. When the mutations in *GLB1* cause deficiencies in the catalytic activity of β-gal, these macromolecules accumulate within the lysosome of cell. Specifically, GM1 and GA1 ganglioside are found to accumulate primarily in the CNS [38], while KS and oligosaccharides accumulate within the visceral tissue [255]. Clinically, GM1-gangliosidosis patients are categorized into one of three disease severities, 1) infantile, 2) late infantile/juvenile, 3) late onset/adult [3], depending upon symptoms and residual β-gal enzyme activity. The incidence of GM1-gangliosidosis is between 1:100,000 and 1:200,000 live births [42]. Those with the most severe form, infantile, have minimal or no residual β-gal enzyme activity [26, 275, 276]. Patients usually present with symptoms around 6 months of age, including severe psychomotor and neurocognitive regression, hypotonia, macular cherry-red spot, hepatosplenomegaly, skeletal dysplasia, coarse facial features, and typically succumb to the disease by 2 years of age [3]. Late infantile and juvenile GM1-gangliosidosis patients will typically have residual β-gal enzyme activity, typically between 1 and 5% of normal activity [26, 275]. Symptoms of the disease are typically similar, but milder, than those observed in infantile GM1-gangliosidosis, and onset around 1-3 years of age. However,

patients will typically not present with the macular cherry-red spot or hepatosplenomegaly [277]. Life expectancy of these patients is approximately 10 years. In adult onset GM1-gangliosidosis, patients have between 4-10% of normal β-gal enzyme activity [26, 275, 276, 278]. This range of enzyme activity yields a broad phenotypic variability, ranging from mild neurological symptoms such as dystonia, to more severe neurocognitive impairments, and onset, which can happen between 3 to 30 years of age. Besides palliative approaches, there are no current treatments for GM1-gangliosidosis.

To test therapies for this disease, an animal model was necessary. Here we describe the characterization of a mouse model that was developed and described in Chapter II using various biochemical and behavioral tests. The 20 bp mutation that was created abolished β-gal enzyme activity, resulting in a mouse model that recapitulates many aspects of human GM1-gangliosidosis.

Materials and Methods

Animal Care and Procedures

All animal care and experimental procedures were conducted under the approval of the Institute Animal Care and Use Committee (IACUC) of the University of Minnesota. All animals were housed in specific pathogen-free conditions and genotyped by PCR described in Chapter II. C57BL/6J (000664) animals were purchased from The Jackson Laboratory.

The humane endpoint for these studies was defined as the presence of limb paralysis, the inability to rear and feed normally, or the loss of ≥15% of peak

body weight. For biochemical analysis, animals were sacrificed by CO_2 asphyxiation and perfused transcardially with 20 mL of ice-cold PBS. Animals utilized for histological analysis were further perfused with 20 mL of 10% neutral buffered formalin (NBF). Tissues isolated for biochemical assays were flash frozen in liquid nitrogen.

Tissue Homogenization

Harvested organs for biochemical analysis were homogenized in 1 mL of T-PER™ Tissue Protein Extraction Reagent (Cat. #78510, Thermo Fisher Scientific) with Halt™ Protease Inhibitor Cocktail (Cat. #78430, Thermo Fischer) added to manufacturers recommendation using a Brinkmann Polytron™ PT 10/35.

Quantitative Reverse Transcript PCR (RT-qPCR)

Glb1 gene expression was determined utilizing RT-qPCR. Tissue samples (~30 mg) were harvested from the brain and liver of animals and placed into RNA*later*™ (Cat. #AM7021, Thermo Fisher) to stabilize RNA until isolation. Tissues were homogenized in RNase-free Eppendorf® Safe-Lock® snap-cap tubes containing stainless steel beads (Cat. #GREENE1-RNA, Next Advance, Troy, NY) using the Bullet Blender® (Next Advance) following manufacturers protocols, in Buffer RLT from the RNeasy Kit (Cat. #74104, Qiagen, Hilden, Germany). Total RNA isolation was completed following the RNeasy Kit manufacturers recommendations. Final RNA concentration was determined

using a NanoDrop 1000 (Thermo Fisher). 1 µg of RNA was used for reverse transcription using the QuanitiTect® Reverse Transcription kit (Cat. #205311, Qiagen) following the manufacturers protocol. Utilizing this cDNA, the qPCR reaction was set up in 96-well plate format: 10 µL TaqMan™ Fast Advanced Master Mix (2X, Cat. #4444556, Applied Biosystems™, Foster City, CA), 1 µL TaqMan® primer/probe mix (20X, Cat. #4331182, Thermo Fisher), 50 ng of cDNA template, and up to 20 µL with nuclease-free water. The reaction was then run using the BioRad CFX96 Touch™ Real-Time PCR Detection System (BioRad, Hercules, CA) under the following conditions: [1] 50ºC, 2 minutes, [2] 95ºC 20 seconds [3] 95ºC 3s, [4] 60ºC 30 seconds; [5] repeat steps 3-4 for 40 cycles. *Glb1* expression was calculated relative to the expression of *Gapdh* (Cat. #4331182, Thermo Fisher) using the $2^{-\Delta\Delta CT}$ algorithm [279].

β-galactosidase (β-gal) Enzyme Assay

β-gal enzyme activity was determined utilizing a fluorometric assay as previously described [280], with slight modification. Briefly, tissue samples were homogenized in 1 mL of T-PER™ Tissue Protein Extraction Reagent (Thermo Fisher Scientific, Waltham, MA) with added Halt™ Protease Inhibitor Cocktail (Thermo Fischer Scientific) added to manufacturers recommendation. To determine β-gal activity, supernatants of the tissue homogenates were diluted with a 0.2 M sodium acetate/0.1 M sodium chloride buffer (pH 4.3) and 40 µL of each was added in triplicate to a 96-well black round-bottom plate (Corning™, Corning, NY) on ice. 20 µL of a substrate solution containing 1.0 mM 4-

methylumbelliferyl-β-D-galactopyranoside (4-MUGal, Millipore-Sigma, St. Louis, MO) was added to each well, and the plate was incubated for 30 minutes at 37°C. To quench the reaction, 200 µL of 1M carbonate buffer (1 M sodium carbonate to pH 10.7 with 1 M sodium bicarbonate) was added. In the presence of β-gal enzyme, the non-fluorescent 4-MUGal is cleaved and releases a fluorescent 4-methylumbelliferone (4-MU) molecule. This fluorescence was measured in a Synergy MX Plate Reader with Gen5 plate reader program (BioTek Instruments, Winooski, VT) with excitation at 360 nm and emission read at 460 nm (80% sensitivity). 4-MU (Sigma-Millipore) is used to generate a standard curve. β-gal enzyme activity is expressed in nmol of 4-MU released per hour, per milligram of protein (nmol/hr/mg), which is determined using a Pierce™ BCA Protein Assay Kit (Thermo Fisher Scientific).

Histopathological Analysis

Following perfusion and fixation with 10% neutral buffered formalin (NBF), tissues were processed into paraffin wax using standard histology techniques, sectioned at a thickness of 4 µm, stained with hematoxylin and eosin (H&E), and evaluated using light microscopy by two A.C.V.P. board-certified pathologists. Additional evaluation was performed on selected tissues stained with Luxol fast blue (LFB)/H&E combination stain, Periodic acid-Schiff (PAS), alcian blue, and toluidine blue using standard laboratory protocols. Major organs examined in β-gal$^{-/-}$ mice include the brain, liver, heart, intestines, and pancreas. All work was

done at the Masonic Cancer Center Comparative Pathology Shared Resource laboratory at the University of Minnesota (St. Paul, MN).

Ganglioside Isolation and Quantification

GM1, GA1, GM2, and GM3 ganglioside accumulation in β-gal$^{-/-}$ tissue was quantified with the following ratio of tissue/volume CHAPS (3-[(3-cholamidopropyl) dimethylammonio]-1-propanesulfonate): cerebellum (1g wet tissue/10 mL CHAPS), cerebral cortex (1g wet tissue/6 mL CHAPS), hippocampus (1 g wet tissue/ 10 mL CHAPS) were homogenized in 2% CHAPS. Protein precipitation with 200 µL of methanol was performed to extract gangliosides GM1, GA1, GM2, and GM3 from 50 µL of homogenate in the presence of internal standards. For GM1, N-CD_3-Stearoyl-GM_1 (Cat. #2050, Matreya LLC Lipids and Biochemicals, State College, PA) was used; for GA1, standard was developed by conversion of N-CD_3-Stearoyl-GM_1 to N-CD_3-Stearoyl-GA_1 using methods described in [281]; for GM2, N-CD_3-Stearoyl-GM_2 (Cat #. 2051) was used; and for GM3, N-CD_3-Stearoyl-GM_2 (Cat. # 2052) was used. The 10% study sample extracts from each tissue type were pooled to prepare a quality control (QC) sample for that tissue. QC samples were injected every 5 study samples to monitor the instrument performance. Samples reported have a QC coefficient of variance <15%.

Sample analysis was performed with a Shimadzu 20AD high performance liquid chromatography (HPLC) system coupled to a 6500QTRAP+ mass spectrometer (AB Sciex, Framingham, MA) operated in positive MRM mode.

Data processing was conducted with Analyst 1.6.3 (Applied Biosystems). Data were reported as the peak area ratios of the analytes in sample to the corresponding internal standards.

Mouse Behavioral Analysis

At 6 months of age, mice were subjected to multiple behavior tests to assess neuromotor and neurocognitive function. All behavioral analyses were conducted in the Mouse Behavior Core at the University of Minnesota.

Neuromotor Testing

Balance Beam

The balance beam protocol was adapted from [282, 283]. Trials were performed on a 1 meter long wooden beam, held 48 cm above the table by a platform on one end (start) and a dark enclosure “safe box” on the other (stop). Before the first trial was conducted each day, the mouse was habituated for 15 seconds in the safe box. To begin the trial, the mouse was placed on the start platform under an aversive light in a dark room. The latency to cross the beam and enter the enclosure was measured, in addition to the number of hind foot slips that occur while crossing the beam. Each mouse was trained on a square beam (25 mm wide) for three days, with four trials per day. On day four, mice were subjected to two trials on beams of increasing difficulty: 25 mm square beam, followed by 27 mm round beam, and lastly the 15 mm wide square beam.

Again, latency to cross and number of hind foot slips were measured. Max trial duration was limited to 60 seconds.

Pole Test

The pole test was conducted as previously described with minor modifications [284]. The test began by placing a mouse head-upward on a vertical pole (10 cm in diameter; 55 cm tall) wrapped in athletic tape to assist with grip. Two measurements were taken: Latency to rotate body to face downward was measured, in addition to total time to descend the pole and place all 4 paws on the base of the apparatus inside of the cage, with a maximum test duration of 60 seconds. If a mouse failed to make the initial rotation to face downward, 60 second was recorded for both the turn and total time to descend. If the mouse fell from the pole during the testing time, it was placed back at the initial starting point while the time continued until 60 seconds. Mice were subjected to a single trial.

Accelerating Rotarod

Rotarod analysis was conducted on an accelerating rotarod (Ugo Basile, Comerio, Italy), adapted from a protocol previously described [285]. Briefly, mice were tested for three consecutive days, undergoing four trials per day, with a minimum inter-trial duration of 30 minutes. Testing was done on a rotarod programmed to accelerate from 5 to 50 rpm over a max trial duration of 300 seconds. 3-5 mice were placed on the divided rod simultaneously and the

apparatus' counter was started. The trial was considered complete when 1) the mouse fell off the rotarod and stopped the counter, 2) the mouse completes two consecutive rotations by holding on to the rod without walking, or 3) when 300 seconds elapsed.

Inverted Screen

Inverted screen testing [286] was completed utilizing a wire mesh apparatus, approximately 25 cm x 25 cm with 25 mm^2 square openings, placed approximately 30 cm over a cushioned surface. Testing began by placing the mouse on the wire mesh, which was then inverted until the animal was completely upside down. Latency to fall was measured for a max trial duration of 60 seconds. Mice were subjected to 3 trials, with a minimum of 15-minute resting period between trials.

Neurocognitive Testing

Barnes Maze

The Barnes maze [287] was conducted on an elevated circular platform, 36 inches in diameter, with 20 equally spaced holes around its perimeter. All of the holes on the platform were blocked except for one, which contained an opening to an escape box. The apparatus was placed directly under a bright light source that served as an aversive stimulus for the mouse to escape the platform. Visual cues were placed on each of the walls that act as navigational cues for the mouse. Mice were trained on the Barnes maze for 4 days, each mouse subjected

to 4 trials per day, for a max of 3 minutes per trial, with a minimum of 30 minutes between trials. Data was collected utilizing the ANY-Maze software (Stoelting Co, Wood Dale, IL).

Spontaneous Alternation T-Maze

The spontaneous alternation T-maze test [288] was utilized to test the spatial and working memory of the animals with a maze consisting of three arms. The starting arm of the maze contained a small compartment which was separated from the rest of the maze by a guillotine door. The two choice arms of the maze contained different visual cues on the end walls. Testing was done in a dark room with the maze lit by a portable canopy light over the choice arms. A mouse was placed in the start chamber for 5 seconds, after which the guillotine door is opened and the mouse was allowed to explore the maze and freely choose either choice arm. Once the animal's body completely entered the choice arm, a removable partition was placed behind the mouse, blocking the animal within the chosen arm for 15 seconds. This first trial is referred to as the free choice trial. The animal was then placed back into the start box for 5 seconds and the test was repeated, for a total of 11 trials (1 free choice, 10 choice trials). Once all trials were completed, the percent of correct alternations was calculated. A correct alternation was defined as successfully alternating arms from left to right, or right to left, on subsequent trials. On the following day, the experiment was repeated and the average percentage of correct alternations was calculated and reported.

Statistical Analysis

Data are reported as mean ± standard error. GraphPad Prism 7 (v. 7.0a, GraphPad Software, Inc, La Jolla, CA) was used to perform all statistical analyses. Survival probability was determined using Kaplan-Meier analysis, followed by the log-rank test (Mantel-Cox) to compare statistical significance of the survival curves for each group. One-way or two-way ANOVA, followed by Tukey's multiple comparisons test was conducted in all other experiments to compare wildtype, heterozygous, and mutant groups.

Results

Loss of *Glb1* expression in β-gal$^{-/-}$ mice

The deletion of 20 bp in *Glb1* results in the introduction of three premature stop codons within exon 8 of the gene (Figure 4C). To determine whether these mutations result in nonsense mediated decay of the mRNA and subsequent loss of *Glb1* expression, quantitative reverse transcription PCR (RT-qPCR) was used, targeting the sequence spanning exons 6 and 7, upstream of the 20 bp mutation. In the brain, relative *Glb1* expression in β-gal$^{-/-}$ mice (0.07-fold) was approximately 7.0% of wildtype levels (1.0-fold), and 11.5% of heterozygous levels (0.61-fold) (Figure 7A). In the liver, relative *Glb1* expression (0.03-fold) in β-gal$^{-/-}$ mice was 3.1% of wildtype levels (1.0-fold) and 4.9% of heterozygous levels (0.70-fold) (Figure 7B). These results show that *Glb1* expression is negligible in β-gal$^{-/-}$ mice.

Loss of β-gal enzyme activity in β-gal$^{-/-}$ mice

The deletion of the catalytic nucleophile (*Glb1*^{E269} [23]) and lack of *Glb1* transcripts in β-gal$^{-/-}$ mice results in loss of β-gal enzyme activity. In the brain of β-gal$^{-/-}$ mice, β-gal activity was 1.9±0.2 nmol/h/mg protein, compared to 95±10.1 nmol/h/mg in heterozygous mice and 195.8±30.2 nmol/h/mg in wildtype mice (Figure 8A). Similarly, β-gal activity in the heart of β-gal$^{-/-}$ mice was abolished, with 0.6±0.5 nmol/h/mg, where heterozygous mice had 20.9±0.9 nmol/h/mg and wildtype mice had 47.1±7.0 nmol/h/mg (Figure 8B). In the liver, β-gal activity in β-gal$^{-/-}$ mice was 0.6±0.3 nmol/h/mg, where β-gal activity in heterozygous mice was 88.7 nmol/h/mg and wildtype was 190.3±23.5 nmol/h/mg (Figure 8C). Lastly, in the spleen, β-gal activity in β-gal$^{-/-}$ mice was 3.3±1.0 nmol/h/mg, whereas activity in heterozygous mice was 264.1±18.6 nmol/h/mg and wildtype mice was 460.9±27.7 nmol/h/mg (Figure 8D). Overall, β-gal enzyme activity is abolished in β-gal$^{-/-}$ mice.

Significant weight loss and decreased lifespan of β-gal$^{-/-}$ mice

At birth, β-gal$^{-/-}$ mice were indistinguishable from their littermates. At 4 months of age, β-gal$^{-/-}$ mice begin showing gait disturbance in their hind limbs, followed by body tremors and ataxia around 5 months. For the first year of life, heterozygous and wildtype female mice continued to gain weight, however, the weight of female β-gal$^{-/-}$ mice peaked at 25.3±0.4 grams at approximately 33 weeks of age (~7.5 months), after which their weight began to decline rapidly

(Figure 9A). Surprisingly, male β-gal$^{-/-}$ mice became significantly heavier than their littermates at 25 weeks of age (45.3±1.2g compared to wildtype, 40.0±1.2g and heterozygous 38.0±0.9g) (Figure 9B). Following this peak weight, male β-gal$^{-/-}$ mice began to lose weight rapidly, similar to female β-gal$^{-/-}$ mice. This decline in weight coincided with the overall decline in health of the β-gal$^{-/-}$ mice.

Similar to the previously published mouse models of GM1-gangliosidosis, at 6 months of age, β-gal$^{-/-}$ mice had a severe neurological disease phenotype. 6-month-old female (Movie 1) and male (Movie 2) β-gal$^{-/-}$ mice had an ataxic gait, with a stiff, curved tail, as if it was being used for balance. At 9 months of age, both female (Movie 3) and male (Movie 4) β-gal$^{-/-}$ mice displayed severe neurological deterioration, manifesting as physical instability and labored ambulation. As the disease progressed, neurological symptoms of β-gal$^{-/-}$ mice significantly worsened, leading to a loss of function in the forelimbs and hindlimbs of β-gal$^{-/-}$ mice, leading to total paralysis.

In agreement with previous mouse models of GM1-gangliosidosis [151, 152], β-gal$^{-/-}$ mice had a significantly shortened lifespan compared to wildtype and heterozygous animals, which have an average lifespan over 2 years. In females, the lifespan of β-gal$^{-/-}$ mice was 264.4±34.9 days (mean±SD) (Figure 10A). Likewise, the lifespan of male β-gal$^{-/-}$ mice was 265.2±21.2 days (Figure 10B).

While β-gal$^{-/-}$ mice are fertile and produce normal litters, at approximately 5 months of age, they cease breeding. Whether this is due to the onset of these neurological symptoms or another physiological reason is unknown.

Accumulation of gangliosides in the brain of β-gal$^{-/-}$ mice

To determine whether the loss of *Glb1* expression and subsequent deficiency in β-gal enzyme activity resulted in ganglioside accumulation, high-performance liquid chromatography, tandem mass spectrometry (HPLC-MS/MS) was implemented to quantify GM1 and GA1 gangliosides in microdissected β-gal$^{-/-}$ brains. As the 18-carbon atom sphingosine chain length is the most abundant GM1 and GA1 ganglioside [289], this was chosen as the biomarker for quantification. In the cerebral cortex, GM1 ganglioside was increased 1.6-fold in β-gal$^{-/-}$ mice compared to control animals, where GA1 ganglioside content was increased 2.5-fold (Figure 11A). In the cerebellum, GM1 ganglioside levels were increased 4.0-fold compared to control mice and GA1 ganglioside was increased 7.3-fold (Figure 11B). Further, in the hippocampus, GM1 ganglioside was 2.2-fold higher than controls and GA1 ganglioside was increased 3.6-fold (Figure 11C).

In addition to quantifying the primary substrate of β-gal, the secondary accumulation of GM2 and GM3 gangliosides was also measured. In all three brain regions analyzed, secondary ganglioside accumulation was significantly increased, except GM3 ganglioside in the cerebellum. In the cerebral cortex, GM2 ganglioside accumulation was 2.6-fold higher than control mice, while there was a 4.5-fold increase of GM3 ganglioside (Figure 11A). In the cerebellum, GM2 ganglioside was 1.5-fold higher than controls and GM3 ganglioside was increased 1.8-fold (Figure 11B). Lastly, in the hippocampus, GM2 ganglioside was increased 2.6-fold and GM3 ganglioside was increased 2.4-fold (Figure 11C).

Severe CNS and visceral cellular vacuolation in β-gal$^{-/-}$ mice

Histopathological examination of the CNS in β-gal$^{-/-}$ mice revealed a striking and marked enlargement of neurons with pale, finely granular to foamy cytoplasm that occasionally displaced the nucleus to the periphery (Figure 12). Neuronal cytoplasmic vacuolation was variable and was observed within the cerebral cortex, thalamus, Cornu Ammonis (mainly CA3) of the hippocampus, brainstem nuclei, cerebellum (Purkinje cells and deep cerebellar nuclei), and spinal cord (ventral and dorsal spinal horns). These observations are consistent with the CNS findings for β-gal$^{-/-}$ mice described previously [151, 152] and are characteristic findings in the brain of patients with GM1-gangliosidosis. This CNS pathology was absent in control mice. In addition to the CNS pathology, we also observed cellular enlargement with cytoplasmic vacuolation involving hepatocytes of the liver, acinar cells of the pancreas, and enterocytes of the intestine (Figure 13).

Additionally, although negative with PAS, toluidine blue, and alcian blue stains, histological analysis utilizing LFB staining on CNS tissue confirmed the presence of complex lipids within the vacuolated cells, which has been described in several animal models of gangliosidoses [136, 290]. These inclusions were observed in the CA3, cerebellar nuclei, cerebellar cortex, pons, and cortex of β-gal$^{-/-}$ mice (Figure 14).

β-gal$^{-/-}$ mice have significant neuromotor dysfunction

To test whether the lack of β-gal activity and subsequent accumulation of gangliosides in the brain of β-gal$^{-/-}$ mice led to neurological deficiencies, female and male mice were subjected to many behavioral analyses at 6 months of age. First, neuromotor function was tested using the balance beam. In this test, β-gal$^{-/-}$ mice showed a severe motor coordination deficit. When measuring latency to cross the balance beam, from Day 1 of testing, the latency to cross the beam of β-gal$^{-/-}$ was significantly longer (female, 28.3±2.2 seconds; male, 44.5±3.1s) compared to heterozygous (female, 12.5±1.5s; male, 17.7±1.6s) and wildtype (female, 14.8±1.2s; male, 13.0±1.4s) (Figure 15A and B). While the latency to cross the beam shortened on subsequent days, β-gal$^{-/-}$ mice took significantly longer to cross the beam compared to control mice. On Day 4, the latency to cross of β-gal$^{-/-}$ mice (female, 18.5±2.3s; male, 20.9±2.8s) was still significantly longer than heterozygous (female, 8.2±1.4s; male, 7.7±0.9s) and wildtype mice (female, 7.1±0.9s; male, 6.0±0.8s).

In addition to the increased latency to cross the beam, the number of hind foot slips (fs) while crossing the beam was significantly higher in β-gal$^{-/-}$ mice. On Day 1, the average number of foots lips of female β-gal$^{-/-}$ mice was 7.6±1.3fs, where heterozygous (0.8±0.2 fs) and wildtype (0.7±0.2 fs) mice averaged less than one foot slip per trial (Figure 15C). Male β-gal$^{-/-}$ mice (15.3±2.6 fs) also had significantly more foot slips compared to heterozygous (1.3±0.3 fs) and wildtype (1.6±0.3 fs) mice (Figure 15D). On each of the 4 trial days, β-gal$^{-/-}$ mice continued to have significantly more foot slips compared to control animals.

On Day 4, mice were tested on beams of increasing difficulty, and again latency to cross and number of hind foot slips were measured. As the difficulty of the beams increased, the latency to cross in both female (25mm square, 18.5±2.3s; 27mm round, 23.5±4.5s; 15mm square, 27.7±4.7s) and male β-gal$^{-/-}$ mice increased (25mm square, 20.9±2.8s; 27mm round, 29.8±6.1s; 15mm square, 30.2±5.7s), in contrast to heterozygous (25mm square, 8.2±1.4s; 27mm round, 6.9±0.8s; 15mm square, 8.5±1.5s) and wildtype (25mm square, 7.1±0.9s; 27mm round, 7.0±0.9s; 15mm square, 8.5±1.3s) mice, which had consistent latencies to cross (Figure 15E). This trend was also observed in male mice. The latency to cross the beam for heterozygous (25mm square, 7.7±0.9s; 27mm round, 8.4±1.1s; 15mm square, 8.3±1.3s) and wildtype (25mm square, 6.0±0.8s; 27mm round, 7.0±1.1s; 15mm square, 5.7±0.6s) mice were consistent between the beams, however, the latency to cross of β-gal$^{-/-}$ mice (25mm square, 20.9±2.8s; 27mm round, 29.8±6.1s; 15mm square, 30.2±5.7s) increased as the beam difficulty increased (Figure 15F).

Similarly, as the beam difficulty increased, the number of hind foot slips in β-gal$^{-/-}$ mice also increased. β-gal$^{-/-}$ females foot slips increased from 3.3±1.1 fs on the 25mm square beam, to 13.8±0.7 fs on the 27mm round beam, to 17.5±1.7 fs on the 15mm square beam (Figure 15G). Similarly, in male β-gal$^{-/-}$ mice, hind foot slips increased (25mm square, 9.2±1.8 fs; 27mm round, 12.7±0.5 fs; 15mm square, 12.7±2.1 fs) (Figure 15H). Overall, the results of the balance beam test showed that β-gal$^{-/-}$ mice have a severe motor coordination deficit.

The second test of neuromotor function was the accelerating rotarod to test motor coordination and motor learning. Over the 3 days of trials, the latency to fall of female β-gal$^{-/-}$ mice (Day 1, 25.3±6.8s; Day 2, 31.8±6.7s; Day 3, 37.2±5.8s) was significantly lower than heterozygous (Day 1, 151.8±7.8s; Day 2, 214.6±7.9s; Day 3, 216.1±6.0s) and wildtype mice (Day 1, 150.6±11.6s; Day 2, 202.1±12.7s; Day 3, 201.6±14.6s) (Figure 16A). In all male mice, the overall latency to fall was shorter than female mice, but β-gal$^{-/-}$ mice had a significantly shortened latency to fall (Day 1, 15.1±1.8s; Day 2, 29.0±8.8s; Day 3, 27.1±9.4s) compared to heterozygous (Day 1, 115.1±16.1s; Day 2, 160.8±10.9s; Day 3, 182.1±12.1s) and wildtype mice (Day 1, 101.9±15.2s; Day 2, 158.8±15.1s; Day 3, 180.8±18.3s) (Figure 16B). These results further showed that β-gal$^{-/-}$ mice have impaired motor coordination and motor learning.

Thirdly, the pole test was utilized to assess bradykinesia, typically observed in other CNS diseases such as Parkinson's disease [291]. Muscle weakness and tremors, which are seen in GM1-gangliosidosis patients, can contribute to bradykinesia. In both β-gal$^{-/-}$ females (50.6±5.8s) and males (52.5±5.5s), the inversion time was significantly longer than heterozygous (female, 9.5±3.9s; male, 10.7±2.2s) and wildtype (female, 10.32±2.5; male, 8.0±2.9s) mice (Figure 17A and B). Similar results were seen in the total time to descend. Female (55.9±4.1s) and male (56.4±3.6s) β-gal$^{-/-}$ took significantly longer to descend the pole in comparison to heterozygous (female, 20.9±4.0s; male, 25.9±2.9s) and wildtype mice (female, 20.7±2.7s; male, 19.0±3.0s) (Figure

17C and XD). If the mice could not complete the inversion task and descend the pole, a maximum time of 60 seconds was recorded. Overall, these results support the observation that β-gal$^{-/-}$ mice have impaired motor function.

The last test used to analyze neuromotor function was the inverted screen test to measure grip strength. The latency to fall of female β-gal$^{-/-}$ mice averaged 17.6±3.7s, where heterozygous and wildtype mice could remain on the inverted screen for 59.1±0.6s and 57.4±1.2s, respectively (Figure 18A). Male β-gal$^{-/-}$ mice showed a similar significant loss of grip strength, only being able to stay on the screen for 3.4±0.5s, compared to 53.4±2.9s in heterozygous mice, and 49.9±2.4s in wildtype mice (Figure 18B). In summation, the results of this test and the extensive behavior tests of motor function showed that β-gal$^{-/-}$ mice have severe neuromotor impairments.

Neurocognitive testing of β-gal$^{-/-}$ mice revealed severe impairments

To test neurocognitive function in β-gal$^{-/-}$ mice, spatial reference memory and learning was tested using the Barnes maze. Over the course of 4 days of testing, the latency to escape the platform of wildtype and heterozygous mice decreased significantly in females from 158.7±9.6 and 159.9±10.0 seconds on Day 1 to 42.4±5.4 and 35.1±5.0 seconds on Day 4 (Figure 19A). Similarly, in males, the latency to escape decreased from 176.9±2.4 seconds in wildtype and 180 seconds in heterozygous mice on Day 1 to 38.2±2.5 seconds and 42.0±10.8 seconds on Day 4 (Figure 19B). These results indicate a normal cognitive

function. In comparison, the latency to escape of female and male β-gal$^{-/-}$ mice decreased from 180 seconds for both groups to 177.3±1.8 seconds and 175.3±4.8 seconds, respectively. The latency to escape did not decrease, suggesting that β-gal$^{-/-}$ mice have a neurocognitive learning disability and impaired spatial reference memory.

Additionally, the spatial working memory of the β-gal$^{-/-}$ mice was tested using the spontaneous alternating T-maze. This test utilizes the normal tendencies of mice to explore a new environment. If an animal's cognition is impaired, mice will not alternate between arms, resulting in a random pattern of arm choice (≤50% successful alternation). In this test, female wildtype and heterozygous mice successfully alternated 72.9±2.4% and 75.0±1.9% of the trials, while β-gal$^{-/-}$ mice correctly alternated 47.9±5.9% of the time (Figure 20A). Similarly, male wildtype and heterozygous mice successfully alternated 74.3±2.8% and 68.8±1.8% of the trials, where β-gal$^{-/-}$ mice correctly alternated 42.0±8.5% of the trials (Figure 20B). These results suggest the decision of β-gal$^{-/-}$ mice was random, indicating a spatial working memory deficiency.

Discussion

Large animal models of GM1-gangliosidosis exist, including felines, canines, and sheep, are available, however the cost and time to use these models makes the mouse a more feasible option for use in developing and testing novel therapies for this debilitating disease. The data presented here

depict the characterization a novel murine model of β-galactosidase deficiency that recapitulates many characteristics of the human lysosomal disease GM1-gangliosidosis. Currently, there are 2 published murine models of this disease, however these models were generated by introducing a synthetic *neo* cassette to disrupt the *Glb1* gene. Here, we describe a mouse model that harbors a mutation that could potentially exist in the human population. Additionally, this is the first model of a lysosomal disease to be described that was generated utilizing CRISPR-Cas9 genome editing. In this mouse line, the removal of 20 bp in exon 8 results in a frameshift mutation introducing 3 premature stop codons in the reading frame of *Glb1*. Additionally, this mutation resulted in the deletion of a highly conserved region of DNA, including the catalytic nucleophile (*Glb1*^{Glu269}, *GLB1*^{Glu268} in humans) yielding an enzyme that is catalytically inactive. While there have been no patients with a mutation resulting in a loss of the catalytic nucleophile described, this mutation is predicted to result in both Morquio syndrome type B and GM1-gangliosidosis, as a catabolic reaction cannot occur [24].

Mice homozygous for this mutation (β-gal$^{-/-}$) have minimal *Glb1* expression and negligible enzyme activity towards a synthetic fluorogenic substrate. The lack of β-gal enzyme activity resulted in a severe cellular vacuolation phenotype in the central nervous system, in addition to visceral organs. This data was corroborated by GM1 ganglioside quantification using HPLC-MS/MS, which showed significant accumulation of GM1 ganglioside and its asialo derivative GA1 ganglioside in multiple regions of the mouse brain. An alternative pathway

of GM1 ganglioside catabolism exists apart from GM1 ganglioside to GA1 ganglioside conversion by neuraminidase. In the presence of ceramide deacylase, GM1 ganglioside can be converted to lyso-GM1, which has been shown to be elevated in patients with GM1-gangliosidosis [292]. It is believed that lyso-GM1 is also neuropathic, similar to other toxic lysosphingolipids like galactosylsphingosine and glucosylsphingosine in Krabbe and Gaucher diseases, respectively. Further, secondary accumulation of glycosphingolipids such as glucosylceramide, lactosylceramide, GM2, GM3, and GD1a gangliosides in GM1-gangliosidosis patients has been reported [293-295]. In the β-gal$^{-/-}$ mouse model reported here, a significant secondary accumulation of GM2 and GM3 gangliosides in the brain was observed. While not previously reported in the other murine models of GM1-gangliosidosis, this secondary accumulation of GM2 and GM3 ganglioside is not specific to GM1-gangliosidosis, but is found to be a common phenotype of many lysosomal diseases with a neurological involvement (reviewed in [296]). Specifically, accumulation of GM2 ganglioside has been implicated in ectopic dendritogenesis, which alters neuroplasticity and synaptic connectivity [297]. This could provide an explanation for the observations of severe motor and cognitive impairments of β-gal$^{-/-}$ mice in behavior testing. These deficiencies are further supported by where gangliosides are accumulating in the CNS of β-gal$^{-/-}$ mice. Specifically, the accumulation present within the Purkinje cells and deep cerebellar nuclei of the cerebellum could contribute to the neuromotor dysfunction observed. Additionally, there was vacuolation present and ganglioside accumulation in the CA3 region of the

hippocampus, a region of the brain that is attributed to the memory and learning and could explain impairments seen in the Barnes maze and T-maze, which had not been described in the previous models of GM1-gangliosidosis [298].

Another surprising finding in this study was the presence of a vacuolated phenotype in the somatic tissue of β-gal$^{-/-}$ mice, in addition to the CNS pathology. While primarily a neurological disease, human patients with infantile GM1-gangliosidosis do present with an enlarged liver and spleen. While this was not observed in β-gal$^{-/-}$ mice, the presence of cellular vacuolation in tissues like the liver and intestine supports the idea that therapies for this disease will require targeting both the CNS and the viscera.

In conclusion, the β-gal$^{-/-}$ mouse model characterized here recapitulates many aspects of the human disease GM1-gangliosidosis, including biochemical and cognitive abnormalities. Overall, this β-gal$^{-/-}$ mouse model will play an important role in the development of new therapies for patients suffering with GM1-gangliosidosis.

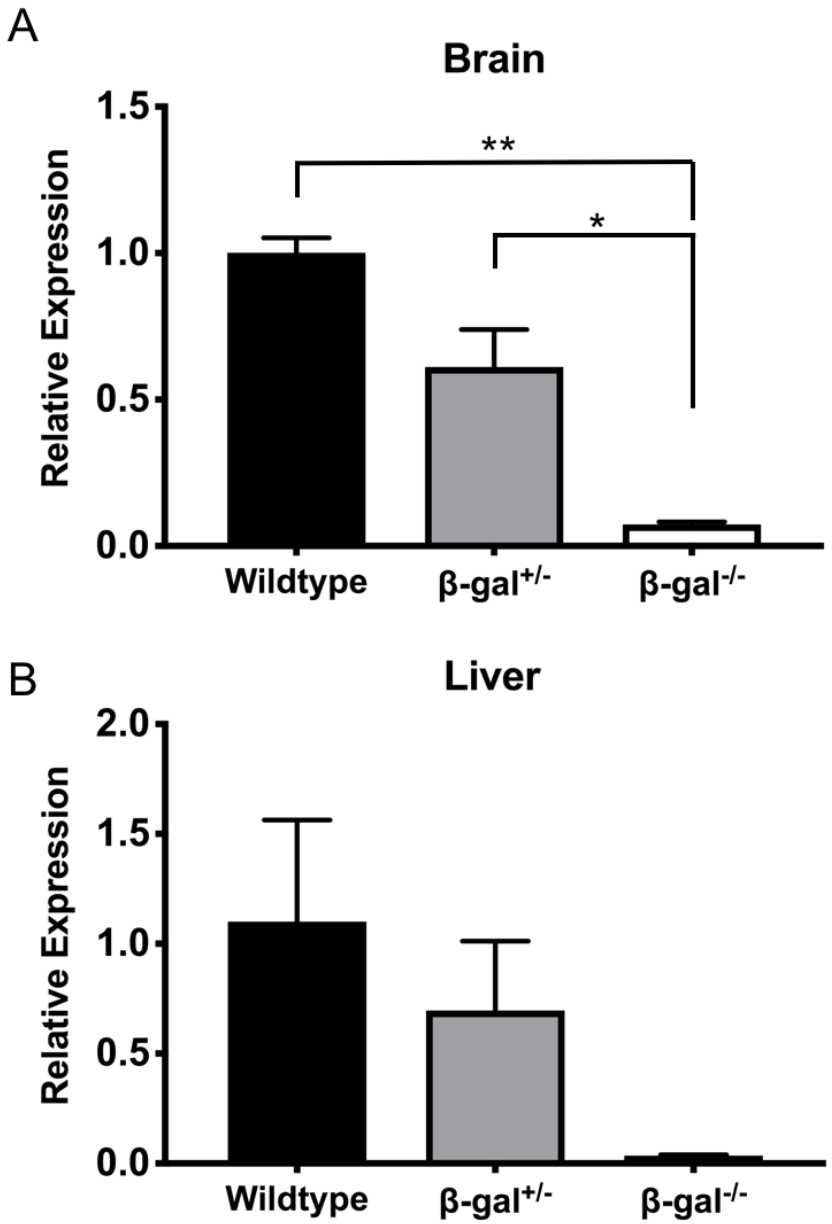

Figure 7. Loss of *Glb1* expression in β-gal$^{-/-}$ mice. Utilizing RT-qPCR to quantify *Glb1* gene expression in the (A) brain and (B) liver of β-gal$^{-/-}$ mice. Expression is relative to *Gapdh* expression. Data are mean ± SEM. *p≤0.05, **p≤0.01 when comparing mutant mice (β-gal$^{-/-}$) to wildtype and heterozygous mice.

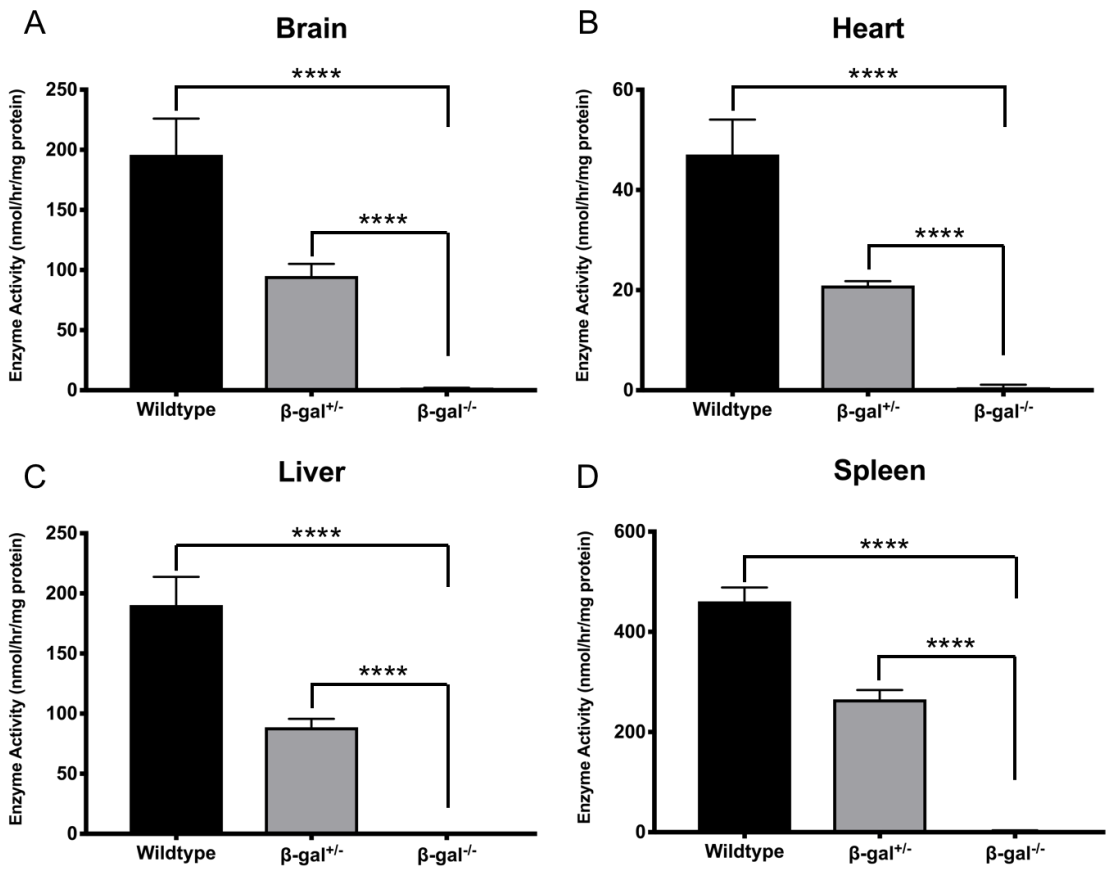

Figure 8. β-galactosidase enzyme activity is abolished in β-gal$^{-/-}$ mice. Enzyme activity determined using the artificial substrate β-D-galactopyranoside in β-gal$^{-/-}$ mouse (A) brain, (B) heart, (C) liver, and (D) spleen. Wildtype n=5, heterozygous (β-gal$^{+/-}$) n=9, mutant (β-gal$^{-/-}$) n=7. Data are mean ± SEM. ****p≤0.0001 when comparing mutant mice to wildtype and heterozygous.

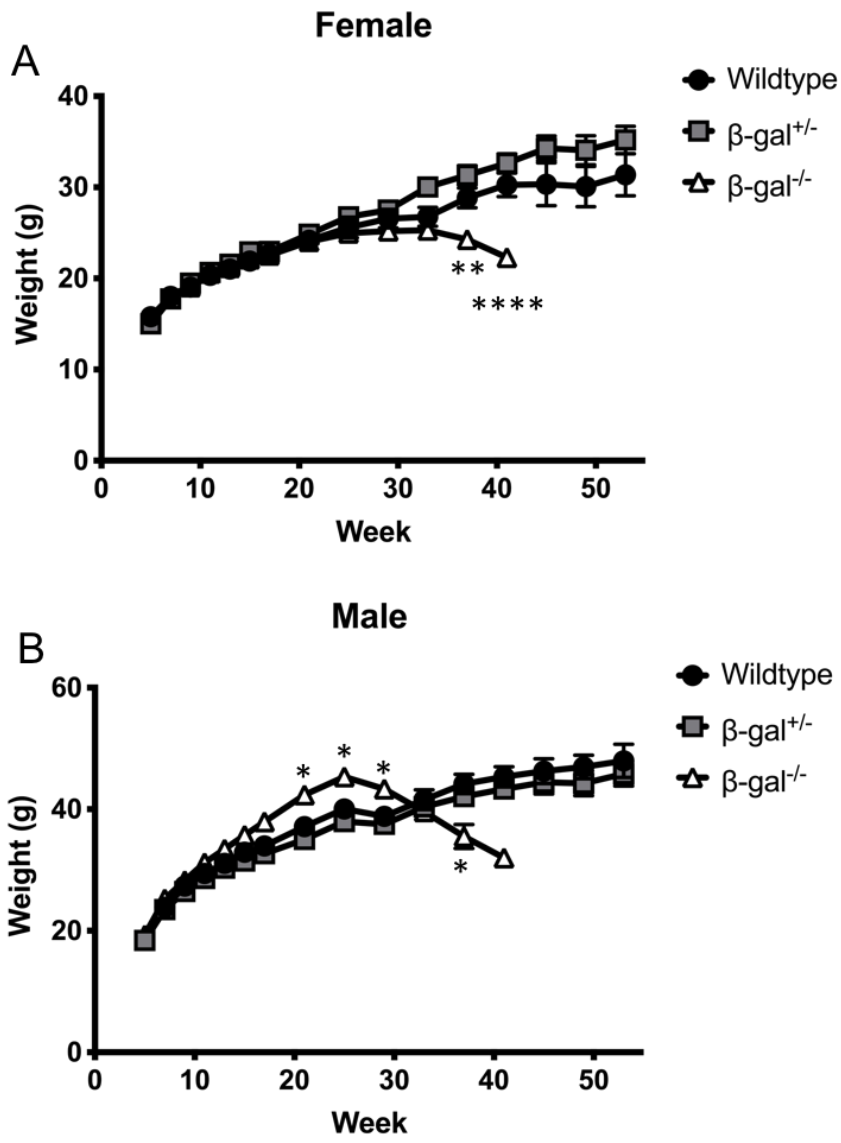

Figure 9. Significant weight loss in β-gal$^{-/-}$ mice. Weight of (A) female and (B) male β-gal$^{-/-}$ mice over one year (n>5 for each group, except β-gal$^{-/-}$ males at timepoint week 41, where n=1). Weight data are mean ± SEM. *p≤0.05, **p≤0.01, ****p≤0.0001.

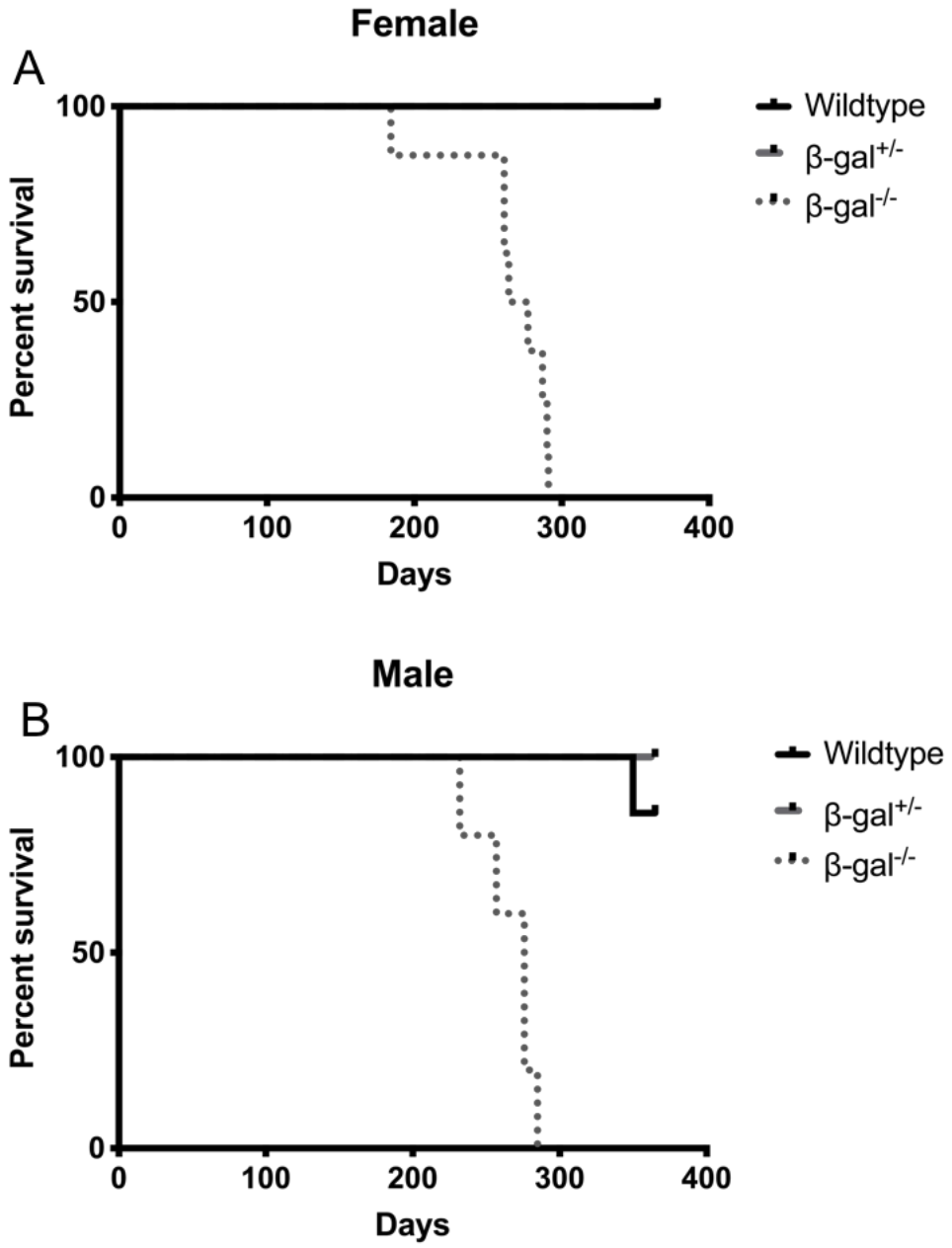

Figure 10. β-gal$^{-/-}$ mice have a significantly reduced lifespan. Kaplan-Meier survival curve of (A) female and (B) β-gal$^{-/-}$ mice (n=5-8 for each group). Survival of β-gal$^{-/-}$ mice significantly reduced ****p≤0.0001.

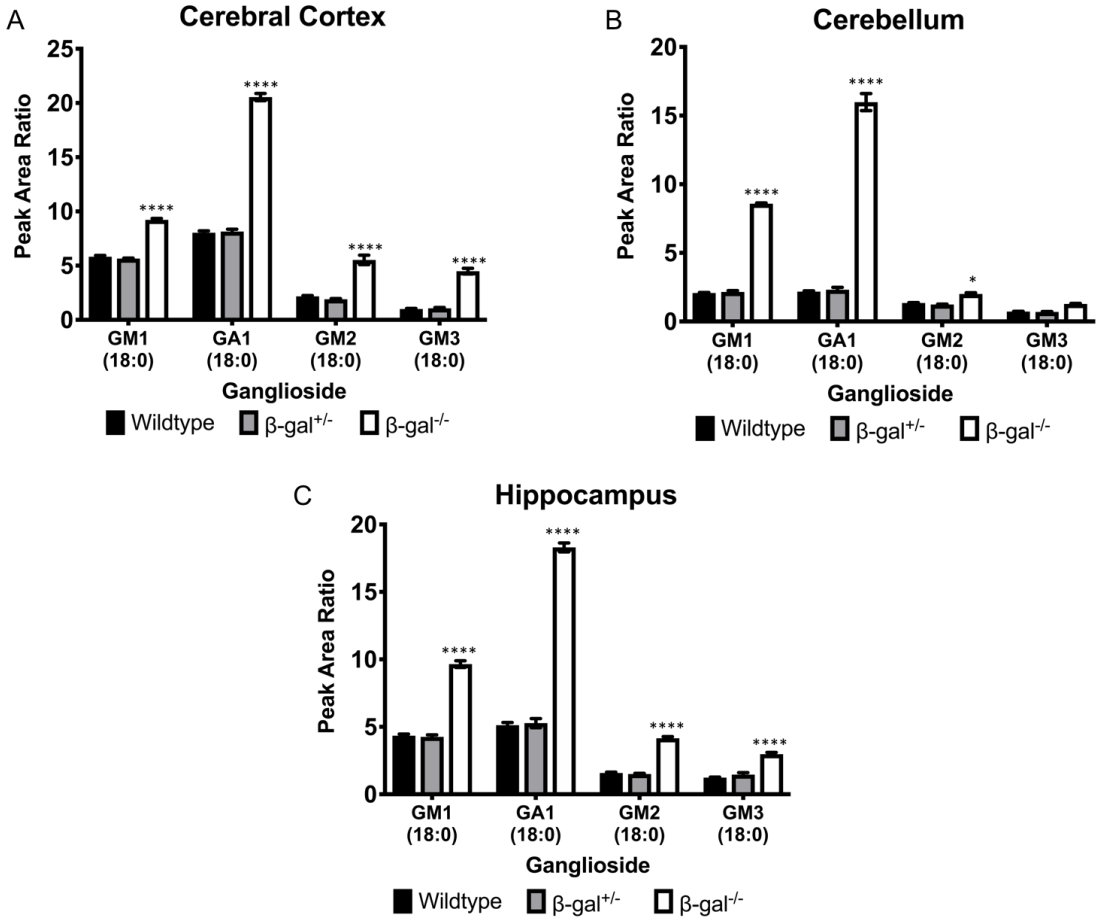

Figure 11. Primary and secondary accumulation of gangliosides in the brain of β-gal$^{-/-}$ mice. GM1, GA1, GM2, and GM3 ganglioside accumulation in the (A) cerebral cortex, (B), cerebellum, and (C) hippocampus of mice (n = 3 for each group) were measured using high performance liquid chromatography tandem-mass spectrometry. Data are reported as the peak area ratios of analytes in the sample to the corresponding internal standard. Data are mean ± SEM. *p≤0.05, ****p≤0.0001.

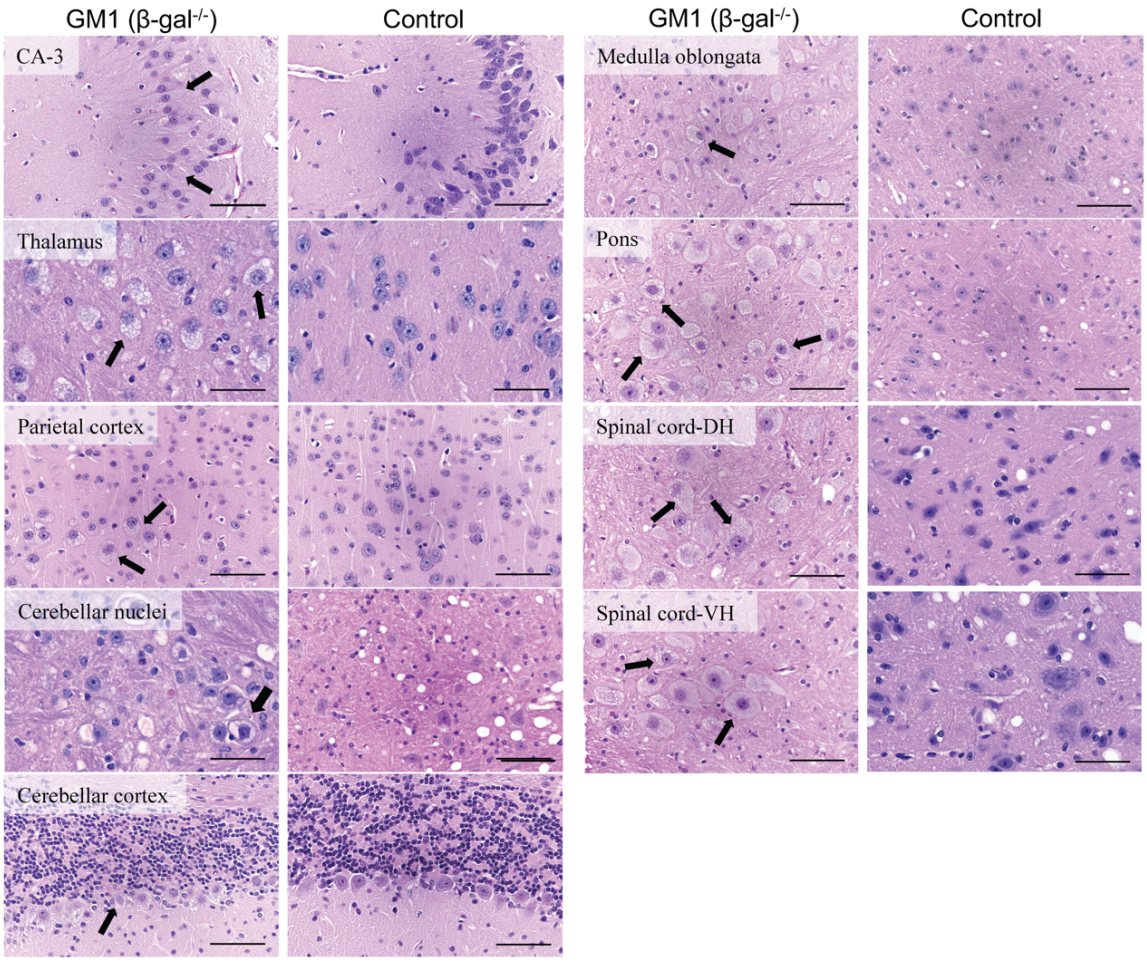

Figure 12. Widespread marked enlargement of neurons with cytoplasmic vacuolation (reflecting significant accumulation of storage material) in the central nervous system of β-gal$^{-/-}$ mice. Hematoxylin and eosin staining of brain and spinal cord of β-gal$^{-/-}$ and control mice. Brain and spinal cord (β-gal$^{-/-}$): objective x40, scale bar indicates 30 μm; spinal cord control: objective x60, scale bar indicates 20 μm. Black arrows indicate vacuolated cells.

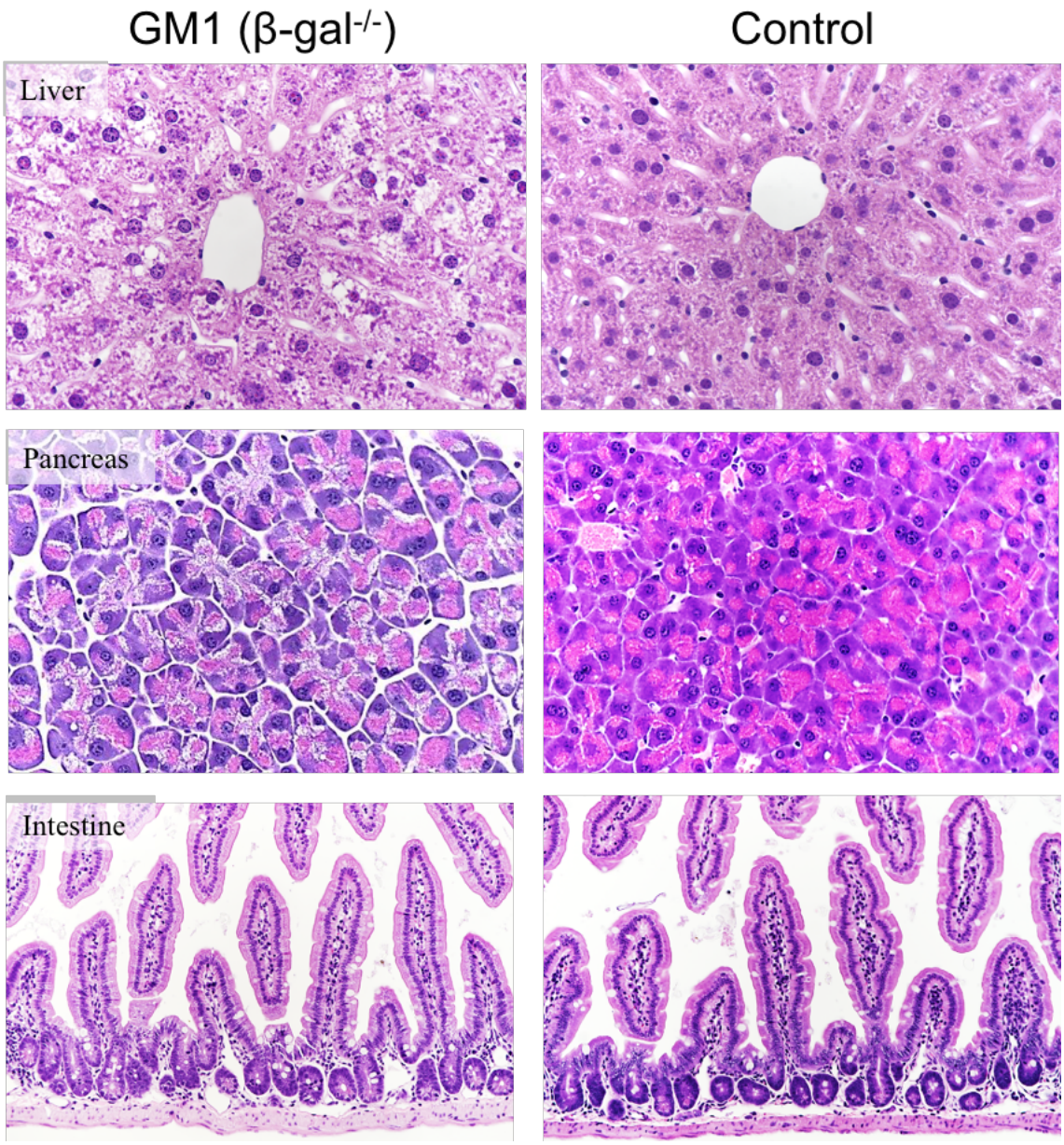

Figure 13. Severe vacuolation phenotype in visceral organs of β-gal$^{-/-}$ mice. Hematoxylin and eosin staining of liver, pancreas and intestine of β-gal$^{-/-}$ and control mice. Liver and pancreas: objective x40, scale bar indicates 30 μm; intestine: upper panels: objective x20, scale bar 60 μm, lower panels: objective x40, scale bar indicates 30 μm.

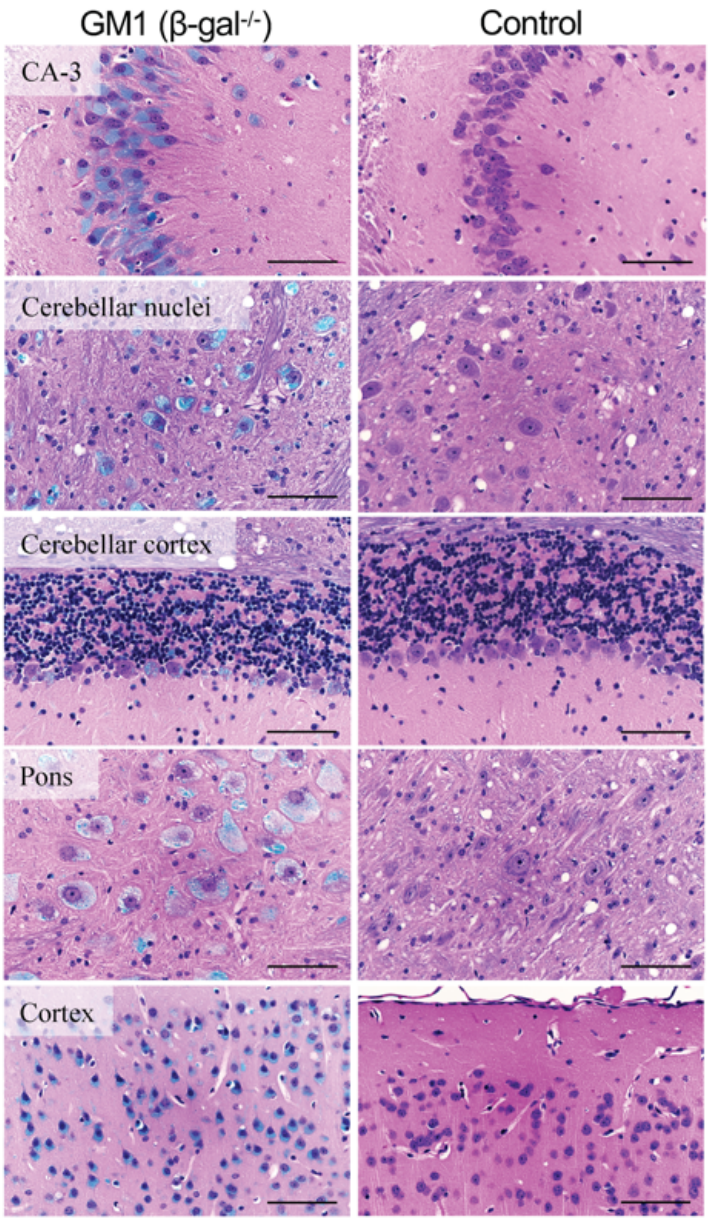

Figure 14. Luxol fast blue positive staining in the neurons of the brain. Histopathological images of Luxol fast blue-stained brain tissue from β-gal$^{-/-}$ mice compared with control mice. Neurons of β-gal$^{-/-}$ mice are enlarged/swollen, and contain abundant intracytoplasmic, granular, Luxol fast blue positive material, with occasional nuclear peripheralization. Objective x40, scale bar indicates 30 μm.

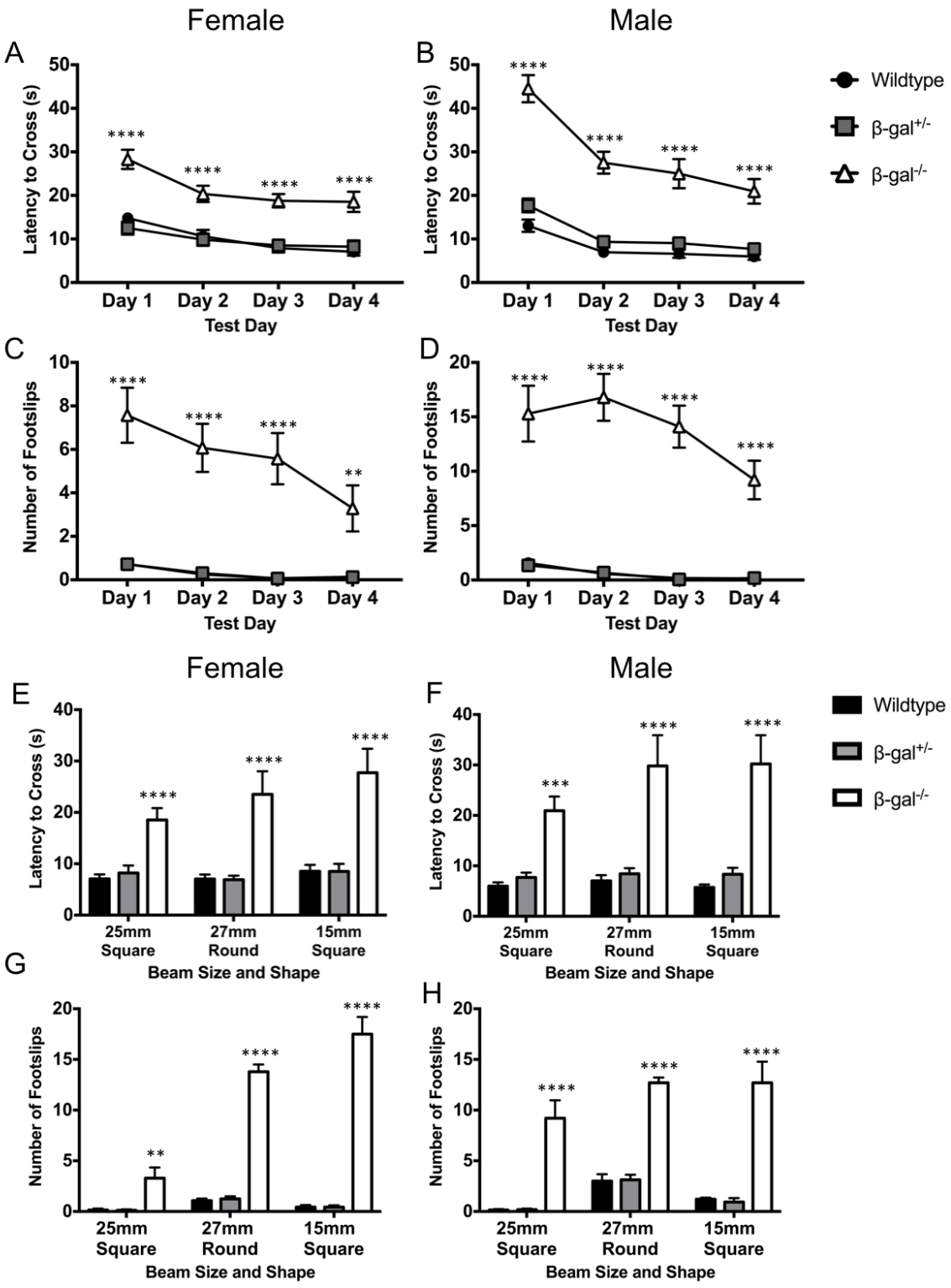
Female
Male
A
B
C
D
E
F
G
H
Latency to Cross (s)
Number of Footslips
Test Day
Day 1
Day 2
Day 3
Day 4
Wildtype
β-gal+/-
β-gal-/-
25mm Square
27mm Round
15mm Square
Beam Size and Shape

Figure 15. Impaired balance and motor coordination in β-gal$^{-/-}$ mice. At 6 months of age, β-gal$^{-/-}$ mice were tested on a balance beam. (A and B) Latency to cross beam and (C and D) number of hind foot slips while crossing the beam. (E and F) Latency to cross beams of increasing difficulty and (G and H) number of hind foot slips while crossing the beam on test day (n = 5-8 for each group). Data are mean ± SEM. **≤P0.01, ***p≤0.001, ****p≤0.0001.

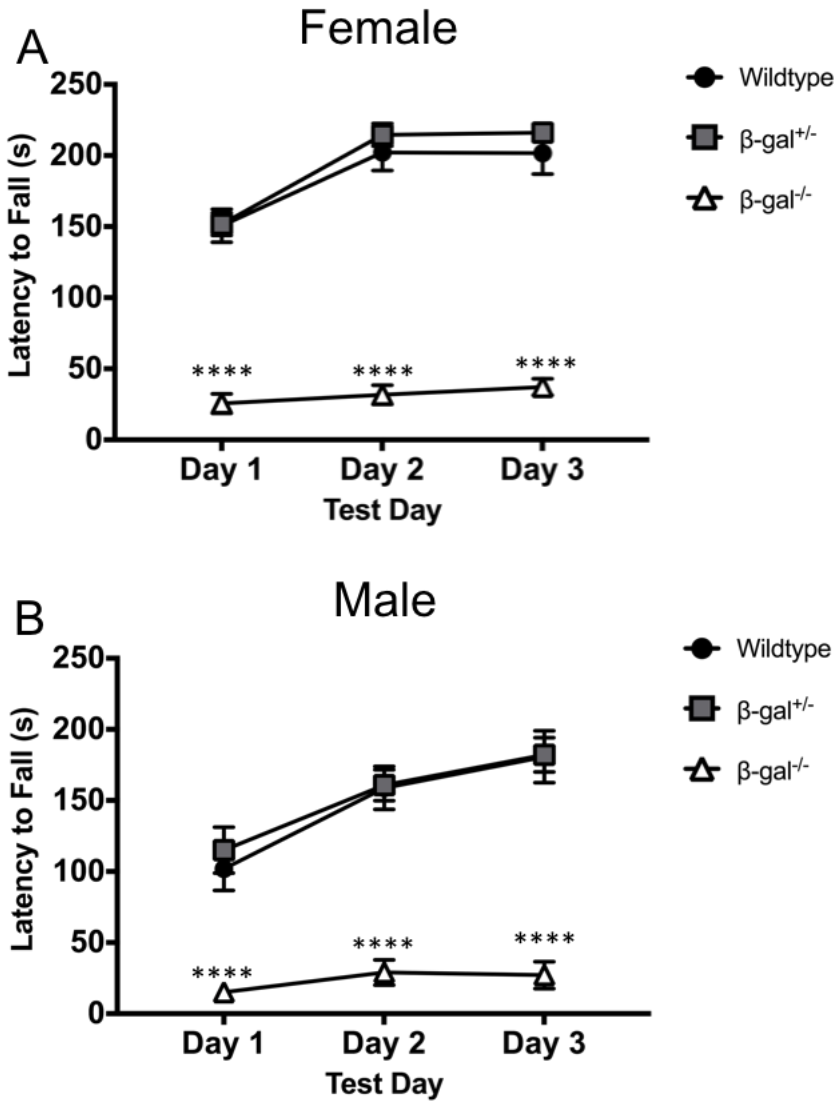

Figure 16. Impaired motor coordination and motor memory in β-gal$^{-/-}$ mice. Latency to fall off accelerating rotarod of (A) female and (B) male β-gal$^{-/-}$ (n = 5-8 for each group) for three test days. Data are mean ± SEM. ****p≤0.0001.

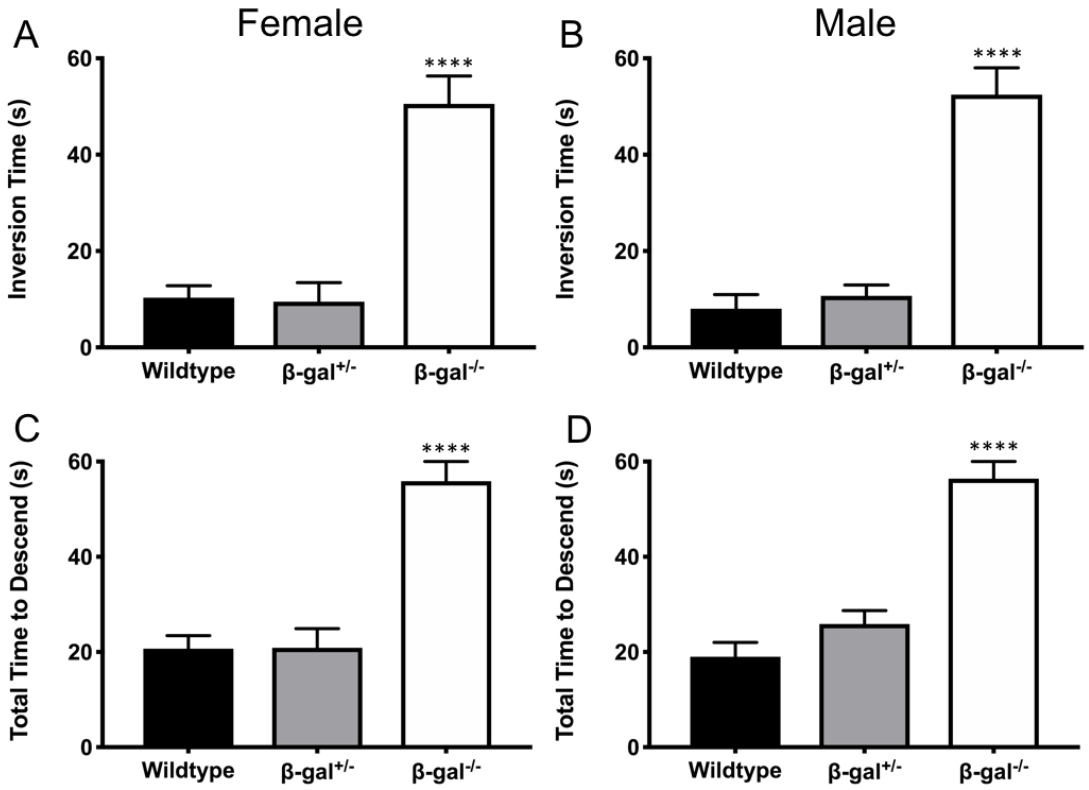

Figure 17. Slowed and impaired fine motor skills in β-gal$^{-/-}$ mice. Time to rotate body on pole and time to descend pole were recorded in a single trial (n=5-8 for each group). Data are mean ± SEM. ****p≤0.0001.

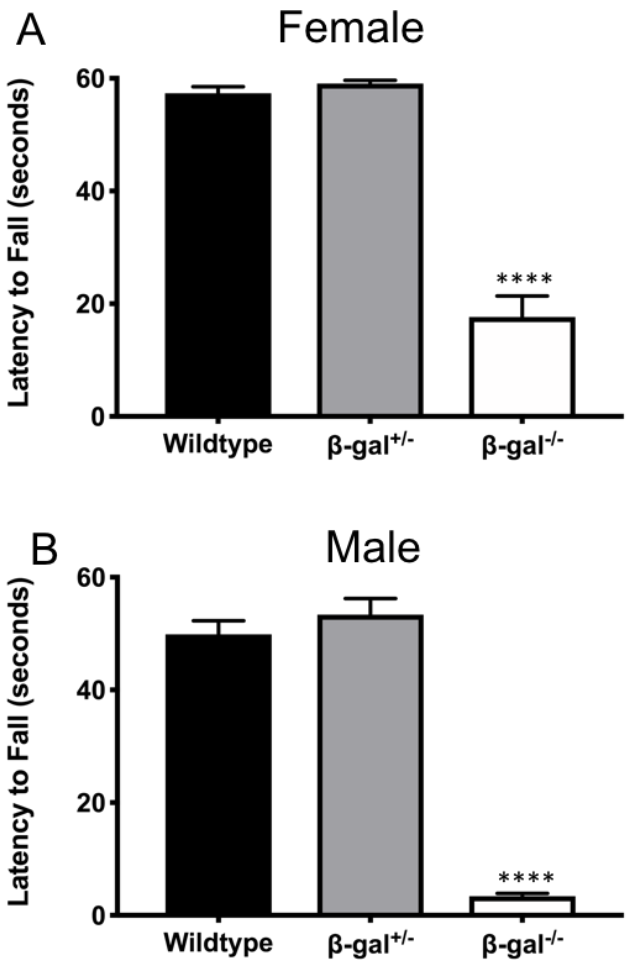

Figure 18. Significant reduction in grip strength in β-gal$^{-/-}$ mice. Assessment of grip strength of (A) female and (B) male mice using the inverted screen test (n=5-11 for each group). Data presented are mean of three trials ± SEM. ****p≤0.0001.

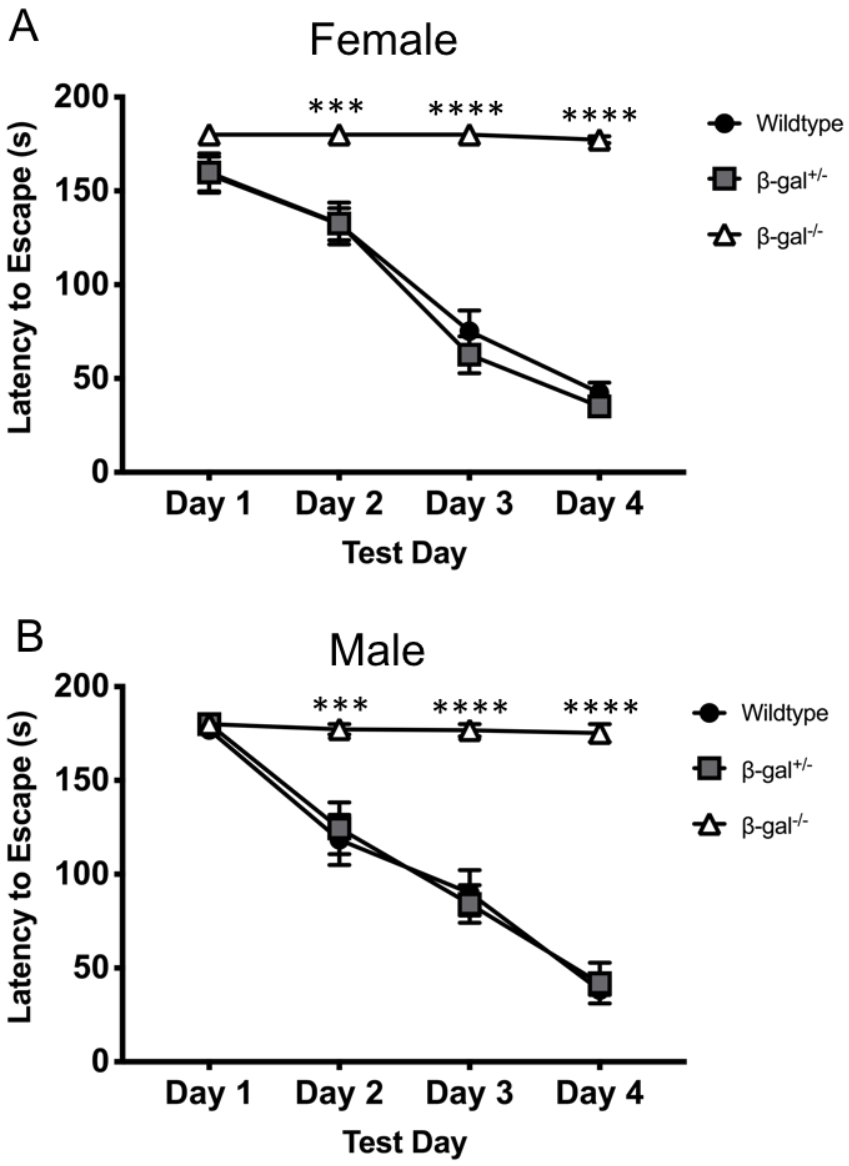

Figure 19. Severe spatial learning and memory deficiency in β-gal$^{-/-}$ mice at 6 months of age. The Barnes maze was used to investigate the ability of (A) female and (B) male β-gal$^{-/-}$ mice (n=5=11 for each group) to learn and remember how to escape the platform over the course of four experimental days consisting of 4 trials per day. Data are mean of three trials ± SEM. ***p≤0.001, ****p≤0.0001.

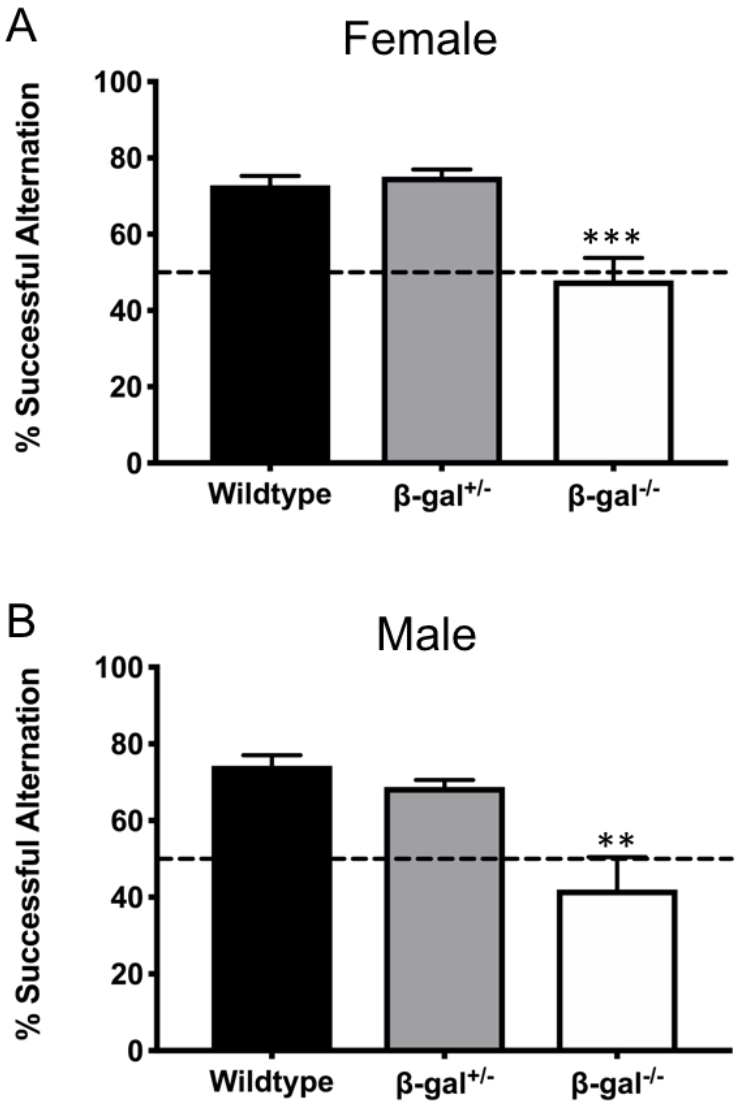

Figure 20. Impairment of spatial working memory in β-gal$^{-/-}$ mice. Measuring the exploratory behavior of (A) female and (B) male mice as a measurement of spatial working memory in the spontaneous alternating T-maze (n=5-8 for each group). Dashed line indicates 50%. Data are mean ± SEM. **p≤0.01, ***p≤0.001.

CHAPTER IV

Characterization of a Mouse Model Harboring a Mutation Found in Morquio Syndrome Type B

Introduction

Morquio syndrome type B, also known as Mucopolysaccharidosis type IV B (MPS IVB, MIM #253010), is an autosomal recessive lysosomal disease caused by deficiencies of β-galactosidase (β-gal; EC 3.2.1.23), a lysosomal hydrolase that is responsible for catalyzing the hydrolysis of the terminal galactose residue on keratan sulfate, GM1 ganglioside, GA1 ganglioside, and galactose-containing oligosaccharides. While there are over 223 disease causing mutations in the β-gal encoding gene, *GLB1*, reported in the Human Gene Mutation Database (v. 2018.3) [25], there are only 22 mutations reported to be associated with Morquio syndrome type B. These mutations reduce the ability of β-gal enzyme to catabolize keratan sulfate (KS), leading to KS accumulation within the lysosome. This storage of KS leads to severe skeletal changes, including skeletal dysplasia, odontoid hypoplasia, short stature, kyphosis, protruding sternum and corneal clouding. In some cases, there is cardiac involvement. Interestingly, there is typically no neurological involvement in Morquio syndrome type B, whereas GM1-gangliosidosis, another disease caused by deficiencies in β-gal, is primarily a neurological disease. Morquio syndrome type B is extremely rare, and the incidence rate is currently unknown. In four natural history studies of patients with MPS diseases [104-107], there were only 2 cases of Morquio syndrome type B reported, which were in Germany. Out of 474 patients reported to have an MPS disease over 15 years, only 2 patients had Morquio syndrome type B [107]. Like GM1-gangliosidosis, there are no current

therapies available for Morquio syndrome type B except for pain relief from abnormal bone growth.

Up to now, the ability to study this disease has been limited, not only by the limited number of patients available, but also due to the lack of an animal model. Currently, most research conducted for Morquio syndrome type B has been limited to studies on patient fibroblasts [100]. Additionally, the mouse models that are available for studying β-gal deficiencies are those that completely lack expression of *Glb1*, resulting in a complete loss of β-gal enzyme activity. Patients with Morquio syndrome type B have missense mutations that result in changes in the secondary and tertiary structure of the β-gal protein, and have a residual enzyme activity between 1.3-11.9% of normal activity [32, 99, 101, 102]. One common mutation is a 2 bp missense mutation that results in an amino acid substitution from tryptophan to leucine (*GLB1*^{W273L}). This mutation was introduced into a murine model (*Glb1*^{W274L}) using CRISPR-Cas9 genome editing (see Chapter II) and the characterization of this line is described here.

Materials and Methods

Animal Care and Procedures

All animal care and experimental procedures were conducted under the approval of the Institute Animal Care and Use Committee (IACUC) of the University of Minnesota. All animals were housed in specific pathogen-free conditions and genotyped by PCR described in Chapter II. C57BL/6J (000664) animals were purchased from The Jackson Laboratory.

The humane endpoint for these studies was defined as the presence of limb paralysis, the inability to rear and feed normally, or the loss of ≥15% of peak body weight. For biochemical analysis, animals were sacrificed by CO_2 asphyxiation and perfused transcardially with 20 mL of ice-cold PBS. Animals utilized for histological analysis were further perfused with 20 mL of 10% neutral buffered formalin (NBF). Tissues isolated for biochemical assays were flash frozen in liquid nitrogen.

Tissue Homogenization

Harvested organs for biochemical analysis were homogenized in 1 mL of T-PER™ Tissue Protein Extraction Reagent (Cat. #78510, Thermo Fisher Scientific) with Halt™ Protease Inhibitor Cocktail (Cat. #78430, Thermo Fischer) added to manufacturers recommendation using a Brinkmann Polytron™ PT 10/35.

β-galactosidase (β-gal) Enzyme Assay

β-gal enzyme activity was determined utilizing a fluorometric assay as previously described [280], with slight modification. Briefly, tissue samples were homogenized in 1 mL of T-PER™ Tissue Protein Extraction Reagent (Thermo Fisher Scientific, Waltham, MA) with added Halt™ Protease Inhibitor Cocktail (Thermo Fischer Scientific) added to manufacturers recommendation. To determine β-gal activity, supernatants of the tissue homogenates were diluted with a 0.2 M sodium acetate/0.1 M sodium chloride buffer (pH 4.3) and 40 µL of

each was added in triplicate to a 96-well black round-bottom plate (Corning™, Corning, NY) on ice. 20 µL of a substrate solution containing 1.0 mM 4-methylumbelliferyl-β-D-galactopyranoside (4-MUGal, Millipore-Sigma, St. Louis, MO) was added to each well, and the plate was incubated for 30 minutes at 37°C. To quench the reaction, 200 µL of 1M carbonate buffer (1 M sodium carbonate to pH 10.7 with 1 M sodium bicarbonate) was added. In the presence of β-gal enzyme, the non-fluorescent 4-MUGal is cleaved and releases a fluorescent 4-methylumbelliferone (4-MU) molecule. This fluorescence was measured in a Synergy MX Plate Reader with Gen5 plate reader program (BioTek Instruments, Winooski, VT) with excitation at 360 nm and emission read at 460 nm (80% sensitivity). 4-MU (Sigma-Millipore) is used to generate a standard curve. β-gal enzyme activity is expressed in nmol of 4-MU released per hour, per milligram of protein (nmol/hr/mg), which is determined using a Pierce™ BCA Protein Assay Kit (Thermo Fisher Scientific).

Histopathological Analysis

Following perfusion and fixation with 10% NBF, tissues were processed into paraffin wax using standard histology techniques, sectioned at a thickness of 4 µm, stained with hematoxylin and eosin (H&E), and evaluated using light microscopy by two A.C.V.P. board-certified pathologists. Tissues that were examined include the lungs, liver, heart, spleen, kidney, adrenal gland, stomach, large and small intestine, brain, eyes, salivary glands, skeletal muscle, sternum, and femur (including hip and stifle joints). All work was done at the Masonic

Cancer Center Comparative Pathology Shared Resource laboratory at the University of Minnesota.

Plasma Heparan Sulfate and Keratan Sulfate Quantification

Liquid chromatography, tandem mass spectrometry was performed by Dr. Shunji Tomatsu at the Nemours/Alfred I. duPont Hospital for Children at the University of Delaware following procedures published previously [299].

Radiographic Analysis

Following perfusion and harvesting of visceral organs, radiographic analysis was performed using a Faxitron UltraFocus X-ray imaging cabinet (Faxitron Bioptics, LLC, Tucson, AZ) at the Veterinary Diagnostic Laboratory at the University of Minnesota (St. Paul, MN).

Statistical Analysis

Data are reported as mean ± standard error. GraphPad Prism 7 (v. 7.0a, GraphPad Software, Inc, La Jolla, CA) was used to perform all statistical analyses. Survival probability was determined using Kaplan-Meier analysis, followed by the log-rank test (Mantel-Cox) to compare statistical significance of the survival curves for each group. One-way or two-way ANOVA, followed by Tukey's multiple comparisons test was conducted in all other experiments to compare wildtype, heterozygous, and mutant groups.

Results

Residual β-gal enzyme activity in *Glb1*^{W274L} mice

In β-gal$^{-/-}$ mice, a loss of 20 bp in exon 8 of the *Glb1* gene, including the catalytic nucleophile, resulted in complete loss of β-gal enzyme activity. Here, we measured the enzyme activity in the *Glb1*^{W274L} mice, to determine whether the common Morquio syndrome type B mutation resulted in a similar residual β-gal enzyme activity that is observed in patients. In the brain, β-gal enzyme activity in homozygous *Glb1*^{W274L} mutant mice (14.5±0.6 nmol/hr/mg of protein) was 13.3% of wildtype activity (108.9±4.0) (Figure 21A). Similarly, in the heart (4.2±0.4), liver (10.3±0.8), and spleen (59.8±8.1) of *Glb1*^{W274L} mice, β-gal enzyme activity was 9.8%, 8.4%, and 12.4% of wildtype activity, respectively (heart, 43.2±7.1; liver, 122.5±4.4; and spleen, 480.3±52.0) (Figure 21B-D). As expected, carriers of the *Glb1*^{W274L} mutation have an intermediate β-gal enzyme activity (brain, 65.0±1.8; heart, 22.0±1.5; liver, 75.3±3.5; and spleen, 322.9±49.2).

Appearance and survival of *Glb1*^{W274L} mice

Over the course of one year, the weight of *Glb1*^{W274L} mice was monitored. In contrast to β-gal$^{-/-}$ mice, weights of both female (Figure 22A) and male (Figure 22B) *Glb1*^{W274L} mice did not differ from wildtype and heterozygous mice. Similarly, *Glb1*^{W274L} mice showed no increase in mortality over one year of observation (Figure 23A and B). Further, *Glb1*^{W274L} mice showed no obvious

visible phenotype over the course of the year. *Glb1*^{W274L} mice also have normal litter sizes and breed for a normal length of time.

Histological and X-ray assessment of *Glb1*^{W274L} mice

Human Morquio syndrome type B patients primarily suffer from a skeletal disease, so highly detailed X-rays were taken at approximately 8 weeks of age to assess any abnormalities found in the bones of the *Glb1*^{W274L} mice. Following assessment by board-certified pathologists, it was deemed that there were no observable differences between *Glb1*^{W274L} mice and a wildtype littermate (Figure 24A-D).

Glycosaminoglycan quantification in *Glb1*^{W274L} mice

As keratan sulfate (KS) is the primary substrate that accumulates in patients with the *GLB1*^{W273L} mutation, tandem mass-spectrometry was utilized to quantify monosulfated (mono-KS) and disulfated KS (di-KS) in plasma samples of 8-week old mice. The results of this experiment showed that both mono-KS and ds-KS were undetectable (<19.5 ng/ml) in mice assayed, including *Glb1*^{W274L} mice. Interestingly, heparan sulfate was quantified and was found to be significantly elevated in plasma samples of *Glb1*^{W274L} mice (ΔDiHS-0S, 57.24$\pm$2.0 ng/mL; ΔDiHS-NS, 6.81$\pm$0.3 ng/mL) compared to wildtype mice (DiHS-0S, 30.7$\pm$9.1 ng/mL; ΔDiHS-NS, 4.1$\pm$0.8 ng/mL) (Figure 25A and B).

Discussion

The introduction of a 2 bp mutation that is commonly found in patients with Morquio syndrome type B into a mouse model results in the first described mouse model of β-galactosidase deficiency that has residual β-gal enzyme activity. The mutation, which causes a substitution of a tryptophan residue to a leucine at position 274 (*Glb1*^{W274L}; *GLB1*^{W273L} in humans), occurs at a highly conserved residue in the *GLB1* gene. This tryptophan residue is important for forming the substrate binding pocket, specifically playing a role in shaping the pocket, and when substituted to an amino acid with a smaller side chain, the ability to cover the pocket was lost [24]. This conformational change in the protein results in a loss of specificity to keratan sulfate [300], which results in its accumulation within the lysosomes of patients with Morquio syndrome type B. Even though β-gal enzyme activity was significantly reduced, ranging from 8.4-13.3% of wildtype levels, accumulation of keratan sulfate was not observed in *Glb1*^{W274L} mice and even after one year, no skeletal phenotype was observed. An explanation for this observation may be the absence of keratan sulfate in skeletal tissues of mice [301]. However, keratan sulfate-containing proteoglycans are found in the cornea of the mouse, beginning around postnatal day 20 [302, 303]. This will have to be carefully examined to determine whether the *Glb1*^{W274L} mice will accumulate corneal keratan sulfate.

While this mouse lacks a Morquio syndrome type B phenotype, it is still valuable for the testing of novel therapies, not only for Morquio, but for patients with GM1-gangliosidosis as well. Previously generated murine models of GM1-gangliosidosis, including the one described in Chapter III, knockout function of

the protein completely. This limits their use in β-gal deficiency studies to developing enzyme replacement therapies [187] or to gene therapies [159, 160, 211, 304, 305]. However, most patients who suffer from GM1-gangliosidosis or Morquio syndrome type B do not have a complete β-gal enzyme deficiency. In reality, many patients with juvenile or adult forms of GM1-gangliosidosis or Morquio syndrome type B have a single amino acid substitution that affects the secondary or tertiary structure of β-gal, reducing its catalytic activity. With the creation of the *Glb1*^{W274L} mouse model, the ability to test enzyme-stabilizing small molecules becomes a possibility.

In conclusion, the first mouse model of β-galactosidase deficiency that has residual enzyme activity has been developed. While the mouse lacks a Morquio syndrome type B pathological phenotype, this model will be important for the development of new therapies for all β-gal deficiencies that a knockout model cannot be used for. Also, it could be helpful for the study of the *GLB1*^{W273L} mutation and others that cause reduced affinity for galactose-containing macromolecules. This has recently been assessed *in silico* by our laboratory for the β-gal protein [33].

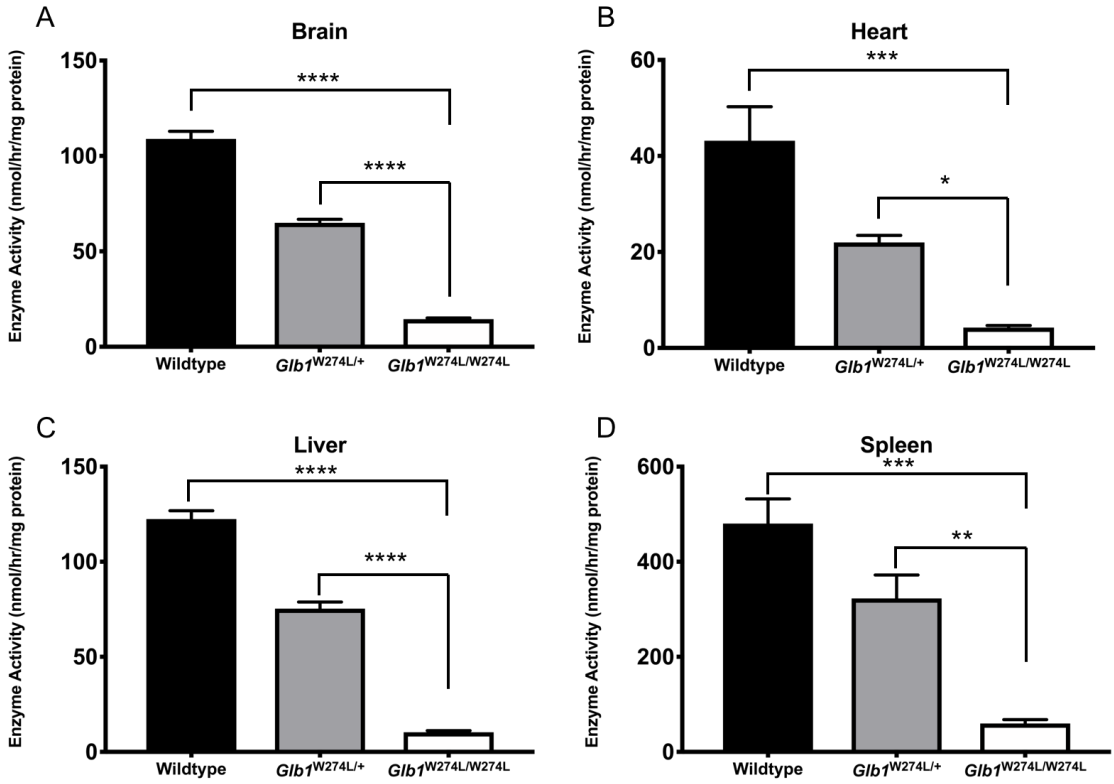

Figure 21. The *Glb1*^{W274L} mutation results in the presence of residual β-gal enzyme activity. Enzyme activity in the (A) brain, (B) heart, (C) liver, and (D) spleen of mice (n=3-4 for each group) determined using the artificial substrate 4-MUGal. Data are mean ± SEM. *p≤0.05, **p≤0.01, ***p≤0.001, ****p≤0.0001.

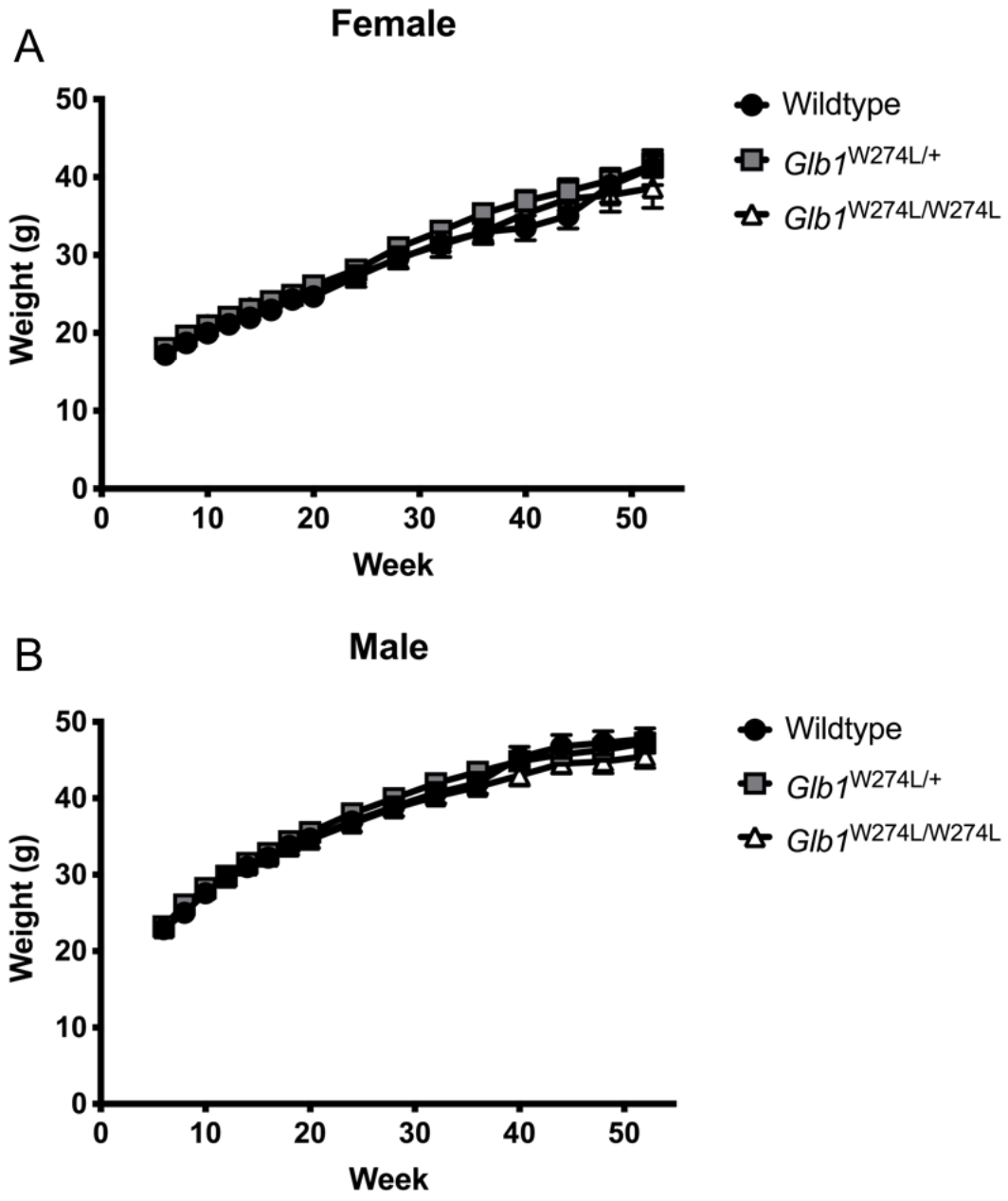

Figure 22. Presence of *Glb1*^{W274L} mutation in mice has no effect on weight. Weight of (A) female and (B) male *Glb1*^{W274L} mice over one year (n>6 for each group). Weight data are mean ± SEM.

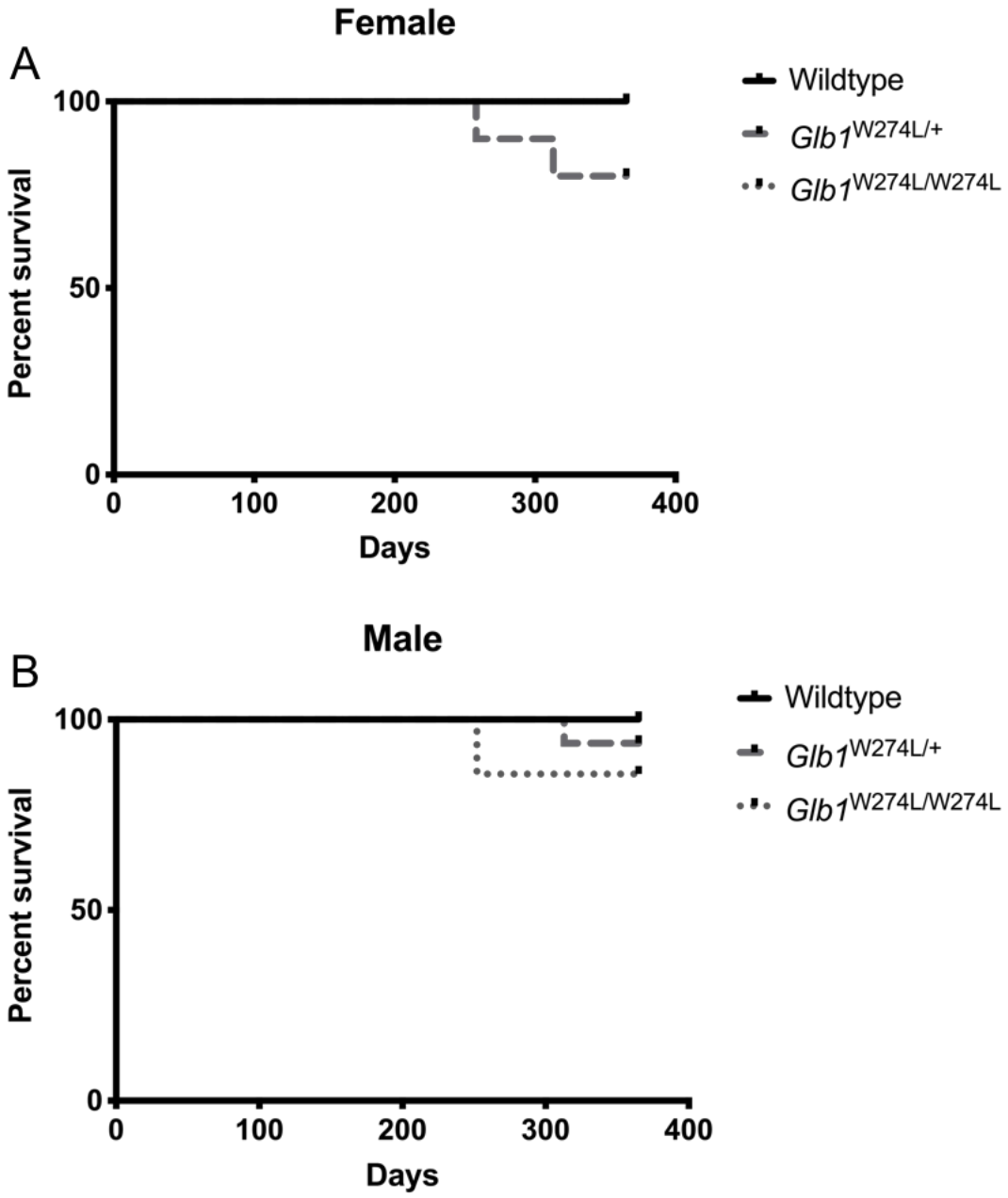

Figure 23. Reduction in enzyme activity in *Glb1*^{W274L} mice has no effect on lifespan over one year. Kaplan-Meier survival curve of (A) female and (B) male *Glb1*^{W274L} mice (n=7-16 for each group).

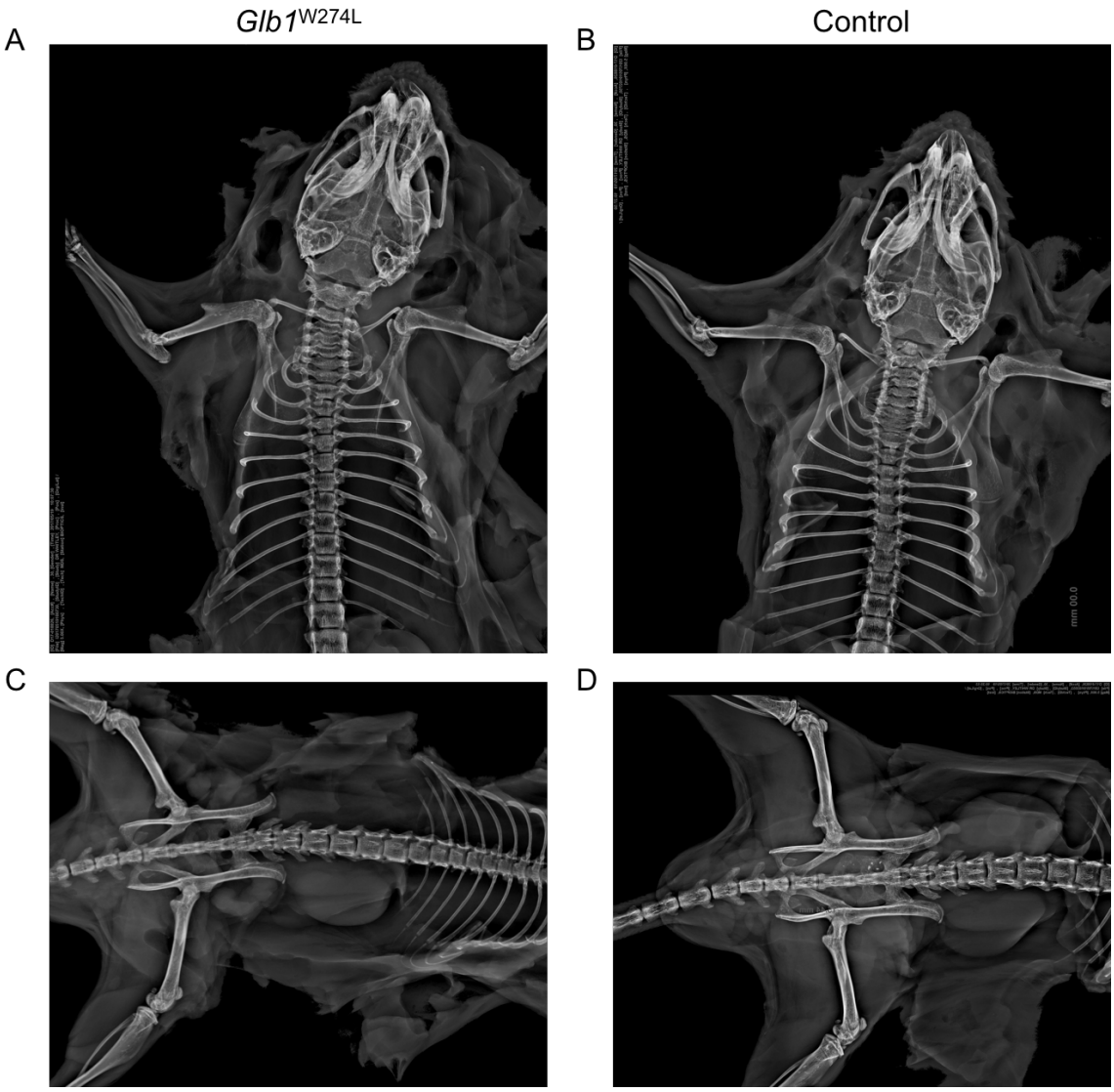

Figure 24. Lack of skeletal abnormalities in *Glb1*^{W274L} mice observed in Morquio syndrome type B patients. X-ray analysis conducted on 2-month-old (A and C) *Glb1*^{W274L} and (B and D) control mice using a Faxitron digital imager.

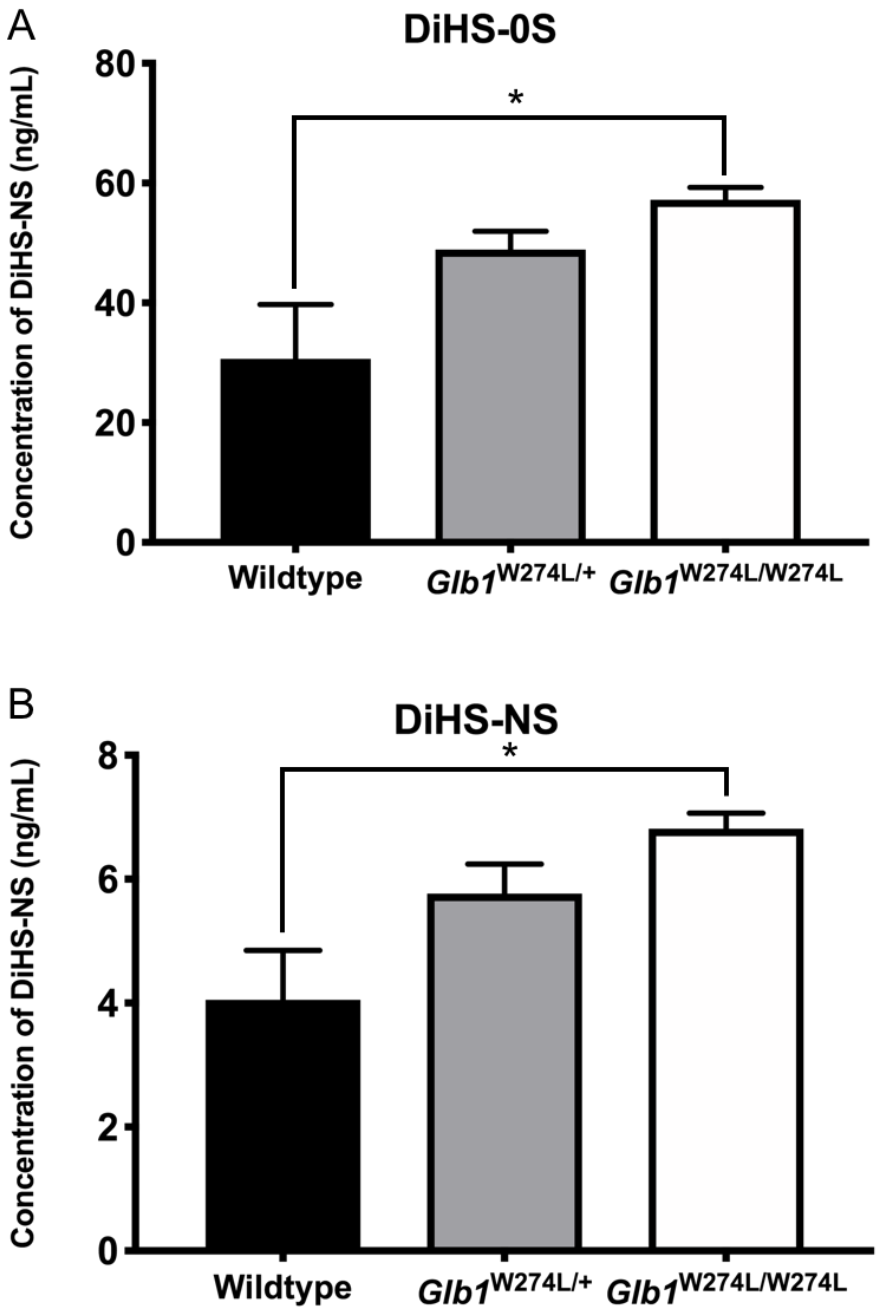

Figure 25. Secondary accumulation of heparan sulfate in the plasma of *Glb1*^{W274L} mice. Using tandem mass spectrometry to measure (A) DiHS-0S and (B) DiHS-NS heparan sulfate moieties in plasma from *Glb1*^{W274L} mice (n=3 for all groups). Data are presented as mean ± SEM. *p≤0.05.

CHAPTER V

AAV-Mediated Gene Therapy for GM1-Gangliosidosis

Introduction

Lysosomal diseases are a group of metabolic diseases caused by deficiencies in lysosomal hydrolases, which lead to an accumulation of substrate within the lysosome of the cell. One of these diseases, GM1-gangliosidosis, is a fatal neurodegenerative disease caused by insufficiencies in the enzyme β-galactosidase (β-gal; EC 3.2.1.23). Because of this deficiency, GM1 and GA1 gangliosides accumulates in the central nervous system (CNS), leading to a cascade of cellular events, often resulting in cell death [3, 84, 86]. Clinically, there are three severities of GM1-gangliosidosis, including infantile, juvenile, and adult forms. Classification into a specific category is determined by residual enzyme activity, and symptom presentation. Typically, as the amount of residual enzyme activity decreases, the more severe disease symptoms a patient will have. In the infantile form, the most severe, residual enzyme activity is between 0 and 2% of normal, where juvenile and adult forms have between 0.3-5% and 5-10% of normal, respectively. In the infantile form, symptoms typically become apparent by 6 months of age, which include delayed or regression of intellectual development, increased muscle weakening, progressive hepatosplenomegaly, seizures, and in some cases corneal clouding and skeletal abnormalities [3], leading to death before the age of 2. In juvenile and adult forms, these symptoms are milder or absent due to the higher residual enzyme activity.

Currently, there are no approved therapies for GM1-gangliosidosis. In the clinic, bone marrow transplant has been attempted [46] as a treatment, even as early as 5 weeks of age (Whitley, personal communication), however patients still

develop the symptoms of the disease. An additional approach has been substrate reduction therapy using miglustat (Zavesca) [47, 174], however this too has had minimal benefits; thus, there is a critical need for a new therapy. To date, there have been many preclinical studies conducted, including using enzyme replacement therapy [186, 187], molecular chaperones [181-183], and gene therapy [159, 160, 211, 304-306], however, none have proceeded to clinical trials. Recently, Sangamo Therapeutics received approval to conduct a Phase I safety trial for two lysosomal disease, MPS I (Hurler syndrome; ClinicalTrials.gov Identifier: NCT02702115) and MPS II (Hunter syndrome; ClinicalTrials.gov Identifier: NCT03041324) which were supported by preclinical studies conducted by our group and colleagues [250, 251]. This study utilized two AAV vectors encoding zinc-finger nucleases (ZFNs) which generate a site-specific DSB in the first intron of the albumin locus, and another vector that encodes the cDNA of the deficient gene with homology sequence to the site of cleavage. Under expression of the albumin promoter, even with a low number of integration events, this system produced enough enzyme to correct the pathology and neurocognitive deficiencies of the diseased mice.

In this chapter, a similar approach adapted from the ZFN experiments is taken to test whether this could be a beneficial approach to treat GM1-gangliosidosis. These preliminary studies were to determine whether a catalytically active β-gal enzyme could be synthesized from an AAV system designed to integrate the human *GLB1* cDNA into the albumin locus. Further,

these initial studies looked at whether the level of β-gal enzyme produced was enough to prevent the neuromotor disease observed in β-gal$^{-/-}$ mice.

Materials and Methods

Animals

All protocols involving animals were approved by the University of Minnesota Institutional Animal Use and Care (IACUC) committee. β-gal$^{-/-}$ and control mice were genotyped by PCR described in Chapter II. All animals were housed in specific pathogen-free conditions.

Mice were sacrificed by CO_2 asphyxiation and perfused transcardially with 20 mL of ice-cold PBS. Tissues isolated for biochemical assays were flash frozen in liquid nitrogen, and stored on dry ice.

Plasmid Design and Adeno-associated Virus (AAV) Vector Production

The plasmid design encoding the nuclease in this system is proprietary and will be designated PS-905. The donor construct providing human *GLB1* (AAV-h*GLB1*) was subcloned from the plasmid Cat #SC119908 from OriGene (Rockville, MD). This plasmid contains the h*GLB1* cDNA sequence flanked by regions of homology to the albumin locus, but lacks a promoter. Packaging of these plasmids into AAV8 vectors was done at the Children's Hospital of Philadelphia Research Vector Core. The titer was verified by SDS PAGE and silver staining.

Hydrodynamic Injection

Hydrodynamic injection of 8-week-old β-gal$^{-/-}$ mice was done as previously described [307, 308]. Briefly, mice were anesthetized with a cocktail of ketamine hydrochloride (10 mg/kg), acepromazine (0.12 mg/kg), and butorphanol (0.012 mg/kg) as an analgesic, all given intraperitoneally. 50 ng of each plasmid was mixed in a volume of Ringer's solution equivalent to 10% of body mass, and injected via tail vein using a 27-gauge butterfly needle over a period of 5-8 seconds. 24 hours after injection, mice were euthanized and assayed for enzyme activity.

Intravenous AAV Injection

Neonatal mice (postnatal day 0-3) were injected with AAV vectors (<30 μL) through the temporal facial vein with a 31-gauge needle. Mice were injected with a dose ratio of 1:6 (nuclease:*GLB1* donor cDNA).

Tissue Homogenization

Harvested organs for biochemical analysis were homogenized in 1 mL of T-PER™ Tissue Protein Extraction Reagent (Cat. #78510, Thermo Fisher Scientific) with Halt™ Protease Inhibitor Cocktail (Cat. #78430, Thermo Fischer) added to manufacturers recommendation using a Brinkmann Polytron™ PT 10/35.

Blood Collection for Enzymatic Assay

Blood samples (<200 µL) were collected monthly by submandibular bleed into a microfuge tube containing 20 µL of heparin to prevent clotting. Plasma was separated from the sample by spinning the tubes for 10 minutes at 3,000 rpm. Plasma samples were then diluted as necessary and assayed for β-gal enzyme activity as described for tissue samples.

Plasma and Tissue β-galactosidase Enzyme Activity

Plasma and tissue β-gal enzyme activity was determined utilizing a fluorometric assay as previously described [280], with slight modification. Briefly, tissue samples were homogenized in 1 mL of T-PER™ Tissue Protein Extraction Reagent (Thermo Fisher Scientific, Waltham, MA) with added Halt™ Protease Inhibitor Cocktail (Thermo Fischer Scientific) added to manufacturers recommendation. To determine β-gal activity, supernatants of the tissue homogenates were diluted with a 0.2 M sodium acetate/0.1 M sodium chloride buffer (pH 4.3) and 40 µL of each was added in triplicate to a 96-well black round-bottom plate (Corning™, Corning, NY) on ice. 20 µL of a substrate solution containing 1.0 mM 4-methylumbelliferyl-β-D-galactopyranoside (4-MUGal, Millipore-Sigma, St. Louis, MO) was added to each well, and the plate was incubated for 30 minutes at 37°C. To quench the reaction, 200 µL of 1M carbonate buffer (1 M sodium carbonate to pH 10.7 with 1 M sodium bicarbonate) was added. In the presence of β-gal enzyme, the non-fluorescent 4-MUGal is cleaved and releases a fluorescent 4-methylumbelliferone (4-MU) molecule. This fluorescence was measured in a Synergy MX Plate Reader with

Gen5 plate reader program (BioTek Instruments, Winooski, VT) with excitation at 360 nm and emission read at 460 nm (80% sensitivity). 4-MU (Sigma-Millipore) is used to generate a standard curve. β-gal enzyme activity is expressed in plasma as nmol 4-MU released per hour, per mL of plasma used (nmol/hr/mL). In tissue, activity is expressed in nmol of 4-MU released per hour, per milligram of protein (nmol/hr/mg), which is determined using a Pierce™ BCA Protein Assay Kit (Thermo Fisher Scientific).

Behavioral Analysis

At 4 months of age, mice were subjected to the accelerating rotarod (Ugo Basile, Comerio, Italy) as previously described [285]. Briefly, mice were tested for three consecutive days, undergoing four trials per day, with a minimum inter-trial duration of 30 minutes. Testing was done on a rotarod programmed to accelerate from 5 to 50 rpm over a max trial duration of 300 seconds. 3-5 mice were placed on the divided rod simultaneously and the apparatus' counter was started. The trial was considered complete when 1) the mouse fell off the rotarod and stopped the counter, 2) the mouse completes two consecutive rotations by holding on to the rod without walking, or 3) when 300 seconds elapsed.

Statistical Analysis

Data are reported as mean ± standard error of the mean. GraphPad Prism 7 (v. 7.0a, GraphPad Software, Inc, La Jolla, CA) was used to perform all

statistical analyses. Unpaired t-test was conducted to compare treated mice to mutant control mice.

Results

Assessing the functionality of PS-905 and h*GLB1* plasmids using hydrodynamic delivery

Hydrodynamic delivery of plasmids was utilized to test whether the two plasmid designs functioned properly and were capable of producing active β-gal protein. At 8-weeks of age, β-gal$^{-/-}$ mice were injected with either the donor plasmid encoding the human *GLB1* cDNA alone (donor only; n=2) or both the donor plasmid and the PS-905 nuclease plasmid (n=2), which is under regulation by a liver-specific promoter. Two-days following injection, mice were sacrificed and β-gal enzyme activity was assessed in the liver and brain. In the group receiving the donor only plasmid, liver β-gal enzyme expression was 5.2±1.7 nmol/hr/mg, compared to 1.1±0.7 nmol/hr/mg in mutant controls and 122.8±17.8 nmol/hr/mg in heterozygous mice. Importantly, mice receiving both the donor cDNA plasmid and PS-905 plasmid had an enzyme activity of 16.9±1.7 nmol/hr/mg protein (Figure 26). These results indicate that the plasmid design is sufficient to produce a functional β-gal enzyme. Knowing this, the plasmids were packaged into AAV8 vectors for use in a preliminary gene therapy study for treating β-gal deficiency in β-gal$^{-/-}$ mice.

Intravenous injection of AAV8-h*GLB1* and AAV8-PS-905 produces a catalytically active and secreted β-gal protein

Neonatal β-gal$^{-/-}$ mice (n=9) were injected with AAV8-PS-905 (5 x 10^9 vg/g body weight) and AAV8-h*GLB1* (3 x 10^{10} vg/g body weight) through the temporal facial vein. As a control, an additional group of β-gal$^{-/-}$ mice received an injection of the donor only (AAV8-h*GLB1*, n=5). Over the course of 4 months post-dosing, plasma enzyme activities were assessed (Figure 27). 30 days following dosing, plasma activity in mice receiving both AAV8-PS-905 and AAV8-h*GLB1* was 13.8±3.1 nmol/hr/mL, which was 4.8-fold higher than heterozygous activity (2.9±0.2 nmol/hr/mL). Strangely, on subsequent measurements, β-gal enzyme activity in AAV8-PS-905+AAV8- h*GLB1* treated mice (Day 60, 4.4±1.4; Day 90, 3.1±0.5; Day 120, 2.9±0.7 nmol/hr/mL) began to diminish and fell to heterozygous levels (Day 60, 2.9±0.6; Day 90, 2.2±0.2; Day 120, 2.0±0.04 nmol/hr/mL) by 120 days post injection. Mice receiving the donor only had no increase in β-gal enzyme activity over the course of 120 days, indicating that there was no episomal transgene expression from the donor which lacks a promoter sequence.

At 120 days post-dosing a subset of mice was sacrificed and β-gal enzyme activity was measured in tissues. Enzyme activity was not present within the brains (Figure 28A) and hearts (Figure 28B) of mice treated with AAV8-PS-905+AAV8-h*GLB1* vectors (n=3). In the liver and spleen, enzyme activity was observed in two of the three animals tested. In the liver, AAV8-PS-905+AAV8-h*GLB1* mice had a β-gal enzyme activity of 39.1±22.9 nmol/hr/mg, compared to

mutant control mice (n=2), which showed no observable enzyme activity (Figure 28C). In the spleen, β-gal enzyme activity in mice receiving treatment with AAV8-PS-905+AAV8-h*GLB1* vectors was increased (41.3±34.1 nmol/hr/mg) compared to mutant β-gal$^{-/-}$ mice receiving no treatment (0.5±0.5 nmol/hr/mg) (Figure 28D).

Neuromotor function is not improved by current dose of h*GLB1*

Behavior analysis with the accelerating rotarod was conducted to determine whether there was a therapeutic effect at the current vector dose and whether it had any effect on neuromotor function. Over the three trial days, β-gal$^{-/-}$ mice that received both AAV8-h*GLB1* and AAV8-PS-905 performed slightly better over subsequent days of testing (Day 1, 61.6±8.9 seconds; Day 2, 86.7±10.3s; Day 3, 88.0±12.5s). However, treated β-gal$^{-/-}$ mice did not improve their performance compared to β-gal$^{-/-}$ mice receiving no treatment (Day 1, 55.6±25.8 seconds; Day 2, 73.8±35.2s; Day 3, 82.6±38.4s), or those only receiving the donor vector AAV8-h*GLB1* (Day 1, 59.8±14.1; Day 2, 96.6±15.7; Day 3, 90.9±13.5). In comparison, the latency to fall of a normal heterozygous mouse progressively increased from 113.6±9.6s on Day 1 to 171.9±11.4s on Day 3, indicating a normal neuromotor function (Figure 29). These results indicate that the current vector dose does not provide a therapeutic effect.

Discussion

Currently, there are no existing treatments for patients suffering with GM1-gangliosidosis, thus it is of the utmost importance that one be developed. Recently, gene therapy has emerged as a potential treatment for many diseases, especially lysosomal diseases. With gene therapy, a convenient single-dose treatment is a possibility. Here, a gene therapy was designed to incorporate the gene that is deficient in patients with GM1-gangliosidosis, *GLB1*, into intron 1 of the albumin locus. Albumin is a the most abundant protein found in human blood, making up over 50% of total protein levels [309]. By incorporating the deficient gene into this locus, *GLB1* expression is driven by the highly active albumin promoter, which results in high expression of the *GLB1* gene, and subsequently increases the amount of β-gal enzyme. Through metabolic cross-correction [175], β-gal can be secreted into the blood stream and taken up by cells across the body to alleviate the GM1-ganglioside pathology. The preliminary data presented here from the initial experiments shows that following neonatal AAV8 injection, a functional β-gal enzyme is being synthesized and secreted into the blood stream and taken up by cells, illustrated by plasma and tissue enzyme activity. This indicates that these plasmids are functional.

While behavior testing on the accelerating rotarod revealed that there was no improvement in motor function of treated mice, there is still optimism that this system can be beneficial. Typically, large proteins are unable to reach the CNS due to the presence of the blood-brain barrier. However, our group has previously published that providing 20-fold of the clinical dose of recombinant IDUA can ameliorating the neurological disease in MPS I mice [310]. Additionally,

recent publications by our group and collaborators showed that a similar approach to that described here to drive expression of the transgene from the albumin locus could produce enough IDUA or IDS enzyme to ameliorate the neurological disease in MPS I [250] and MPS II [251] mice. This means that more commitment should be focused to increasing the amount of β-gal protein that is synthesized by this system, in hopes of treating both the primary CNS disease and the secondary systemic disease.

The first hurdle is to understand what is occurring in these animals as they age. For some reason, β-gal enzyme activity dropped significantly between day 30 and 60 in the plasma and continued to decline until reaching a lower limit, or low plateau, around heterozygous enzyme levels. A similar observation was made in mice that were treated with the Sleeping Beauty transposon system expressing another IDUA [308]. Aronovich *et al.* [308] showed that by suppressing the immune system of the mice using cyclophosphamide, enzyme activity could be maintained. The loss of enzyme activity seen in this study has not been previously reported in gene therapy studies for GM1-gangliosidosis, however plasma β-gal enzyme activity has not been monitored in those studies. A key difference between the approach taken in this chapter and those reported previously is the cDNA sequence of the *Glb1* gene. In our approach, the human *GLB1* cDNA was utilized, while previous studies utilized the mouse *Glb1* sequence. Thus, it is possible that an immune response to the new protein is occurring.

An alternative hypothesis to the loss of enzyme activity could be due to the difference in biochemical properties of the protein. It has been described that the human β-gal protein is temperature sensitive and requires protective protein/cathepsin A (PPCA) to function properly within the lysosome, and protect human β-gal (hβ-gal) from intralysosomal proteolytic inactivation [311], but the mouse β-gal (mβ-gal) does not. Lambourne *et al.*[311] also showed that enzyme activity of mβ-gal is significantly higher than hβ-gal activity, has a longer half-life, and is more stable than hβ-gal. Taking all of this into consideration, it may be more appropriate to utilize the mouse *Glb1* cDNA for subsequent experiments.

Overall, while the level of enzyme activity produced is not sufficient to ameliorate the disease neuromotor phenotype, the preliminary data presented show that this AAV approach produces a functional β-gal enzyme that can be secreted and measured in the plasma of treated mice for at least 120 days. Further, it showed that the secreted enzyme can be taken measured in peripheral tissues. These results are important, because it is the first step in developing a permanent, single-injection therapy for treating β-galactosidase deficiencies.

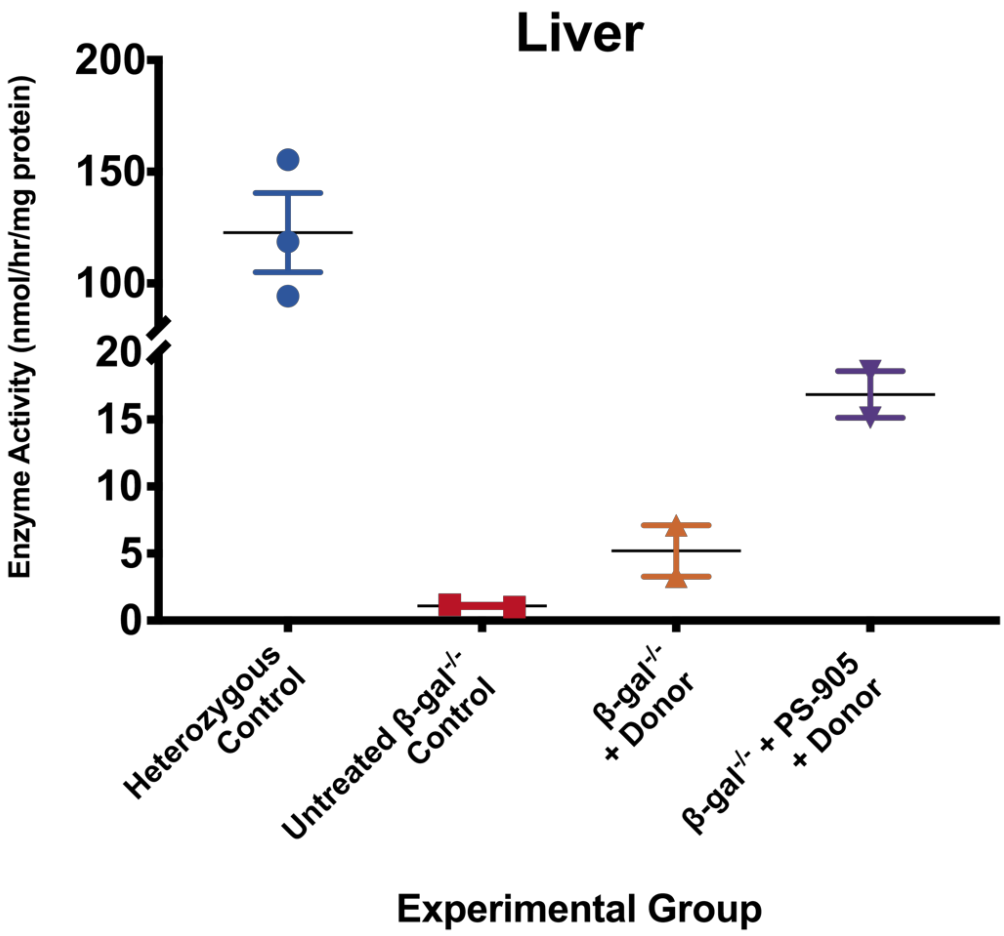

Figure 26. β-gal enzyme expression in liver following hydrodynamic delivery of *GLB1* constructs. Age-matched mice were assigned into four groups: 1) Heterozygous control (β-gal$^{+/-}$) (n=3, blue circles); 2) Untreated β-gal$^{-/-}$ control (n=2, red squares); 3) β-gal$^{-/-}$ mice injected with 50 ng h*GLB1* plasmid (donor) only (n=2, orange upward triangles); 4) β-gal$^{-/-}$ mice injected with 50 ng each of PS-905 plasmid + donor plasmid (n=2, purple downward triangles). Data are presented as mean ± SEM. *p≤0.05.

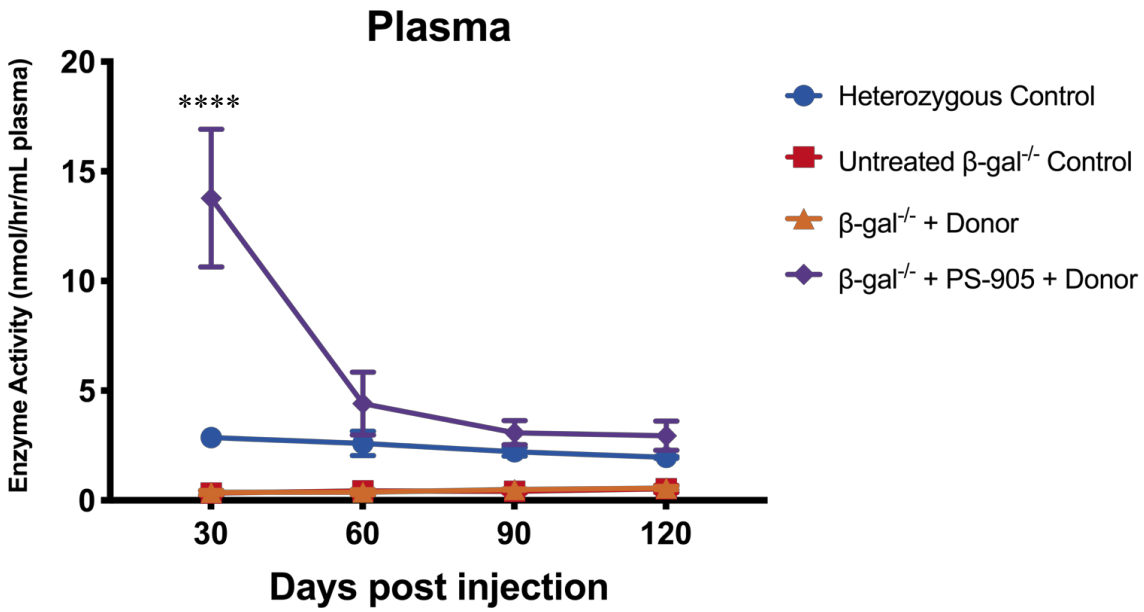

Figure 27. Significant decline and stabilization of plasma β-gal enzyme activity after 120 days post-treatment. Neonatal mice (P0-P2) were assigned into four groups: 1) Heterozygous control (β-gal$^{+/-}$) (n=8, blue circles); 2) Untreated β-gal$^{-/-}$ control (n=6, red squares); 3) β-gal$^{-/-}$ mice injected with AAV8-h*GLB1* (donor) only (n=5 orange upward triangles); 4) β-gal$^{-/-}$ mice injected with both AAV8-PS-905 + AAV8-*hGLB1* (n=9, purple downward triangles). Plasma was collected every 30 days. Data are presented as mean ± SEM. ****p≤0.0001.

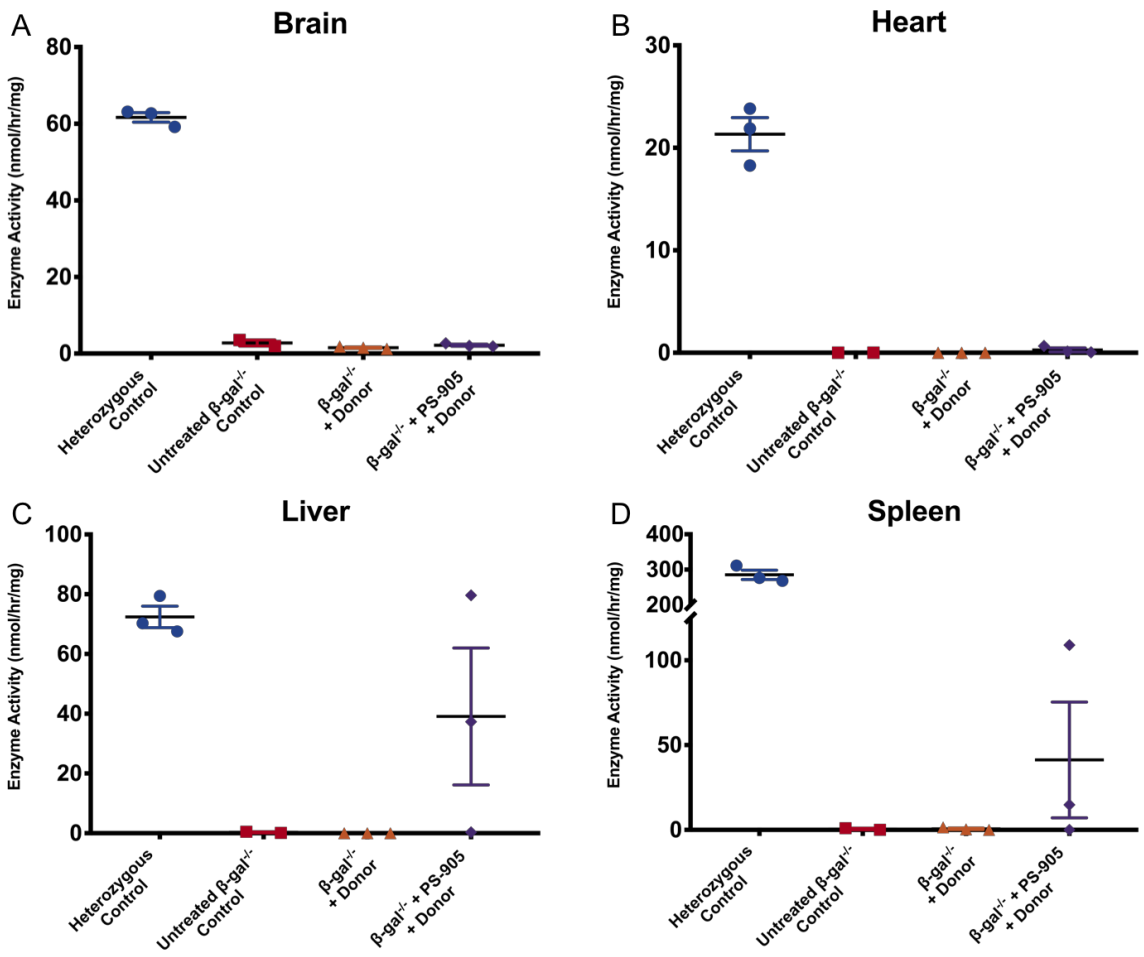

Figure 28. Presence of β-gal enzyme activity in the liver and spleen of two treated β-gal$^{-/-}$ mice. A subset of animals (n=2-3 for each group) from each group were sacrificed 120 days post-treatment and β-gal enzyme activity was measured in the (A) brain, (B) heart, (C) liver, and (D) spleen. Data are presented as mean ± SEM.

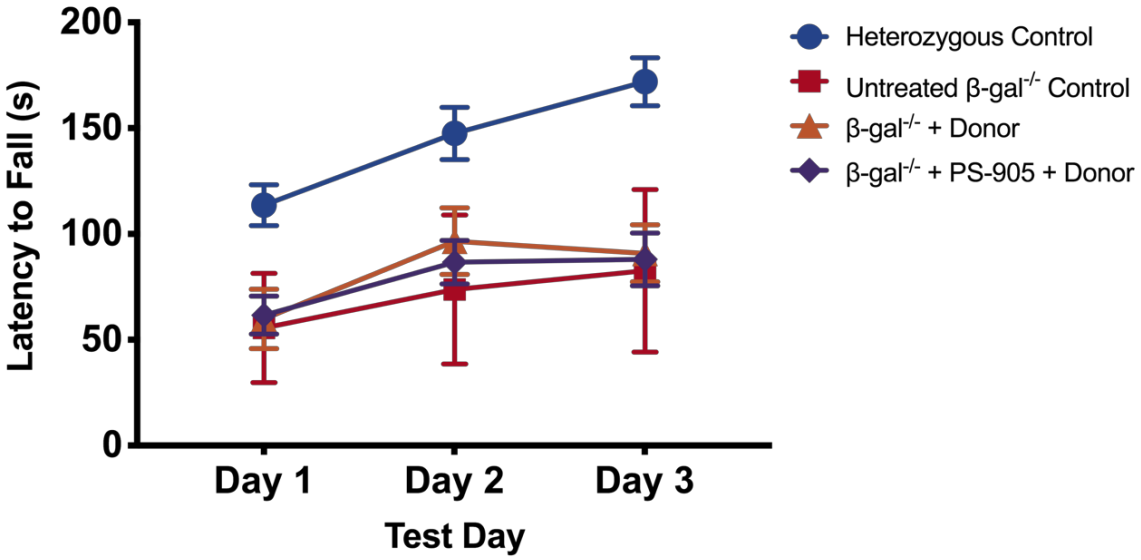

Figure 29. Treated β-gal$^{-/-}$ mice show no improvements in the accelerating rotarod. Mice were subjected to the accelerating rotarod at 120 days old for three days, four trials per day, to assess neuromotor function. n≥5 for each group. Data are presented as mean ± SEM.

CHAPTER VI

Conclusions and Future Directions

β-galactosidase is a unique lysosomal hydrolase, in that when it is deficient, depending on where the mutation is located in the *GLB1* gene and what effect it has on β-gal enzyme activity, it is responsible for two distinct lysosomal diseases: one affecting the central nervous system (GM1-gangliosidosis), and another affecting the skeletal system (Morquio syndrome type B). To be able to develop and test potential therapeutics for these diseases, an appropriate animal that recapitulates the phenotype of the human disease is essential. The work compiled in this thesis describes the development of two novel mouse models of these two lysosomal diseases. Additionally, the preliminary analysis of a novel gene therapy for these diseases is discussed.

Previous techniques utilized for developing novel mouse models, including pronuclear injection and ES cell manipulation, were inefficient and time consuming. Further, pronuclear injection relies upon random integration of the transgene, which could result in 1) inactivation of necessary genes, or 2) integration into a region that activates an oncogene. With ES cell manipulation, targeted mutagenesis via homologous recombination was made possible. While this method allows for specific manipulation of genes, the efficiency of homologous recombination is extremely low, and the experimental timeframe is extensive and tedious. With the advent of CRISPR-Cas9 genome editing, the ability to generate targeted mutations with high efficiency and in a short time frame is possible. Towards this end, Chapter II describes the successful introduction of two mutations into the β-galactosidase-encoding gene, *Glb1*, using CRISPR-Cas9 genome editing. This is the first description of using

CRISPR-Cas9 genome editing to generate a mouse model of a lysosomal disease. To introduce a 2 bp mutation commonly found in patients with Morquio syndrome type B, a donor oligonucleotide encoding the mutated sequence was used. Sequencing of potential founders showed that two mice had undergone HDR, and contained the *Glb1*^{W274L} mutation. The second potential repair pathway following double-stranded DNA cleavage is NHEJ. Of the offspring sequenced, one was found to contain a 20 bp deletion that resulted in a frameshift and 3 premature stop codons, removing the catalytic nucleophile of the β-gal enzyme. By using CRISPR-Cas9, this was all accomplished in a single experiment, showing just how powerful this system is for genome modification.

To determine whether these mutations resulted in a phenotype that is similar to human patients, these mice were characterized. Chapter III investigated the phenotype of mice harboring a 20 bp mutation in the *Glb1* gene, which resulted in a loss of β-gal enzyme activity and subsequent accumulation of GM1 and GA1 ganglioside within the CNS and visceral tissue. Further, this ganglioside accumulation resulted in a severe neurological phenotype in these mice, which presented as a loss of motor function and cognitive ability. This observation of motor dysfunction is a phenotype described significantly in previous reports [157-160]. However, this was the first description that mice lacking β-gal enzyme activity are also cognitively impaired. It will be key to use these tests as outcome measures for novel therapies for this disease, because it will be important that the treatment reaches all parts of the CNS.

In Chapter IV, the initial characterization experiments of the mouse harboring the common Morquio syndrome type B mutation, *Glb1*^{W274L} (position 273 in humans) showed that this mutation recapitulated the human β-gal enzyme deficiency, as mice had between 8.4%-13.3% of wildtype β-gal enzyme activity. This is the first description of a mouse model that has residual β-gal enzyme activity. However, even though the enzyme activity was approximately 10% of wildtype levels, these mice showed no visible phenotype, even after a year. It was surprising that this minimal enzyme activity did not produce a phenotype at all. This is an important observation, because if 10% of normal enzyme activity is enough to keep up with the catabolism of the target macromolecules, this should be the goal of any potential therapies for these diseases. This level of activity has previously been assumed to be the minimum activity to prevent storage in lysosomal diseases [312]. One way to test whether this is a possible "threshold" of minimum enzyme activity is to cross β-gal deficient mice to *Glb1*^{W274L} mice to reduce the enzyme activity even further and see whether a neurological phenotype arises.

With the murine models of GM1-gangliosidosis and Morquio syndrome type B established, the most important next step is to utilize them in developing a new therapy. In Chapter V, preliminary experiments are discussed regarding a proprietary gene therapy system that is designed to integrate the human *GLB1* cDNA into the albumin locus of neonatal β-gal$^{-/-}$ mice. This system was designed to express the *GLB1* transgene under the regulation of the albumin promoter. Preliminary data from these experiments showed that functional β-gal protein

was being synthesized and secreted into the bloodstream. While the data was limited, β-gal enzyme activity was present in the liver and spleen of two of the three animals analyzed. Additionally, even though plasma β-gal activity was maintained for 120 days at heterozygous levels and found in peripheral tissue, the level of β-gal expression was not sufficient to prevent the onset of neurological symptoms of the disease. In current and future experiments, it will be important to determine a dose that is effective to treat both the CNS and the systemic disease. One alternative approach, instead of using more vector, is to create a cDNA encoding a fusion protein. This has been applied for enzyme replacement therapy in pre-clinical studies for lysosomal diseases. For MPS I [192] and GM1-gangliosidosis [187], the ribosome-inactivating toxin B subunit (RTB) lectin, which exploits endocytic pathways to enter cells, was fused to IDUA and β-gal, respectively. While only shown to be functional *in vitro* with β-gal, the fusion construct was shown to improve neurocognitive function and reduce GAG accumulation in MPS I mice. A similar approach has been applied with a monoclonal antibody against the human insulin receptor for treating MPS I [313]. These both could be applied to treating the CNS disease of GM1-gangliosidosis.

For Morquio syndrome type B, developing a novel gene therapy will require addressing several challenges. This is because it is primarily a skeletal disease, and targeting the skeletal system through metabolic cross-correction is especially difficult due to the bone being located in an avascular area. One way to increase delivery and target the bone and cartilage is to fuse an aspartic acid octapeptide (D8) to the β-gal protein. This has been shown to be effective when

fused to alkaline phosphatase [314] and the lysosomal enzymes β-glucuronidase [315] and *N*-acetylgalactosamine-6-sulfatase [316]. Alternatively, pharmacological chaperone therapy with small molecules could be utilized to treat Morquio syndrome type B or any β-gal deficient patients with missense mutations. Proof-of-principle experiments have been conducted on various lysosomal diseases using pharmacological chaperones [183, 317-321].

Further, an aspect to take into consideration for therapy of these diseases is timing of the treatment. Most in the field of lysosomal diseases believe that the earlier the treatment, the better the outcome will be for the patient. However, even when a patient is treated when symptoms arise around 6 months of age, irreversible damage has occurred. In MPS I, mouse fetuses deficient for IDUA have a significant accumulation of GAG, suggesting that the disease starts *in utero* (Figure 30). This may be the case in GM1-gangliosidosis as well. It was reported that a premature fetus lacking β-gal enzyme activity displayed a vacuolated phenotype in the basal ganglions of the brain [322]. Additionally, many newborns with lysosomal diseases present with nonimmune hydrops, which is an abnormal accumulation of fluid in two or more fetal compartments [323, 324]. Because these symptoms arise *in utero*, current therapeutic timing may not be sufficient to prevent the onset of the disease. With the advancements of *in utero* prenatal screening tests, including genetic screening, it may be important to begin testing and treating these patients in the fetal stage of development. Many groups have done pre-clinical *in utero* experiments for various diseases [325-327], however their use in human patients in clinical trials

has not been tested yet and will require further assessment for safety and efficacy.

Closing Remark

Collectively, the studies conducted and described in this dissertation provide hope for patients and families suffering from β-galactosidase deficiencies. Two new models of these diseases now exist and are being utilized for the development of a new therapy that has shown promising preliminary results. Knowing that a similar gene therapy system has been approved and implemented in clinical trials for other lysosomal diseases should provide a clear and concise path to treatment once more pre-clinical studies have been conducted with the system described above. We show that this system can produce catalytically active β-gal enzyme that is secreted into the bloodstream and be measured in peripheral tissue. Once the appropriate dose is determined, this therapy could be utilized as a platform strategy to treat most lysosomal diseases, in addition to many other monogenic diseases.

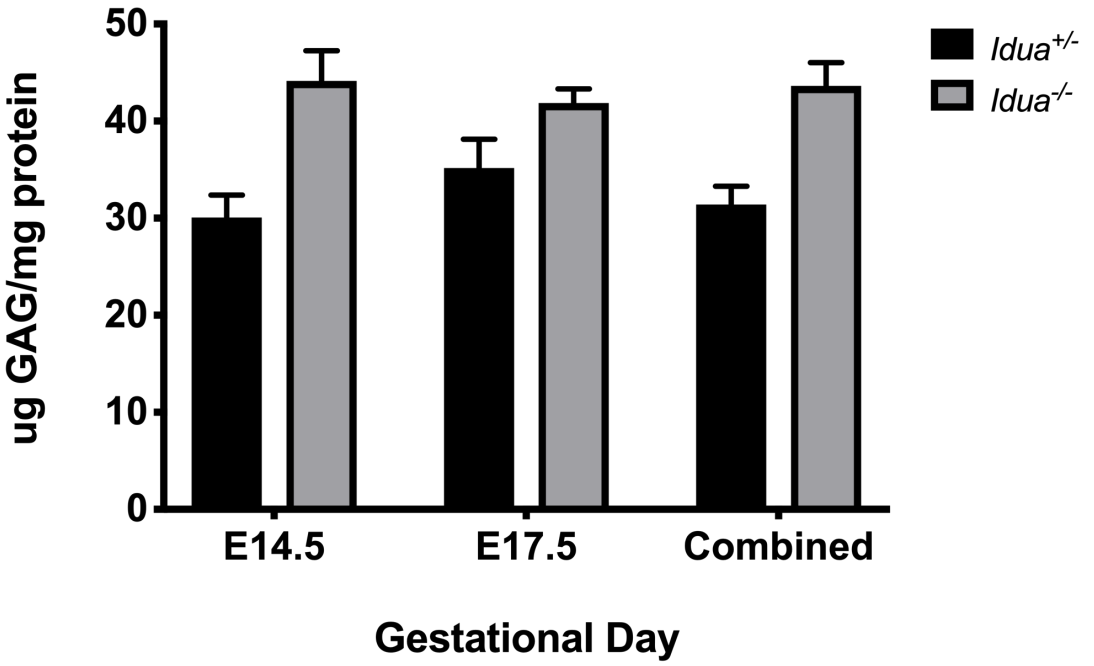

Figure 30. Significant accumulation of glycosaminoglycans in fetal MPS I mice. MPS I (*Idua*$^{-/-}$) and heterozygous control (*Idua*$^{+/-}$) embryos were isolated at embryonic days E14.5 and E17.5, homogenized, and assessed for glycosaminoglycan (GAG) content with the Blyscan™ Glycasaminoglycan Assay (Biocolor Ltd, United Kingdom). Data are presented as mean ± SEM. ***p≤0.001.

Bibliography

[1] M. Fuller, P.J. Meikle, J.J. Hopwood, Epidemiology of lysosomal storage diseases: an overview, in: A. Mehta, M. Beck, S.-P. G. (Eds.), Fabry Disease: Perspectives from 5 Years of FOS, Oxford PharmaGenesis, Oxford, 2006.
[2] F.M. Platt, B. Boland, A.C. van der Spoel, The cell biology of disease: lysosomal storage disorders: the cellular impact of lysosomal dysfunction J Cell Biol 199 (2012) 723-734.
[3] Y. Suzuki, E. Nanba, J. Matsuda, K. Higaki, A. Oshima, Beta-galactosidase deficiency (beta-galactosidosis): GM1 gangliosidosis and Morquio B disease., in: C.R. Scriver, A.L. Beaudet, W.S. Sly, D. Valle (Eds.), The metabolic and molecular basis of inherited disease, McGraw-Hill, New York, 2001, pp. 3775-3809.
[4] Y. Yamamoto, C.A. Hake, B.M. Martin, K.A. Kretz, A.J. Ahern-Rindell, S.L. Naylor, M. Mudd, J.S. O'Brien, Isolation, characterization, and mapping of a human acid β-galactosidase cDNA DNA and Cell Biology 9 (1990) 119-127.
[5] T. Yakano, Y. Yamanouchi, Assignment of human β-galactosidase-A gene to 3p21.33 by fluorescence in situ hybridization Human Genetics 92 (1993) 403-404.
[6] H. Morreau, N.J. Galjart, N. Gillemans, R. Willemsen, G.T. van der Horst, A. d'Azzo, Alternative splicing of β-galactosidase mRNA generates the classic lysosomal enzyme and a β-galactosidase-related protein The Journal of Biological Chemistry 264 (1989) 20655-20663.
[7] A. Hinek, M. Rabinovitch, F. Keeley, Y. O'kamura-Oho, J. Callahan, The 67-kD elastin/laminin-binding protein is related to an enzymatically inactive, alternative spliced form of β-galactosidase Journal of Clinical Investigation 91 (1993) 1198-1205.
[8] A. Hinek, A.V. Pshezhetsky, M. von Itzstein, B. Starcher, Lysosomal sialidase (neuraminidase-1) is targeted to the cell surface in a multiprotein complex that facilitates elastic fiber assembly J Biol Chem 281 (2006) 3698-3710.
[9] A. Hinek, T.D. Bodnaruk, S. Bunda, Y. Wang, K. Liu, Neuraminidase-1, a subunit of the cell surface elastin receptor, desialylates and functionally inactivates adjacent receptors interacting with the mitogenic growth factors PDGF-BB and IGF-2 Am J Pathol 173 (2008) 1042-1056.
[10] A. Hinek, F.W. Keeley, J. Callahan, Recycling of the 67-kDa elastin binding protein in arterial myocytes is imperative for secretion of tropoelastin Experimental Cell Research 220 (1995) 312-324.
[11] A. Scandolera, L. Odoul, S. Salesse, A. Guillot, S. Blaise, C. Kawecki, P. Maurice, H. El Btaouri, B. Romier-Crouzet, L. Martiny, L. Debelle, L. Duca, The Elastin Receptor Complex: A Unique Matricellular Receptor with High Anti-tumoral Potential Front Pharmacol 7 (2016) 32.
[12] S. Privitera, C.A. Prody, J.W. Callahan, A. Hinek, The 67-kDa enzymatically inactive alternatively spliced variant of β-galactosidase is identical to the elastin/laminin-binding protein The Journal of Biological Chemistry 273 (1998) 6319-6326.

[13] L. Duca, N. Floquet, A.J. Alix, B. Haye, L. Debelle, Elastin as a matrikine Crit Rev Oncol Hematol 49 (2004) 235-244.
[14] L. Duca, C. Blanchevoye, B. Cantarelli, C. Ghoneim, S. Dedieu, F. Delacoux, W. Hornebeck, A. Hinek, L. Martiny, L. Debelle, The elastin receptor complex transduces signals through the catalytic activity of its Neu-1 subunit J Biol Chem 282 (2007) 12484-12491.
[15] A. Oshima, A. Tsuji, Y. Nagao, H. Sakuraba, Y. Suzuki, Cloning, sequencing, and expression of cDNA for human β-galactosidase. Biochem Biophys Res Commun 157 (1988) 238-244.
[16] J.W. Callahan, Molecular basis of GM1 gangliosidosis and Morquio disease, type B. Structure-function studies of lysosomal β-galactosidase and the non-lysosomal β-galactosidase-like protein. Biochemica et Biophysica Acta 1455 (1999) 85-103.
[17] S. Zhang, J.D. McCarter, Y. Okamura-Oho, F. Yaghi, A. Hinek, S.G. Withers, J.W. Callahan, Kinetic mechanism and characterization of human β-galactosidase precursor secreted by permanently transfected Chinese hamster ovary cells Biochemical Journal 304 (1994) 281-288.
[18] A. van der Spoel, E. Bonten, A. d'Azzo, Processing of lysosomal β-galactosidase, the c-terminal precursor fragment is an essential domain of the mature enzyme The Journal of Biological Chemistry 275 (2000) 10035-10040.
[19] Y. Okamura-Oho, S. Zhang, W. Hilson, A. Hinek, J.W. Callahan, Early proteolytic cleavage with loss of a C-terminal fragment underlies altered processing of the β-galactosidase precursor in galactosialidosis. Biochem J. 313 (1996) 787-794.
[20] Y. Okamura-Oho, S. Zhang, J.W. Callahan, M. Murata, A. Oshima, Y. Suzuki, Maturation and degradation of β-galactosidase in the post-Golgi compartment are regulated by cathepsin B and a non-cysteine protease. FEBS Letters 419 (1997) 231-234.
[21] A. van der Spoel, E. Bonten, A. d'Azzo, Processing of lysosomal β-galactosidase, the c-terminal precursor fragment is an essential domain of the mature enzyme. The Journal of Biological Chemistry 275 (2000) 10035-10040.
[22] A. D'Azzo, A. Hoogeveen, A.J.J. Reuser, D. Robinson, H. Galjaard, Molecular defect in combined β-galactosidase and neuraminidase deficiency in man. Proc Natl Acad Sci U S A 79 (1982) 4535-4539.
[23] J.D. McCarter, D.L. Burgoyne, S. Miao, S. Zhang, J.W. Callahan, S.G. Wither, Identification of Glu-268 as the catalytic nucleophile of human lysosomal β-galactosidase precursor by mass spectrometry. The Journal of Biological Chemistry 272 (1997) 396-400.
[24] U. Ohto, K. Usui, T. Ochi, K. Yuki, Y. Satow, T. Shimizu, Crystal structure of human beta-galactosidase: structural basis of Gm1 gangliosidosis and morquio B diseases. J Biol Chem 287 (2012) 1801-1812.
[25] P.D. Stenson, M. Mort, E.V. Ball, K. Evans, M. Hayden, S. Heywood, M. Hussain, A.D. Phillips, D.N. Cooper, The Human Gene Mutation Database: towards a comprehensive repository of inherited mutation data for medical

research, genetic diagnosis and next-generation sequencing studies. Hum Genet 136 (2017) 665-677.
[26] K. Yoshida, A. Oshima, M. Shimmoto, Y. Fukuhara, H. Sakuraba, N. Yanagisawa, Y. Suzuki, Human β-galactosidase gene mutations in GM1-gangliosidosis: a common mutation among Japanese adult/chronic cases. American Journal of Human Genetics 49 (1991) 435-442.
[27] K. Yoshida, A. Oshima, H. Sakuraba, T. Nakano, N. Yanagisawa, S.-i. Iwasaki, K. Takamiya, Y. Suzuki, GM1 gangliosidosis in adults: clinical and molecular analysis of 16 Japanese patients. Annals of Neurology 31 (1992) 328-332.
[28] J. Nishimoto, E. Nanba, K. Inui, S. Okada, K. Suzuki, GM1-gangliosidosis (genetic β-galactosidase deficiency): identification of four mutations in different clinical phenotypes among Japanese patients. American Journal of Human Genetics 49 (1991) 566-574.
[29] N.-C. Chiu, W.-H. Qian, A.L. Shanske, S.S. Brooks, R.-M. Boustany, A common mutation site in the β-galactosidase gene originates in Puerto Rico. Pediatric Neurology 14 (1996) 53-56.
[30] G. Mosna, S. Fattore, G. Tubiello, S. Brocca, E. Gianazza, R. Gatti, C. Danesino, A. Minelli, M. Piantanida, A homozygous missense arginine to histidine substitution at position 482 of the β-galactosidase in an Italian infantile GM1-gangliosidosis patient. Human Genetics 90 (1992) 247-250.
[31] N. Ishii, T. Oohira, A. Oshima, H. Sakuraba, F. Endo, I. Matsuda, K. Sukegawa, T. Orii, Y. Suzuki, Clinical and molecular analysis of a Japanese boy with Morquio B disease. Clinical Genetics 48 (1995) 103-108.
[32] A. Oshima, K. Yoshida, M. Shimmoto, Y. Fukuhara, H. Sakuraba, Y. Suzuki, Human β-galactosidase gene mutations in Morquio B Disease. American Journal of Human Genetics 49 (1991) 1091-1093.
[33] L. Ou, M.J. Przybilla, C.B. Whitley, SAAMP 2.0: An algorithm to predict genotype-phenotype correlation of lysosomal storage diseases. Clin Genet 93 (2018) 1008-1014.
[34] A. Hinek, S. Zhang, A.C. Smith, J.W. Callahan, Impaired elastic-fiber assembly by fibroblasts from patients with either Morquio B disease or infantile GM1-gangliosidosis is linked to deficiency in the 67-kD spliced variant of beta-galactosidase. Am J Hum Genet 67 (2000) 23-36.
[35] A. Caciotti, M.A. Donati, T. Bardelli, A. d'Azzo, G. Massai, L. Luciani, E. Zammarchi, A. Morrone, Primary and secondary elastin-binding protein defect leads to impaired elastogenesis in fibroblasts from GM1-gangliosidosis patients. American Journal of Pathology 167 (2005) 1689-1698.
[36] R.M. Norman, H. Urich, A.H. Tingey, R.A. Goodbody, Tay-Sachs' disease with visceral involvement and its relationship to Niemann-Pick's disease. J. Path. Bact. 78 (1959) 409-421.
[37] B.H. Landing, F.N. Silverman, J.M. Craig, M.D. Jacoby, M.E. Lahey, D.L. Chadwick, Familial neurovisceral lipidosis, an analysis of eight cases of a syndrome previously reported as "Hurler-Variant," "Pseudo-Hurler disease," and

“Tay-Sachs disease with visceral involvement”. American Journal of Diseases of Children 108 (1964) 503-522.
[38] J.S. O’Brien, M.B. Stern, B.H. Landing, J.K. O’Brien, G.N. Donnell, Generalized gangliosidosis, another inborn error of ganglioside metabolism? American Journal of Diseases of Children 109 (1965) 338-346.
[39] S. Okada, J.S. O’Brien, Generalized gangliosidosis: beta-galactosidase deficiency. Science 160 (1968) 1002-1004.
[40] S.-C. Li, Y.-T. Li, S. Moriya, T. Miyagi, Degradation of GM1 and GM2 by mammalian sialidases. Biochemical Journal 360 (2001) 233-237.
[41] J.W. Callahan, L.S. Wolfe, Isolation and characterization of keratan sulfates from the liver of a patient with GM1-gangliosidosis type I. Biochimica et Biophysica Acta 215 (1970) 527-543.
[42] N. Brunetti-Pierri, F. Scaglia, GM1 gangliosidosis: review of clinical, molecular, and therapeutic aspects. Mol Genet Metab 94 (2008) 391-396.
[43] M.H. Severini, C. Silva, A. Sopelsa, J.C. Coelho, R. Giugliani, High frequency of type 1 GM1 gangliosidosis in southern Brazil. Clinical Genetics 56 (1999) 168-169.
[44] I. Sinigerska, D. Chandler, V. Vaghjiani, I. Hassanova, R. Gooding, A. Morrone, I. Kremensky, L. Kalaydjieva, Founder mutation causing infantile GM1-gangliosidosis in the Gypsy population. Mol Genet Metab 88 (2006) 93-95.
[45] H.M. Lenicker, P. Vassallo Agius, E.P. Young, S.P. Attard Montalto, Infantile generalized GM1 gangliosidosis: high incidence in the Maltese islands. Journal of Inherited Metabolic Diseases 20 (1997) 723-724.
[46] J.P. Shield, J. Stone, C.G. Steward, Bone marrow transplantation correcting beta-galactosidase activity does not influence neurological outcome in juvenile GM1-gangliosidosis. J Inherit Metab Dis 28 (2005) 797-798.
[47] J.R. Jarnes Utz, S. Kim, K. King, R. Ziegler, L. Schema, E.S. Redtree, C.B. Whitley, Infantile gangliosidoses: mapping a timeline of clinical changes. Mol Genet Metab 121 (2017) 170-179.
[48] R.K. Yu, Y. Nakatani, M. Yanagisawa, The role of glycosphingolipid metabolism in the developing brain. J Lipid Res 50 Suppl (2009) S440-445.
[49] E. Posse de Chaves, S. Sipione, Sphingolipids and gangliosides of the nervous system in membrane function and dysfunction. FEBS Lett 584 (2010) 1748-1759.
[50] A. Prinetti, N. Loberto, V. Chigorno, S. Sonnino, Glycosphingolipid behaviour in complex membranes. Biochim Biophys Acta 1788 (2009) 184-193.
[51] B. Wang, J. Brand-Miller, The role and potential of sialic acid in human nutrition. Eur J Clin Nutr 57 (2003) 1351-1369.
[52] S. Ngamukote, M. Yanagisawa, T. Ariga, S. Ando, R.K. Yu, Developmental changes of glycosphingolipids and expression of glycogenes in mouse brains. J Neurochem 103 (2007) 2327-2341.
[53] L. Svennerholm, K. Bostrom, P. Fredman, J.-E. Mansson, B. Rosengren, B.-M. Rynmark, Human brain gangliosides: developmental changes from early fetal stage to advanced age. Biochimica et Biophysica Acta 1005 (1989) 109-117.

[54] I. Kracun, H. Rosner, V. Drnovsek, M. Heffer-Lauc, C. Cosovic, G. Lauc, Human brain gangliosides in development, aging and disease. International Journal of Developmental Biology 35 (1991) 289-295.
[55] M.C. Nowycky, G. Wu, R.W. Ledeen, Glycobiology of ion transport in the nervous system, in: R. Yu, C. Schengrund (Eds.), Glycobiology of the nervous system. Advances in Neurobiology, Springer, New York, NY, 2014.
[56] E. Bieberich, S. MacKinnon, J. Silva, R.K. Yu, Regulation of apoptosis during neuronal differentiation by ceramide and b-series complex gangliosides. J Biol Chem 276 (2001) 44396-44404.
[57] M. Okada, M. Itoh Mi, M. Haraguchi, T. Okajima, M. Inoue, H. Oishi, Y. Matsuda, T. Iwamoto, T. Kawano, S. Fukumoto, H. Miyazaki, K. Furukawa, S. Aizawa, K. Furukawa, B-series Ganglioside deficiency exhibits no definite changes in the neurogenesis and the sensitivity to Fas-mediated apoptosis but impairs regeneration of the lesioned hypoglossal nerve. J Biol Chem 277 (2002) 1633-1636.
[58] G. Wu, Z.H. Lu, J. Wang, Y. Wang, X. Xie, M.F. Meyenhofer, R.W. Ledeen, Enhanced susceptibility to kainate-induced seizures, neuronal apoptosis, and death in mice lacking gangliotetraose gangliosides: protection with LIGA 20, a membrane-permeant analog of GM1. J Neurosci 25 (2005) 11014-11022.
[59] H. Rahmann, Brain gangliosides and memory function. Behav Brain Res 66 (1995) 105-116.
[60] K. Simons, D. Toomre, Lipid rafts and signal transduction. Nature Reviews Molecule and Cell Biology 1 (2000) 31-41.
[61] S. Sonnino, L. Mauri, V. Chigorno, A. Prinetti, Gangliosides as components of lipid membrane domains. Glycobiology 17 (2007) 1R-13R.
[62] R.W. Ledeen, G. Wu, The multi-tasked life of GM1 ganglioside, a true factotum of nature. Trends Biochem Sci 40 (2015) 407-418.
[63] J. Holmgren, I. Lonnroth, J.-E. Mansson, L. Svennerholm, Interaction of cholera toxin and membrane GM1 ganglioside of small intestine. Proc Natl Acad Sci U S A 72 (1975) 2520-2524.
[64] J. Fantini, N. Yahi, N. Garmy, Cholesterol accelerates the binding of Alzheimer's β-amyloid peptide to ganglioside GM1 through a universal hydrogen-bond-dependent sterol tuning of glycolipid conformation. Front Phys 4 (2013) 1-10.
[65] J. Fantini, N. Yahi, Molecular basis for the glycosphingolipid-binding specificity of alpha-synuclein: key role of tyrosine 39 in membrane insertion. J Mol Biol 408 (2011) 654-669.
[66] K. Ikeda, T. Yamaguchi, S. Fukunaga, M. Hoshino, K. Matsuzaki, Mechanism of amyloid beta-protein aggregation mediated by GM1 ganglioside clusters. Biochemistry 50 (2011) 6433-6440.
[67] Z. Martinez, M. Zhu, S. Han, A.L. Fink, GM1 specifically interacts with α-synuclein and inhibits fibrillation. Biochemistry 46 (2007) 1868-1877.

[68] G. Wu, Z.H. Lu, N. Kulkarni, R.W. Ledeen, Deficiency of ganglioside GM1 correlates with Parkinson's disease in mice and humans. J Neurosci Res 90 (2012) 1997-2008.
[69] F.H. Geisler, F.C. Dorsey, W.P. Coleman, Recovery of motor function after spinal-cord injury - a randomized, placebo-controlled trial with GM1-ganglioside. The New England Journal of Medicine 324 (1991) 1829-1838.
[70] F.H. Geisler, W.P. Coleman, G. Grieco, D. Poonian, S.S. Group, The Syngen multicenter acute spinal cord injury study. Spine 26 (2001) S87-S98.
[71] V. Rubovitch, Y. Zilberstein, J. Chapman, S. Schreiber, C.G. Pick, Restoring GM1 ganglioside expression ameliorates axonal outgrowth inhibition and cognitive impairments induced by blast traumatic brain injury. Sci Rep 7 (2017) 41269.
[72] M. Hadjiconstantinou, A.P. Mariani, N.H. Neff, GM1 ganglioside-induced recovery of nigrostriatal dopaminergic neurons after MPTP: an immunohistochemical study. Brain Research 484 (1989) 297-303.
[73] J.S. Schneider, A. Kean, L. DiStefano, GM1 ganglioside rescues substantia nigra pars compacta neurons and increases dopamine synthesis in residual nigrostriatal dopaminergic neurons in MPTP-treated mice. Journal of Neuroscience Research 42 (1995) 117-123.
[74] J.S. Schneider, A. Pope, K. Simpson, J. Taggart, M.G. Smith, L. DiStefano, Recovery from experimental parkinsonism in primates with GM1 ganglioside treatment. Science 256 (1992) 843-846.
[75] J.S. Schneider, S. Sendek, C. Daskalakis, F. Cambi, GM1 ganglioside in Parkinson's disease: Results of a five year open study. J Neurol Sci 292 (2010) 45-51.
[76] J.S. Schneider, S.M. Gollomp, S. Sendek, A. Colcher, F. Cambi, W. Du, A randomized, controlled, delayed start trial of GM1 ganglioside in treated Parkinson's disease patients. Journal of the Neurological Sciences 324 (2013) 140-148.
[77] L. Svennerholm, G. Brane, I. Karlsson, A. Lekman, I. Ramstrom, C. Wikkelso, Alzheimer disease - effect of continous intracerebroventricular treatment with GM1 ganglioside and a systematic activation programme. Dementia and Geriatric Cognitive Disorders 14 (2002) 128-136.
[78] A. Di Pardo, V. Maglione, M. Alpaugh, M. Horkey, R.S. Atwal, J. Sassone, A. Ciammola, J.S. Steffan, K. Fouad, R. Truant, S. Sipione, Ganglioside GM1 induces phosphorylation of mutant huntingtin and restores normal motor behavior in Huntington disease mice. Proc Natl Acad Sci U S A 109 (2012) 3528-3533.
[79] M. Jeyakumar, Central nervous system inflammation is a hallmark of pathogenesis in mouse models of GM1 and GM2 gangliosidosis. Brain 126 (2003) 974-987.
[80] V.L. Dawson, T.M. Dawson, Nitric oxide in neurodegeneration, Nitric Oxide in Brain Development, Plasticity, and Disease, 1998, pp. 215-229.
[81] P.J.L.M. Strijbos, Nitric oxide in cerebral ischemic neurodegeneration and excitotoxicity. Critical Reviews in Neurobiology 12 (1998) 223-243.

[82] M.K. Barthwal, N. Srivastava, M. Dikshit, Role of nitric oxide in a progressive neurodegeneration model of Parkinson's disease in the rat. Redox Rep 6 (2001) 297-302.
[83] S.M. de la Monte, J.R. Wands, Alzheimer's disease is type 3 diabetes - evidence reviewed. Journal of Diabetes Science and Technology 2 (2008) 1101-1113.
[84] A. Tessitore, P.M.M. del, R. Sano, Y. Ma, L. Mann, A. Ingrassia, E.D. Laywell, D.A. Steindler, L.M. Hendershot, A. d'Azzo, GM1-ganglioside-mediated activation of the unfolded protein response causes neuronal death in a neurodegenerative gangliosidosis. Mol Cell 15 (2004) 753-766.
[85] W. Paschen, Endoplasmic reticulum: a primary target in various acute disorders and degenerative diseases of the brain. Cell Calcium 34 (2003) 365-383.
[86] R. Sano, I. Annunziata, A. Patterson, S. Moshiach, E. Gomero, J. Opferman, M. Forte, A. d'Azzo, GM1-ganglioside accumulation at the mitochondria-associated ER membranes links ER stress to Ca(2+)-dependent mitochondrial apoptosis. Mol Cell 36 (2009) 500-511.
[87] A. Takamura, K. Higaki, K. Kajimaki, S. Otsuka, H. Ninomiya, J. Matsuda, K. Ohno, Y. Suzuki, E. Nanba, Enhanced autophagy and mitochondrial aberrations in murine G(M1)-gangliosidosis. Biochem Biophys Res Commun 367 (2008) 616-622.
[88] M.C. Maiuri, E. Zalckvar, A. Kimchi, G. Kroemer, Self-eating and self-killing: crosstalk between autophagy and apoptosis. Nature Reviews Molecular Cell Biology 8 (2007) 741-752.
[89] J.H. Zhu, C. Horbinski, F. Guo, S. Watkins, Y. Uchiyama, C.T. Chu, Regulation of autophagy by extracellular signal-regulated protein kinases during 1-methyl-4-phenylpyridinium-induced cell death. Am J Pathol 170 (2007) 75-86.
[90] P.I. Moreira, S.L. Siedlak, X. Wang, M.S. Santos, C.R. Oliveira, M. Tabaton, A. Nunomura, L.I. Szweda, G. Aliev, M.A. Smith, X. Zhu, G. Perry, Autophagocytosis of mitochondria is prominent in Alzheimer disease. Journal of Neuropathology & Experimental Neurology 66 (2007) 525-532.
[91] A. Yamamoto, M.L. Cremona, J.E. Rothman, Autophagy-mediated clearance of huntingtin aggregates triggered by the insulin-signaling pathway. The Journal of Cell Biology 172 (2006) 719-731.
[92] M. Koike, M. Shibata, S. Waguri, K. Yoshimura, I. Tanida, E. Kominami, T. Gotow, C. Peters, K. von Figura, N. Mizushima, P. Saftig, Y. Uchiyama, Participation of autophagy in storage of lysosomes in neurons from mouse models of neuronal ceroid-lipofuscinoses (Batten Disease). The American Journal of Pathology 167 (2005) 1713-1728.
[93] T. Fukuda, L. Ewan, M. Bauer, R.J. Mattaliano, K. Zaal, E. Ralston, P.H. Plotz, N. Raben, Dysfunction of endocytic and autophagic pathways in a lysosomal storage disease. Ann Neurol 59 (2006) 700-708.
[94] C.D. Pacheco, R. Kunkel, A.P. Lieberman, Autophagy in Niemann-Pick C disease is dependent upon Beclin-1 and responsive to lipid trafficking defects. Hum Mol Genet 16 (2007) 1495-1503.

[95] J.S. O'Brien, E. Gugler, A. Giedion, U. Wiessmann, N. Herschkowitz, Spondyloepiphyseal dysplasia, corneal clouding, normal intelligence and acid β-galactosidase deficiency. Clinical Genetics 9 (1976) 495-504.
[96] A.I. Arbisser, K.A. Donnelly, C.I. Scott Jr, N. DiFerrante, J. Singh, R.E. Stevenson, A.S. Aylesworth, R.R. Howell, Morquio-like syndrome with beta galactosidase deficiency and normal hexosamine sulfatase activity: mucopolysaccharidosis IVB. American Journal of Medical Genetics 1 (1977) 195-205.
[97] J.E. Trojak, C.K. Ho, R.A. Roesel, L.S. Levin, S.E. Kopits, G.H. Thomas, S. Toma, Morquio-like syndrome (MPS IVB) associated with deficiency of a beta-galactosidase. Johns Hopkins Medical Journal 146 (1980) 75-79.
[98] E. Pronicka, A. Tylki, B. Czartoryska, D. Gorska, Three cases of beta-galactosidase deficiency. Klinische Padiatrie 193 (1981) 343-346.
[99] D. Hofer, K. Paul, K. Fantur, M. Beck, F. Burger, C. Caillaud, K. Fumic, J. Ledvinova, A. Lugowska, H. Michelakakis, B. Radeva, U. Ramaswami, B. Plecko, E. Paschke, GM1 gangliosidosis and Morquio B disease: expression analysis of missense mutations affecting the catalytic site of acid beta-galactosidase. Hum Mutat 30 (2009) 1214-1221.
[100] Y. Tatano, N. Takeuchi, J. Kuwahara, H. Sakuraba, T. Takahashi, G. Takada, K. Itoh, Elastogenesis in cultured dermal fibroblasts from patients with lysosomal β-galactosidase, protective protein/cathepsin A and neuraminidase-1 deficiencies. The Journal of Medical Investigation 53 (2006) 103-112.
[101] R. Santamaria, A. Chabas, J.W. Callahan, D. Grinberg, L. Vilageliu, Expression and characterization of 14 GLB1 mutant alleles found in GM1-gangliosidosis and Morquio B patients. J Lipid Res 48 (2007) 2275-2282.
[102] E. Paschke, I. Milos, H. Kreimer-Erlacher, G. Hoefler, M. Beck, M. Hoeltzenbein, W. Kleijer, T. Levade, H. Michelakakis, R. B, Mutation analyses in 17 patients with deficiency in acid β-galactosidase: three novel point mutations and high correlation of mutation W273L with Morquio disease type B. Human Genetics 109 (2001) 159-166.
[103] M. Beck, E.M. Petersen, J. Spranger, P. Beighton, Morquio's disease type B (beta-galactosidase deficiency) in three siblings. South African Medical Journal 72 (1987) 704-707.
[104] J. Nelson, J. Crowhurst, B. Carey, L. Greed, Incidence of the mucopolysaccharidoses in Western Australia. Am J Med Genet A 123A (2003) 310-313.
[105] J. Nelson, Incidence of the mucopolysaccharidoses in Northern Ireland. Human Genetics 101 (1997) 355-358.
[106] H.-Y. Lin, S.-P. Lin, C.-K. Chuang, D.-M. Niu, M.-R. Chen, F.-J. Tsai, M.-C. Chao, P.-C. Chiu, S.-J. Lin, L.-P. Tsai, W.-L. Hwu, J.-L. Lin, Incidence of the mucopolysaccharidoses in Taiwan, 1984-2004. American Journal of Medical Genetics Part A 149A (2009) 960-964.
[107] F. Baehner, C. Schmiedeskamp, F. Krummenauer, E. Miebach, M. Bajbouj, C. Whybra, A. Kohlschutter, C. Kampmann, M. Beck, Cumulative

incidence rates of the mucopolysaccharidoses in Germany. J Inherit Metab Dis 28 (2005) 1011-1017.
[108] H. Groebe, M. Krins, H. Schmidberger, K. von Figura, K. Harzer, H. Kresse, E. Paschke, A. Sewell, K. Ullrich, Morquio syndrome (mucopolysaccharidosis IV b) associated with beta-galactosidase deficiency. Report of two cases. American Journal of Human Genetics 32 (1980) 258-272.
[109] J.J. van Gemund, M.A.H. Giesberts, R.F. Eerdmans, W. Blom, W.J. Kleijer, Morquio-B disease, spondyloepiphyseal dysplasia associated with acid β-galactosidase deficiency. Report of three cases in one family Human Genetics 64 (1983) 50-54.
[110] R. Giugliani, M. Jackson, S.J. Skinner, C.M. Vimal, A.H. Fensom, N. Fahmy, A. Sjovall, P.F. Benson, Progressive mental regression in siblings with Morquio disease type B (mucopolysaccharidosis IV B). Clinical Genetics 32 (1987) 313-325.
[111] F. Kubaski, H.H. Kecskemethy, H.T. Harcke, S. Tomatsu, Bone mineral density in mucopolysaccharidosis IVB. Mol Genet Metab Rep 8 (2016) 80-84.
[112] R. Santamaria, A. Chabas, M.J. Coll, C.S. Miranda, L. Vilageliu, D. Grinberg, Twenty-one novel mutations in the GLB1 gene identified in a large group of GM1-gangliosidosis and Morquio B patients: possible common origin for the prevalent p.R59H mutation among gypsies. Hum Mutat 27 (2006) 1060.
[113] J.L. Funderburgh, Keratan sulfate: structure, biosynthesis, and function. Glycobiology 10 (2000) 951-958.
[114] B. Caterson, J. Melrose, Keratan sulfate, a complex glycosaminoglycan with unique functional capability. Glycobiology 28 (2018) 182-206.
[115] J.L. Funderburgh, M.M. Mann, M.L. Funderburgh, Keratocyte phenotype mediates proteoglycan structure: a role for fibroblasts in corneal fibrosis. J Biol Chem 278 (2003) 45629-45637.
[116] F. Bettelheim, A., B. Plessy, The hydration of proteoglycans of bovine cornea. Biochemica et Biophysica Acta 381 (1975) 203-214.
[117] Y. Sommarin, M. Wendel, Z. Shen, U. Hellman, Osteoadherin, a cell-binding keratan sulfate proteoglycan in bone, belongs to the family of leucine-rich repeat proteins of the extracellular matrix. The Journal of Biological Chemistry 273 (1998) 16723-17629.
[118] K. Ninomiya, T. Miyamoto, J. Imai, N. Fujita, T. Suzuki, R. Iwasaki, M. Yagi, S. Watanabe, Y. Toyama, T. Suda, Osteoclastic activity induces osteomodulin expression in osteoblasts. Biochem Biophys Res Commun 362 (2007) 460-466.
[119] M. Zanetti, Two subpopulations of differentiated chondrocytes identified with a monoclonal antibody to keratan sulfate. The Journal of Cell Biology 101 (1985) 53-59.
[120] P.J. Roughley, J.S. Mort, The role of aggrecan in normal and osteoarthritic cartilage. Journal of Experimental Orthopaedics 1 (2014).
[121] C. Kiani, L. Chen, Y.J. Wu, A.J. Yee, B.B. Yang, Structure and function of aggrecan. Cell Research 12 (2002) 19-32.

[122] S. Muthupalani, P.A. Torres, B.C. Wang, B.J. Zeng, S. Eaton, I. Erdelyi, R. Ducore, R. Maganti, J. Keating, B.J. Perry, F.S. Tseng, N. Waliszewski, M. Pokras, R. Causey, R. Seger, P. March, A. Tidwell, R. Pfannl, T. Seyfried, E.H. Kolodny, J. Alroy, GM1-gangliosidosis in American black bears: clinical, pathological, biochemical and molecular genetic characterization. Mol Genet Metab 111 (2014) 513-521.
[123] W.J.C. Donnelly, B.J. Sheahan, T.A. Rogers, GM1 gangliosidosis in friesian calves. The Journal of Pathology 111 (1973) 173-179.
[124] W.J. Donnelly, B.J. Sheahan, M. Kelly, Beta-galactosidase deficiency in GM1 gangliosidosis of Friesian calves. Res. Vet Sci. 15 (1973) 139-141.
[125] A.J. Ahern-Rindell, D.J. Prieur, R.D. Murnane, S.S. Raghavan, P.F. Daniel, R.H. McCluer, S.U. Walkley, S.M. Parish, Inherited lysosomal storage disease associated with deficiencies of β-galactosidase and α-neuraminidase in sheep. American Journal of Medical Genetics 31 (1988) 39-56.
[126] R.D. Murnane, D.J. Prieur, A.J. Ahern-Rindell, S.M. Parish, L.L. Collier, The lesions of an ovine lysosomal storage disease. Initial characterization. American Journal of Pathology 134 (1989) 263-270.
[127] B.J. Skelly, M. Jeffrey, R.J. Franklin, B.J. Winchester, A new form of ovine GM1-gangliosidosis. Acta Neuropathologica 89 (1995) 374-379.
[128] S.J. Ryder, M.M. Simmons, A lysosomal storage disease of Romney sheep that resembles human type 3 GM1 gangliosidosis. Acta Neuropathologica 101 (2001) 255-228.
[129] D.H. Read, D.D. Harrington, T.W. Keenan, E.J. Hinsman, Neuronal-visceral GM1 gangliosidosis in a dog with β-galactosidase deficiency. Science 194 (1976) 442-445.
[130] M. Rodriguez, J.S. O'Brien, R.S. Garrett, H.C. Powell, Canine GM1 gangliosidosis: an ultrastructural and biochemical study. Journal of Neuropathology & Experimental Neurology 41 (1982) 618-629.
[131] J. Alroy, U. Ograd, A.A. Ucci, S.H. Schelling, K.L. Schunk, C.D. Warren, S.S. Raghavan, E.H. Kolodny, Neurovisceral and skeletal GM1-gangliosidosis in dogs with β-galactosidase deficiency. Science 229 (1985) 470-472.
[132] J. Alroy, U. Orgad, R. DeGasperi, R. Richard, C.D. Warren, K. Knowles, J.G. Thalhammer, S.S. Raghavan, Canine GM1-gangliosidosis, a clinical, morphologic, histochemical, and biochemical comparison of two different models. American Journal of Pathology 140 (1992) 675-689.
[133] G.K. Saunders, P.A. Wood, R.K. Myers, L.G. Shell, R. Carithers, GM1 gangliosidosis in Portuguese Water Dogs: pathological and biochemical findings. Vet. Pathol. 25 (1988) 265-269.
[134] Z.H. Wang, B. Zeng, H. Shibuya, G.S. Johnson, J. Alroy, G.M. Pastores, S. Raghavan, E.H. Kolodny, Isolation and characterization of the normal canine β-galactosidase gene and its mutation in a dog model of GM1-gangliosidosis. Journal of Inherited Metabolic Diseases 23 (2000) 593-606.
[135] G. Müller, W. Baumgartner, A. Moritz, A. Sewell, B. Kustermann-Kuhn, Biochemical findings in a breeding colony of Alaskan Huskies suffering from GM1-gangliosidosis. Journal of Inherited Metabolic Diseases 21 (1998) 430-431.

[136] G. Müller, S. Alldinger, A. Moritz, A. Zurbriggen, N. Kirchhof, A. Sewell, W. Baumgärtner, GM1-gangliosidosis in Alaskan huskies: clinical and pathologic findings. Veterinary Pathology 38 (2001) 281-290.
[137] R. Kreutzer, T. Leeb, G. Muller, A. Moritz, W. Baumgartner, A duplication in the canine beta-galactosidase gene GLB1 causes exon skipping and GM1-gangliosidosis in Alaskan huskies. Genetics 170 (2005) 1857-1861.
[138] O. Yamato, Y. Masuoka, M. Tajima, S. Omae, Y. Maede, K. Ochiai, E. Hayashida, T. Umemura, M. Iijima, GM1 gangliosidosis in shiba dogs. Veterinary Record 146 (2000) 493-496.
[139] O. Yamato, Y. Masuoka, M. Yonemura, A. Hatakeyama, H. Satoh, A. Kobayashi, M. Nakayama, T. Asano, T. Shoda, M. Yamasaki, K. Ochiai, T. Umemura, Y. Maede, Clinical and clinico-pathologic characteristics of shiba dogs with a deficiency of lysosomal acid β-galactosidase: a canine model of human GM1 gangliosidosis. The Journal of Veterinary Medical Science 65 (2003) 213-217.
[140] D. Hasegawa, O. Yamato, Y. Nakamoto, T. Ozawa, A. Yabuki, K. Itamoto, T. Kuwabara, M. Fujita, K. Takahashi, S. Mizoguchi, H. Orima, Serial MRI features of canine GM1 gangliosidosis: a possible imaging biomarker for diagnosis and progression of the disease. Scientific World Journal (2012) 250197.
[141] M.M. Uddin, S. Arata, Y. Takeuchi, H.-S. Chang, K. Mizukami, A. Yabuki, M.M. Rahman, M. Kohyama, M.A. Hossain, K. Takayama, O. Yamato, Molecular epidemiology of canine GM1 gangliosidosis in the Shiba Inu breed in Japan: relationship between regional prevalence and carrier frequency. BMC Veterinary Research 9 (2013) 1-5.
[142] H.J. Baker Jr, J.R. Lindsey, G.M. McKhann, D.F. Farrell, Neuronal GM1 gangliosidosis in a siamese cat with β-galactosidase deficiency. Science 174 (1971) 838-839.
[143] D.F. Farrell, H.J. Baker Jr, R.M. Herndon, J.R. Lindsey, G.M. McKhann, Feline GM1 gangliosidosis: biochemical and ultrastructural comparisons with the disease in man. Journal of Neuropathology and Experimental Neurology 32 (1973) 1-18.
[144] R. De Maria, S. Divari, S. Bo, S. Sonnino, D. Lotti, M.T. Capucchio, M. Castagnaro, β-galactosidase deficiency in a Korat cat: a new form of feline GM1-gangliosidosis. Acta Neuropathologica 96 (1998) 307-314.
[145] C.G. Barker, W.F. Blakemore, A. Dell, A.C. Palmer, P.R. Tiller, B.G. Winchester, GM1 gangliosidosis (type I) in a cat. Biochemical Journal 235 (1986) 151-158.
[146] I.C. Barnes, D.F. Kelly, C.A. Pennock, A.J. Randell, Hepatic beta galactosidase and feline GM1 gangliosidosis. Neuropathology and Applied Neurobiology 7 (1981) 463-476.
[147] J.A. Murray, W.F. Blakemore, K.C. Barnett, Ocular lesions in cats with GM1-gangliosidosis with visceral involvement. The Journal of Small Animal Practice 18 (1977) 1-10.

[148] Y. Kawasaki, I. Nagatani, Y. Terashima, H. Koike, N. Miyoshi, A. Oishi, Assessment of neuological function in three cats with homozygous or heterozygous GM1-gangliosidosis by brainstem auditory evoked potential. Journal of the Japan Veterinary Medical Association 62 (2009) 148-154.
[149] H. Ueno, O. Yamato, T. Sugiura, M. Kohyama, A. Yabuki, K. Miyoshi, K. Matsuda, T. Uchide, GM1 gangliosidosis in a Japanese domestic cat: a new variant identified in Hokkaido, Japan. J Vet Med Sci 78 (2016) 91-95.
[150] M.M. Uddin, M.A. Hossain, M.M. Rahman, M.A. Chowdhury, T. Tanimoto, A. Yabuki, K. Mizukami, H.-S. Chang, O. Yamato, Identification of Bangladeshi Domestic cats with GM1 gangliosidosis caused by the c.1448G^|^gt;C mutation of the feline GLB1 gene: case study. Journal of Veterinary Medical Science 75 (2013) 395-397.
[151] C.N. Hahn, M. del Pilar Martin, M. Schröder, M.T. Vanier, Y. Hara, K. Suzuki, K. Suzuki, A. d'Azzo, Generalized CNS disease and massive GM1-ganglioside accumulation in mice defective in lysosomal acid β-galactosidase. Human Molecular Genetics 6 (1997) 205-211.
[152] J. Matsuda, O. Suzuki, A. Oshima, A. Ogura, Y. Noguchi, Y. Yamamoto, T. Asano, K. Takimoto, K. Sukegawa, Y. Suzuki, M. Naiki, β-Galactosidase-deficient mouse as an animal model for GM1-gangliosidosis. Glycoconjugate Journal 14 (1997) 729-736.
[153] M. Capecchi, Altering the genome by homologous recombination. Science 244 (1989) 1288-1292.
[154] H. Tanaka, K. Suzuki, Substrate specificities of the two genetically distinct human brain β-galactosidases. Brain Research 122 (1977) 325-335.
[155] J. Matsuda, O. Suzuki, A. Oshima, A. Ogura, M. Naiki, Y. Suzuki, Neurological manifestations of knockout mice with β-galactosidase deficiency. Brain & Development 19 (1997) 19-20.
[156] L. Mangiarini, K. Sathasivam, M. Seller, B. Cozens, A. Harper, C. Hetherington, M. Lawton, Y. Trottier, G.P. Bates, Exon 1 of the HD gene with an expanded CAG repeat is sufficient to cause a progressive neurological phenotype in transgenic mice. Cell 87 (1996) 493-506.
[157] R. Sano, A. Tessitore, A. Ingrassia, A. d'Azzo, Chemokine-induced recruitment of genetically modified bone marrow cells into the CNS of GM1-gangliosidosis mice corrects neuronal pathology. Blood 106 (2005) 2259-2268.
[158] S. Ichinomiya, H. Watanabe, K. Maruyama, H. Toda, H. Iwasaki, M. Kurosawa, J. Matsuda, Y. Suzuki, Motor and reflex testing in GM1-gangliosidosis model mice. Brain Dev 29 (2007) 210-216.
[159] R.C. Baek, M.L. Broekman, S.G. Leroy, L.A. Tierney, M.A. Sandberg, A. d'Azzo, T.N. Seyfried, M. Sena-Esteves, AAV-mediated gene delivery in adult GM1-gangliosidosis mice corrects lysosomal storage in CNS and improves survival. PLoS One 5 (2010) e13468.
[160] C.M. Weismann, J. Ferreira, A.M. Keeler, Q. Su, L. Qui, S.A. Shaffer, Z. Xu, G. Gao, M. Sena-Esteves, Systemic AAV9 gene transfer in adult GM1 gangliosidosis mice reduces lysosomal storage in CNS and extends lifespan. Hum Mol Genet 24 (2015) 4353-4364.

[161] R. Barrangou, C. Fremaux, H. Deveau, M. Richards, P. Boyaval, S. Moineau, D.A. Romero, P. Horvath, CRISPR provides acquired resistance against viruses in prokaryotes. Science 315 (2007) 1709-1712.
[162] M. Jinek, K. Chylinski, I. Fonfara, M. Hauer, J.A. Doudna, E. Charpentier, A programmable dual-RNA-guided DNA endonuclease in adaptive bacterial immunity. Science 337 (2012) 816-821.
[163] F.J. Mojica, C. Diez-Villasenor, J. Garcia-Martinez, C. Almendros, Short motif sequences determine the targets of the prokaryotic CRISPR defence system. Microbiology 155 (2009) 733-740.
[164] D.C. Swarts, C. Mosterd, M.W. van Passel, S.J. Brouns, CRISPR interference directs strand specific spacer acquisition. PLoS One 7 (2012) e35888.
[165] C. Wyman, R. Kanaar, DNA double-strand break repair: all's well that ends well. Annu Rev Genet 40 (2006) 363-383.
[166] L.S. Symington, J. Gautier, Double-strand break end resection and repair pathway choice. Annu Rev Genet 45 (2011) 247-271.
[167] J.R. Chapman, M.R. Taylor, S.J. Boulton, Playing the end game: DNA double-strand break repair pathway choice. Mol Cell 47 (2012) 497-510.
[168] F.M. Platt, G.R. Neises, G. Reinkensmeier, M.J. Townsend , V.H. Perry, R.L. Proia, B. Winchester, R.A. Dwek, T.D. Butters, Prevention of lysosomal storage in Tay-Sachs mice treated with N-butyldeoxynojirimycin. Science 276 (1997) 428-431.
[169] J.L. Kasperzyk, M.M. El-Abbadi, E.C. Hauser, A. D'Azzo, F.M. Platt, T.N. Seyfried, N-butyldeoxygalactonojirimycin reduces neonatal brain ganglioside content in a mouse model of GM1 gangliosidosis. J Neurochem 89 (2004) 645-653.
[170] D.S. Regier, R.L. Proia, A. D'Azzo, C.J. Tifft, The GM1 and GM2 gangliosidosis: natural history and progress toward therapy. Pediatric Endocrinology Reviews 13 Suppl 1 (2016) 663-673.
[171] B. Bembi, F. Marchetti, V.I. Guerci, G. Ciana, R. Addobbati, D. Grasso, R. Barone, R. Cariati, L. Fernandez-Guillen, T. Butters, M.G. Pittis, Substrate reduction therapy in the infantile form of Tay-Sachs disease. Neurology 66 (2006) 278-280.
[172] G.H. Maegawa, P.L. van Giersbergen, S. Yang, B. Banwell, C.P. Morgan, J. Dingemanse, C.J. Tifft, J.T. Clarke, Pharmacokinetics, safety and tolerability of miglustat in the treatment of pediatric patients with GM2 gangliosidosis. Mol Genet Metab 97 (2009) 284-291.
[173] B.E. Shapiro, G.M. Pastores, J. Gianutsos, C. Luzy, E.H. Kolodny, Miglustat in late-onset Tay-Sachs disease: a 12-month, randomized, controlled clinical study with 24 months of extended treatment. Genet Med 11 (2009) 425-433.
[174] F. Deodato, E. Procopio, A. Rampazzo, R. Taurisano, M.A. Donati, C. Dionisi-Vici, A. Caciotti, A. Morrone, M. Scarpa, The treatment of juvenile/adult GM1-gangliosidosis with Miglustat may reverse disease progression. Metab Brain Dis 32 (2017) 1529-1536.

[175] J.C. Fratantoni, C.W. Hall, E.F. Neufeld, Hurler and Hunter syndromes: mutual correction of the defect in cultured fibroblasts. Science 162 (1968) 570-572.
[176] R. Kornfeld, S. Kornfeld, Assembly of asparagine-linked oligosaccharides. Annual Review of Biochemistry 51 (1985) 631-664.
[177] S. Kornfeld, Trafficking of lysosomal enzymes in normal and disease states. Journal of Clinical Investigation 77 (1986) 1-6.
[178] K. von Figura, A. Hasilik, Lysosomal enzymes and their receptors. Annual Review of Biochemistry 55 (1986) 167-193.
[179] A. Gonzalez-Noriega, J.H. Grubb, V. Talkad, W.S. Sly, Chloroquine inhibits lysosomal enzyme pinocytosis and enhances lysosomal enzyme secretion by impairing receptor recycling. The Journal of Cell Biology 85 (1980) 839-852.
[180] G.D. Vladutiu, M.C. Rattazzi, Excretion-reuptake route of beta-hexosaminidase in normal and I-cell disease cultured fibroblasts. Journal of Clinical Investigation 63 (1979) 595-601.
[181] L. Tominaga, Y. Ogawa, M. Taniguchi, K. Ohno, J. Matsuda, A. Oshima, Y. Suzuki, E. Nanba, Galactonojirimycin derivatives restore mutant human β-galactosidase activities expressed in fibroblasts from enzyme-deficient knockout mouse. Brain & Development 23 (2001) 284-287.
[182] J.-Q. Fan, S. Ishii, N. Asano, Y. Suzuki, Accelerated transport and maturation of lysosomal α–galactosidase A in Fabry lymphoblasts by an enzyme inhibitor. Nature Medicine 5 (1999) 112-115.
[183] J. Matsuda, O. Suzuki, A. Oshima, Y. Yamamoto, A. Noguchi, K. Takimoto, M. Itoh, Y. Matsuzaki, Y. Yasuda, S. Ogawa, Y. Sakata, E. Nanba, K. Higaki, Y. Ogawa, L. Tominaga, K. Ohno, H. Iwasaki, H. Watanabe, R.O. Brady, Y. Suzuki, Chemical chaperone therapy for brain pathology in G(M1)-gangliosidosis. Proc Natl Acad Sci U S A 100 (2003) 15912-15917.
[184] R.J. Desnick, E.H. Schuchman, Enzyme replacement therapy for lysosomal diseases: lessons from 20 years of experience and remaining challenges. Annu Rev Genomics Hum Genet 13 (2012) 307-335.
[185] G.D. Reynolds, H.J. Baker, R.H. Reynolds, Enzyme replacement using liposome carriers in feline GM1 gangliosidosis fibroblasts. Nature 275 (1978) 754-755.
[186] T.I. Samoylova, D.R. Martin, N.E. Morrison, M. Hwang, A.M. Cochran, A.M. Samoylov, H.J. Baker, N.R. Cox, Generation and characterization of recombinant feline beta-galactosidase for preclinical enzyme replacement therapy studies in GM1 gangliosidosis. Metab Brain Dis 23 (2008) 161-173.
[187] J. Condori, W. Acosta, J. Ayala, V. Katta, A. Flory, R. Martin, J. Radin, C.L. Cramer, D.N. Radin, Enzyme replacement for GM1-gangliosidosis: Uptake, lysosomal activation, and cellular disease correction using a novel beta-galactosidase:RTB lectin fusion. Mol Genet Metab 117 (2016) 199-209.
[188] K. Sandvig, B. van Deurs, Endocytosis and intracellular transport of ricin: recent discoveries. FEBS Letters 452 (1999) 67-70.

[189] M.R. Jackman, W. Shurety, J.A. Ellis, J.P. Luzio, Inhibition of apical but not basolateral endocytosis of ricin and folate in Caco-2 cells by cytochalasin D. Journal of Cell Science 107 (1994) 2547-2556.
[190] A.E. Frankel, T. Fu, C. Burbage, E. Tagge, B. Harris, J. Vesely, M.C. Willingham, Lectin-deficient ricin toxin intoxicates cells bearing the D-mannose receptor. Carbohydrate Research 300 (1997) 251-258.
[191] B.M. Simmons, P.D. Stahl, J.H. Russell, Mannose receptor-mediated uptake of ricin toxin and ricin A chain by macrophages. Multiple intracellular pathways for a chain translocation. The Journal of Biological Chemistry 261 (1986) 7912-7920.
[192] L. Ou, M.J. Przybilla, B. Koniar, C.B. Whitley, RTB lectin-mediated delivery of lysosomal alpha-l-iduronidase mitigates disease manifestations systemically including the central nervous system. Mol Genet Metab 123 (2018) 105-111.
[193] L. Ou, T.L. Herzog, C.M. Wilmot, C.B. Whitley, Standardization of alpha-L-iduronidase enzyme assay with Michaelis-Menten kinetics. Mol Genet Metab 111 (2014) 113-115.
[194] U. Matte, G. Baldo, R. Giugliani, Non viral gene transfer approaches for lysosomal storage disorders, in: X. Yuan (Ed.), Non-Viral Gene Therapy, Intech Open, 2011.
[195] A. Herschhorn, A. Hizi, Retroviral reverse transcriptases. Cell Mol Life Sci 67 (2010) 2717-2747.
[196] M. Sena-Esteves, S.M. Camp, J. Alroy, X.O. Breakefield, E.M. Kaye, Correction of acid β-galactosidase deficiency in GM1 gangliosidosis human fibroblasts by retrovirus vector-mediated gene transfer: higher efficiency of release and cross-correction by the murine enzyme. Human Gene Therapy 11 (2000) 715-727.
[197] L. Naldini, U. Blomer, F.H. Gage, D. Trono, I.M. Verma, Efficient transfer, integration, and sustained long-term expression of the transgene in adult rat brains injected with a lentiviral vector. Proc Natl Acad Sci U S A 93 (1996) 11382-11388.
[198] L. Naldini, U. Blomer, P. Gallay, D. Ory, R. Mulligan, F.H. Gage, I.M. Verma, D. Trono, In vivo gene delivery and stable transduction of nondividing cells by a lentiviral vector. Science 272 (1996) 263-267.
[199] H. Kobayashi, D. Carbonaro, K. Pepper, D. Petersen, S. Ge, H. Jackson, H. Shimada, R. Moats, D.B. Kohn, Neonatal gene therapy of MPS I mice by intravenous injection of a lentiviral vector. Mol Ther 11 (2005) 776-789.
[200] C. Di Domenico, G.R.D. Villani, D. Di Napoli, E. Gonzalez Y Reyero, A. Lombardo, L. Naldini, P. Di Natale, Gene therapy for a Mucopolysaccharidosis type I murine model with lentiviral-IDUA vector. Human Gene Therapy 16 (2005) 81-90.
[201] M. Cavazzana-Calvo, E. Payen, O. Negre, G. Wang, K. Hehir, F. Fusil, J. Down, M. Denaro, T. Brady, K. Westerman, R. Cavallesco, B. Gillet-Legrand, L. Caccavelli, R. Sgarra, L. Maouche-Chretien, F. Bernaudin, R. Girot, R. Dorazio, G.J. Mulder, A. Polack, A. Bank, J. Soulier, J. Larghero, N. Kabbara, B. Dalle, B.

Gourmel, G. Socie, S. Chretien, N. Cartier, P. Aubourg, A. Fischer, K. Cornetta, F. Galacteros, Y. Beuzard, E. Gluckman, F. Bushman, S. Hacein-Bey-Abina, P. Leboulch, Transfusion independence and HMGA2 activation after gene therapy of human beta-thalassaemia. Nature 467 (2010) 318-322.
[202] A. Aiuti, L. Biasco, S. Scaramuzza, F. Ferrua, M.P. Cicalese, C. Baricordi, F. Dionisio, A. Calabria, S. Giannelli, M.C. Castiello, M. Bosticardo, C. Evangelio, A. Assanelli, M. Casiraghi, S. Di Nunzio, L. Callegaro, C. Benati, P. Rizzardi, D. Pellin, C. Di Serio, M. Schmidt, C. Von Kalle, J. Gardner, N. Mehta, V. Neduva, D.J. Dow, A. Galy, R. Miniero, A. Finocchi, A. Metin, P.P. Banerjee, J.S. Orange, S. Galimberti, M.G. Valsecchi, A. Biffi, E. Montini, A. Villa, F. Ciceri, M.G. Roncarolo, L. Naldini, Lentiviral hematopoietic stem cell gene therapy in patients with Wiskott-Aldrich syndrome. Science 341 (2013) 1233151.
[203] N. Cartier, S. Hacein-Bey-Abina, C.C. Bartholomae, G. Veres, M. Schmidt, I. Kutschera, M. Vidaud, U. Abel, L. Dal-Cortivo, L. Caccavelli, N. Mahlaoui, V. Kiermer, D. Mittelstaedt, C. Bellesme, N. Lahlou, F. Lefrere, S. Blanche, M. Audit, E. Payen, P. Leboulch, B. l'Homme, P. Bougneres, C. Von Kalle, A. Fischer, M. Cavazzana-Calvo, P. Aubourg, Hematopoietic stem cell gene therapy with a lentiviral vector in X-linked adrenoleukodystrophy. Science 326 (2009) 818-823.
[204] A. Ciuffi, Mechanisms governing lentivirus integration site selection. Current Gene Thearpy 8 (2008) 419-429.
[205] A. Biffi, C.C. Bartholomae, D. Cesana, N. Cartier, P. Aubourg, M. Ranzani, M. Cesani, F. Benedicenti, T. Plati, E. Rubagotti, S. Merella, A. Capotondo, J. Sgualdino, G. Zanetti, C. von Kalle, M. Schmidt, L. Naldini, E. Montini, Lentiviral vector common integration sites in preclinical models and a clinical trial reflect a benign integration bias and not oncogenic selection. Blood 117 (2011) 5332-5339.
[206] J. Matrai, M.K. Chuah, T. VandenDriessche, Recent advances in lentiviral vector development and applications. Mol Ther 18 (2010) 477-490.
[207] A.J. Berk, Adenoviridae, in: K. D.M., P.M. Howley (Eds.), Fields Virology, Lippincott WIlliams & Wilkins, Philadelphia, PA, 2013, pp. 1704-1731.
[208] O. Meier, U.F. Greber, Adenovirus endocytosis. J Gene Med 6 Suppl 1 (2004) S152-163.
[209] M.A. Kay, J.C. Glorioso, L. Naldini, Viral vectors for gene therapy: the art of turning infectious agents into vehicles of therapeutics. Nature Medicine 7 (2001) 33-40.
[210] M.S. Horwitz, Adenoviruses., in: B. Fields, K. D.M., P.M. Howley, C. R.M. (Eds.), Fields Virology, Lippincott-Raven, Philadelphia, Pennsylvania, 1996, pp. 2149-2171.
[211] N. Takaura, T. Yagi, M. Maeda, E. Nanba, A. Oshima, Y. Suzuki, T. Yamano, A. Tanaka, Attenuation of ganglioside GM1 accumulation in the brain of GM1 gangliosidosis mice by neonatal intravenous gene transfer. Gene Therapy 10 (2003) 1487-1493.
[212] Gene Therapy Clinical Trials Worldwide, in: M. Edelstein (Ed.), John WIley and Sons Ltd, Journal of Gene Medicine, 2018.

[213] R.W. Atchison, B.C. Casto, W.M. Hammon, Adenovirus-associated defective virus particles. Science 149 (1965) 754-755.
[214] M.D. Hoggan, N.R. Blacklow, W.P. Rowe, Studies of small DNA viruses found in various adenovirus preparations: physical, biological, and immunological characteristics. Proc Natl Acad Sci U S A 55 (1966) 1467-1474.
[215] J.E. Conway, S. Zolotukhin, N. Muzyczka, G.S. Hayward, B.J. Byrne, Recombinant adeno-associated virus type 2 replication and packaging is entirely supported by a herpes simplex virus type 1 amplican expressing rep and cap. Journal of Virology 71 (1997) 8780-8789.
[216] J.A. Rose, J.V. Maizel, J.K. Inman, A.J. Shatkin, Structural proteins of adenovirus-associated viruses. Journal of Virology 8 (1971) 766-770.
[217] R.J. Samulski, N. Muzyczka, AAV-mediated gene therapy for research and therapeutic purposes. Annu Rev Virol 1 (2014) 427-451.
[218] L.Y. Huang, S. Halder, M. Agbandje-McKenna, Parvovirus glycan interactions. Curr Opin Virol 7 (2014) 108-118.
[219] J.S. Bartlett, R. Wilcher, R.J. Samulski, Infectious entry pathway of aden-associated virus and adeno-associated virus vectors. Journal of Virology 74 (2000) 2777-2785.
[220] M. Nonnenmacher, T. Weber, Adeno-associated virus 2 infection requires endocytosis through the CLIC/GEEC pathway. Cell Host Microbe 10 (2011) 563-576.
[221] G.P. Gao, M.R. Alvira, L. Wang, R. Calcedo, J. Johnston, J.M. Wilson, Novel adeno-associated viruses from rhesus monkeys as vectors for human gene therapy. Proc Natl Acad Sci U S A 99 (2002) 11854-11859.
[222] G. Gao, L.H. Vandenberghe, M.R. Alvira, Y. Lu, R. Calcedo, X. Zhou, J.M. Wilson, Clades of Adeno-associated viruses are widely disseminated in human tissues. J Virol 78 (2004) 6381-6388.
[223] S. Mori, L. Wang, T. Takeuchi, T. Kanda, Two novel adeno-associated viruses from cynomolgus monkey: pseudotyping characterization of capsid protein. Virology 330 (2004) 375-383.
[224] M. Schmidt, E. Grot, P. Cervenka, S. Wainer, C. Buck, J.A. Chiorini, Identification and characterization of novel adeno-associated virus isolates in ATCC virus stocks. J Virol 80 (2006) 5082-5085.
[225] G. Gao, L.H. Vandenberghe, J.M. Wilson, New recombinant serotypes of AAV vectors. Current Gene Thearpy 5 (2005) 285-297.
[226] J.S. Bartlett, R.J. Samulski, T.J. McCown, Selective and rapid uptake of adeno-associated virus type 2 in brain. Human Gene Therapy 9 (1998) 1181-1186.
[227] A.C. Fischer, S.E. Beck, C.I. Smith, B.L. Laube, F.B. Askin, S.E. Guggino, R.J. Adams, T.R. Flotte, W.B. Guggino, Successful transgene expression with serial doses of aerosolized rAAV2 vectors in rhesus macaques. Molecular Therapy 8 (2003) 918-926.
[228] S.A. Nicklin, H. Buening, K.L. Dishart, M. de Alwis, A. Girod, U. Hacker, A.J. Thrasher, R.R. Ali, M. Hallek, A.H. Baker, Efficient and selective AAV2-

mediated gene transfer directed to human vascular endothelial cells. Mol Ther 4 (2001) 174-181.
[229] J.E. Rabinowitz, W. Xiao, R.J. Samulski, Insertional mutagenesis of AAV2 capsid and the production of recombinant virus. Virology 265 (1999) 274-285.
[230] W. Shi, J.S. Bartlett, RGD inclusion in VP3 provides adeno-associated virus type 2 (AAV2)-based vectors with a heparan sulfate-independent cell entry mechanism. Molecular Therapy 7 (2003) 515-525.
[231] H. Nakai, S. Fuess, T.A. Storm, S. Muramatsu, Y. Nara, M.A. Kay, Unrestricted hepatocyte transduction with adeno-associated virus serotype 8 vectors in mice. J Virol 79 (2005) 214-224.
[232] N. Kaludov, B. Handelman, J.A. Chiorini, Scalable purification of aden-associated virus type 2, 4, or 5 using ion-exchange chromatography. Human Gene Therapy 13 (2002) 1235-1243.
[233] C. Summerford, R.J. Samulski, Viral receptors and vector purification: new approaches for generating clinical-grade reagents. Nature Medicine 5 (1999) 587-588.
[234] R.M. Kotin, M. Siniscalco, R.J. Samulski, X. Zhu, L. Hunter, C.A. Laughlin, S. McLaughlin, N. Muzyczka, M. Rocchi, K. Berns, Site-specific integration by adeno-associated virus. Proc Natl Acad Sci U S A 87 (1990) 2211-2215.
[235] R.M. Kotin, J.C. Menninger, D.C. Ward, K.I. Berns, Mapping and direct visualization of a region-specific viral DNA integration site on chromosome 19q13-qter. Genomics 10 (1991) 831-834.
[236] D.M. McCarty, S.M. Young, Jr., R.J. Samulski, Integration of adeno-associated virus (AAV) and recombinant AAV vectors. Annu Rev Genet 38 (2004) 819-845.
[237] K. Rapti, V. Louis-Jeune, E. Kohlbrenner, K. Ishikawa, D. Ladage, S. Zolotukhin, R.J. Hajjar, T. Weber, Neutralizing antibodies against AAV serotypes 1, 2, 6, and 9 in sera of commonly used animal models. Mol Ther 20 (2012) 73-83.
[238] M. Desrosiers, D. Dalkara, Neutralizing antibodies against adeno-associated virus (AAV): measurement and influence on retinal gene delivery, in: C. Boon, J. Wijnholds (Eds.), Retinal Gene Therapy. Methods in Molecular Biology, Humana Press, New York, NY, 2018.
[239] S.J. Gray, S. Nagabhushan Kalburgi, T.J. McCown, R. Jude Samulski, Global CNS gene delivery and evasion of anti-AAV-neutralizing antibodies by intrathecal AAV administration in non-human primates. Gene Ther 20 (2013) 450-459.
[240] J.R. Mendell, S. Al-Zaidy, R. Shell, W.D. Arnold, L.R. Rodino-Klapac, T.W. Prior, L. Lowes, L. Alfano, K. Berry, K. Church, J.T. Kissel, S. Nagendran, J. L'Italien, D.M. Sproule, C. Wells, J.A. Cardenas, M.D. Heitzer, A. Kaspar, S. Corcoran, L. Braun, S. Likhite, C. Miranda, K. Meyer, K.D. Foust, A.H.M. Burghes, B.K. Kaspar, Single-dose gene-replacement therapy for spinal muscular atrophy. N Engl J Med 377 (2017) 1713-1722.
[241] C. Mueller, G. Gernoux, A.M. Gruntman, F. Borel, E.P. Reeves, R. Calcedo, F.N. Rouhani, A. Yachnis, M. Humphries, M. Campbell-Thompson, L.

Messina, J.D. Chulay, B. Trapnell, J.M. Wilson, N.G. McElvaney, T.R. Flotte, 5 year expression and neutrophil defect repair after gene therapy in alpha-1 antitrypsin deficiency. Mol Ther 25 (2017) 1387-1394.
[242] A.C. Nathwani, U.M. Reiss, E.G. Tuddenham, C. Rosales, P. Chowdary, J. McIntosh, M. Della Peruta, E. Lheriteau, N. Patel, D. Raj, A. Riddell, J. Pie, S. Rangarajan, D. Bevan, M. Recht, Y.M. Shen, K.G. Halka, E. Basner-Tschakarjan, F. Mingozzi, K.A. High, J. Allay, M.A. Kay, C.Y. Ng, J. Zhou, M. Cancio, C.L. Morton, J.T. Gray, D. Srivastava, A.W. Nienhuis, A.M. Davidoff, Long-term safety and efficacy of factor IX gene therapy in hemophilia B. N Engl J Med 371 (2014) 1994-2004.
[243] A.W. Nienhuis, A.C. Nathwani, A.M. Davidoff, Gene therapy for hemophilia. Mol Ther 25 (2017) 1163-1167.
[244] L.A. George, S.K. Sullivan, A. Giermasz, J.E.J. Rasko, B.J. Samelson-Jones, J. Ducore, A. Cuker, L.M. Sullivan, S. Majumdar, J. Teitel, C.E. McGuinn, M.V. Ragni, A.Y. Luk, D. Hui, J.F. Wright, Y. Chen, Y. Liu, K. Wachtel, A. Winters, S. Tiefenbacher, V.R. Arruda, J.C.M. van der Loo, O. Zelenaia, D. Takefman, M.E. Carr, L.B. Couto, X.M. Anguela, K.A. High, Hemophilia B gene therapy with a high-specific-activity factor IX variant. N Engl J Med 377 (2017) 2215-2227.
[245] J. Bennett, J. Wellman, K.A. Marshall, S. McCague, M. Ashtari, J. DiStefano-Pappas, O.U. Elci, D.C. Chung, J. Sun, J.F. Wright, D.R. Cross, P. Aravand, L.L. Cyckowski, J.L. Bennicelli, F. Mingozzi, A. Auricchio, E.A. Pierce, J. Ruggiero, B.P. Leroy, F. Simonelli, K.A. High, A.M. Maguire, Safety and durability of effect of contralateral-eye administration of AAV2 gene therapy in patients with childhood-onset blindness caused by RPE65 mutations: a follow-on phase 1 trial. The Lancet 388 (2016) 661-672.
[246] I.J. Constable, C.M. Pierce, C.M. Lai, A.L. Magno, M.A. Degli-Esposti, M.A. French, I.L. McAllister, S. Butler, S.B. Barone, S.D. Schwartz, M.S. Blumenkranz, E.P. Rakoczy, Phase 2a randomized clinical trial: safety and post hoc analysis of subretinal rAAV.sFLT-1 for wet age-related macular degeneration. EBioMedicine 14 (2016) 168-175.
[247] E.P. Rakoczy, C.-M. Lai, A.L. Magno, M.E. Wikstrom, M.A. French, C.M. Pierce, S.D. Schwartz, M.S. Blumenkranz, T.W. Chalberg, M.A. Degli-Esposti, I.J. Constable, Gene therapy with recombinant adeno-associated vectors for neovascular age-related macular degeneration: 1 year follow-up of a phase 1 randomised clinical trial. The Lancet 386 (2015) 2395-2403.
[248] E.M. Agency, European Medicines Agency recommends first gene therapy for approval. 2012.
[249] FDA approves novel gene therapy to treat patients with a rare form of inherited vision loss. US Food and Drug Administration. 2017, US Food and Drug Administration Newsroom Website: Press Release.
[250] L. Ou, R.C. DeKelver, M. Rohde, S. Tom, R. Radeke, S. St. Martin, Y. Santiago, S. Sproul, M.J. Przybilla, B.L. Koniar, K.M. Podetz-Pedersen, K. Laoharawee, R.D. Cooksley, K.E. Meyer, M.C. Holmes, R.S. McIvor, T. Wechsler, C.B. Whitley, ZFN-mediated in vivo genome editing corrects murine

Hurler syndrome. Molecular Therapy (2018). https://doi.org/10.1016/j.ymthe.2018.10.018.
[251] K. Laoharawee, R.C. DeKelver, K.M. Podetz-Pedersen, M. Rohde, S. Sproul, H.O. Nguyen, T. Nguyen, S.J. St Martin, L. Ou, S. Tom, R. Radeke, K.E. Meyer, M.C. Holmes, C.B. Whitley, T. Wechsler, R.S. McIvor, Dose-dependent prevention of metabolic and neurologic disease in murine MPS II by ZFN-mediated in vivo genome editing Molecular Therapy 26 (2018) 1127-1136.
[252] M. Jasin, Genetic manipulation of genomes with rare-cutting endonucleases. Trends in Genetics 12 (1996) 224-228.
[253] Y.-G. Kim, J. Cha, S. Chandrasegaran, Hybrid restriction enzymes: zinc finger fusions to FokI cleavage domain. Proceedings of the National Academy of Sciences. 93 (1996) 1156-1160.
[254] M. Christian, T. Cermak, E.L. Doyle, C. Schmidt, F. Zhang, A. Hummel, A.J. Bogdanove, D.F. Voytas, Targeting DNA double-strand breaks with TAL effector nucleases. Genetics 186 (2010) 757-761.
[255] K. Suzuki, Cerebral GM1-gangliosidosis: chemical pathology of visceral organs. Science 159 (1968) 1471-1472.
[256] J.S. O'Brien, E. Giedion, A. Giedion, U. Wiessmann, N. Herschkowitz, C. Meier, J. Leroy, Sponyloepiphyseal dysplasia, corneal clouding, normal intelligence and acid β-galactosidase deficiency. Clinical Genetics 9 (1976) 495-504.
[257] P. Mali, L. Yang, K.M. Esvelt, J. Aach, M. Guell, J.E. DiCarlo, J.E. Norville, G.M. Church, RNA-guided human genome engineering via Cas9. Science 339 (2013) 823-826.
[258] Y. Fu, J.D. Sander, D. Reyon, V.M. Cascio, J.K. Joung, Improving CRISPR-Cas nuclease specificity using truncated guide RNAs. Nat Biotechnol 32 (2014) 279-284.
[259] T. Aida, K. Chiyo, T. Usami, H. Ishikubo, R. Imahashi, Y. Wada, K.F. Tanaka, T. Sakuma, T. Yamamoto, K. Tanaka, Cloning-free CRISPR/Cas system facilitates functional cassette knock-in in mice. Genome Biol 16 (2015) 87.
[260] W. Wang, P.M. Kutny, S.L. Byers, C.J. Longstaff, M.J. DaCosta, C. Pang, Y. Zhang, R.A. Taft, F.W. Buaas, H. Wang, Delivery of Cas9 protein into mouse zygotes through a series of electroporation dramatically increases the efficiency of model creation. J Genet Genomics 43 (2016) 319-327.
[261] S.T. Yen, M. Zhang, J.M. Deng, S.J. Usman, C.N. Smith, J. Parker-Thornburg, P.G. Swinton, J.F. Martin, R.R. Behringer, Somatic mosaicism and allele complexity induced by CRISPR/Cas9 RNA injections in mouse zygotes. Dev Biol 393 (2014) 3-9.
[262] G.E. Truett, P. Heeger, R.L. Mynatt, A.A. Truett, J.A. Walker, M.L. Warman, Preparation of PCR-quality mouse genomic DNA with hot sodium hydroxide and tris (HotSHOT). BioTechniques 29 (2000) 52-54.
[263] M. Stemmer, T. Thumberger, M. Del Sol Keyer, J. Wittbrodt, J.L. Mateo, CCTop: An intuitive, flexible and reliable CRISPR/Cas9 target prediction tool. PLoS One 10 (2015) e0124633.

[264] G. Ahmad, M. Amiji, Use of CRISPR/Cas9 gene-editing tools for developing models in drug discovery. Drug Discov Today 23 (2018) 519-533.
[265] R. Barrangou, J.A. Doudna, Applications of CRISPR technologies in research and beyond. Nat Biotechnol 34 (2016) 933-941.
[266] S.H. Sternberg, S. Redding, M. Jinek, E.C. Greene, J.A. Doudna, DNA interrogation by the CRISPR RNA-guided endonuclease Cas9. Nature 507 (2014) 62-67.
[267] C. Anders, O. Niewoehner, A. Duerst, M. Jinek, Structural basis of PAM-dependent target DNA recognition by the Cas9 endonuclease. Nature 513 (2014) 569-573.
[268] P. Mali, J. Aach, P.B. Stranges, K.M. Esvelt, M. Moosburner, S. Kosuri, L. Yang, G.M. Church, CAS9 transcriptional activators for target specificity screening and paired nickases for cooperative genome engineering. Nat Biotechnol 31 (2013) 833-838.
[269] P.D. Hsu, D.A. Scott, J.A. Weinstein, F.A. Ran, S. Konermann, V. Agarwala, Y. Li, E.J. Fine, X. Wu, O. Shalem, T.J. Cradick, L.A. Marraffini, G. Bao, F. Zhang, DNA targeting specificity of RNA-guided Cas9 nucleases. Nat Biotechnol 31 (2013) 827-832.
[270] V. Pattanayak, S. Lin, J.P. Guilinger, E. Ma, J.A. Doudna, D.R. Liu, High-throughput profiling of off-target DNA cleavage reveals RNA-programmed Cas9 nuclease specificity. Nat Biotechnol 31 (2013) 839-843.
[271] Y. Fu, J.A. Foden, C. Khayter, M.L. Maeder, D. Reyon, J.K. Joung, J.D. Sander, High-frequency off-target mutagenesis induced by CRISPR-Cas nucleases in human cells. Nat Biotechnol 31 (2013) 822-826.
[272] H. Yang, H. Wang, C.S. Shivalila, A.W. Cheng, L. Shi, R. Jaenisch, One-step generation of mice carrying reporter and conditional alleles by CRISPR/Cas-mediated genome engineering. Cell 154 (2013) 1370-1379.
[273] S. Kim, D. Kim, S.W. Cho, J. Kim, J.S. Kim, Highly efficient RNA-guided genome editing in human cells via delivery of purified Cas9 ribonucleoproteins. Genome Res 24 (2014) 1012-1019.
[274] X. Liang, J. Potter, S. Kumar, Y. Zou, R. Quintanilla, M. Sridharan, J. Carte, W. Chen, N. Roark, S. Ranganathan, N. Ravinder, J.D. Chesnut, Rapid and highly efficient mammalian cell engineering via Cas9 protein transfection. J Biotechnol 208 (2015) 44-53.
[275] H. Galjaard, A.J.J. Reuser, Clinical, biochemical and genetic heterogeneity in gangliosidoses, in: R.A. Harkness, F. Cockburn (Eds.), The Cultured Cell and Inherited Metabolic Disease, Springer, Dordrecht, 1977.
[276] L. Pinsky, E. Powell, J. Callahan, GM1-gangliosidosis types 1 and 2: enzymatic differences in cultured fibroblasts. Nature 228 (1970) 1093-1095.
[277] J.S. Kannebley, L. Silveira-Moriyama, L.O. Bastos, C.E. Steiner, Clinical findings and natural history in ten unrelated families with juvenile and adult GM1 gangliosidosis. JIMD Rep 24 (2015) 115-122.
[278] Y. Suzuki, T. Furukawa, A. Hoogeveen, F. Verheijen, H. Galjaard, Adult type GMl-gangliosidosis: A complementation study on somatic cell hybrids. Brain and Development 1 (1979) 83-86.

[279] K.J. Livak, T.D. Schmittgen, Analysis of relative gene expression data using real-time quantitative PCR and the 2(-Delta Delta C(T)) Method. Methods 25 (2001) 402-408.
[280] E.C. Hauser, J.L. Kasperzyk, A. d'Azzo, T.N. Seyfried, Inheritance of lysosomal acid β-galactosidase activity and gangliosides in crosses of DBA2J and knockout mice. Biochemical Genetics 42 (2004) 241-257.
[281] N. Kasai, L.O. Sillerud, R.K. Yu, A convenient method for the preparation of asialo-GM1. Lipids 17 (1982) 107-110.
[282] R.J. Carter, J. Morton, S.B. Dunnett, Motor coordination and balance in rodents. Current Protocols in Neuroscience (2001) 8.12.11-18.12.14.
[283] A.L. Southwell, J. Ko, P.H. Patterson, Intrabody gene therapy ameliorates motor, cognitive, and neuropathological symptoms in multiple mouse models of Huntington's disease. J Neurosci 29 (2009) 13589-13602.
[284] N. Ogawa, Y. Hirose, S. Ohara, T. Ono, Y. Watanabe, A simple quantitative bradykinesia test in MPTP-treated mice. Research Communications in Chemical Pathology and Pharmacology 50 (1985) 435-441.
[285] E. Hockly, B. Woodman, A. Mahal, C.M. Lewis, G. Bates, Standardization and statistical approaches to therapeutic trials in the R6/2 mouse. Brain Research Bulletin 61 (2003) 469-479.
[286] M. Jeyarkumar, T.D. Butters, M. Cortina-Borja, V. Hunnam, R.L. Proia, V.H. Perry, R.A. Dwek, F.M. Platt, Delayed symptom onset and increased life expectancy in Sandhoff disease mice treated with N-butyldeoxynojirimycin. Proc Natl Acad Sci U S A 96 (1999) 6388-6393.
[287] C.A. Barnes, Memory deficits associated with senescence: a neurophysiological and behavioral study in the rat. Journal of Comparative and Physiological Psychology 93 (1979) 74-104.
[288] R. Gerlai, A new continuous alternation task in T-maze detects hippocampal dysfunction in mice. A strain comparison and lesion study. Behavioural Brain Research 95 (1998) 91-101.
[289] A. Rosenberg, N. Stern, Changes in sphingosine and fatty acid components of the gangliosides in developing rat and human brain. Journal of Lipid Research 7 (1966) 122-131.
[290] B.F. Porter, B.C. Lewis, J.F. Edwards, J. Alroy, B.J. Zeng, P.A. Torres, K.N. Bretzlaff, E.H. Kolodny, Pathology of GM2 gangliosidosis in Jacob sheep. Vet Pathol 48 (2011) 807-813.
[291] A. Berardelli, J.C. Rothwell, P.D. Thompson, M. Hallett, Pathophysiology of bradykinesia in Parksonson's disease. Brain 124 (2001) 2131-2146.
[292] T. Kobayashi, I. Goto, S. Okada, T. Orii, K. Ohno, T. Nakano, Accumulation of lysosphingolipids in tissues from patients with GM1 and GM2 gangliosidosis. Journal of Neurochemistry 59 (1992) 1452-1458.
[293] K. Suzuki, K. Suzuki, S. Kamoshita, Chemical pathology of GM1-gangliosidosis (generalized gangliosidosis). Journal of Neuropathology and Experimental Neurology 28 (1969) 25-73.
[294] D.A. Siegel, S.U. Walkley, Growth of ectopic dendrites on cortical pyramidal neurons in neuronal storage diseases correlates with abnormal

accumulation of GM2 ganglioside. Journal of Neurochemistry 62 (1994) 1852-1862.
[295] S. Grassi, E. Chiricozzi, L. Mauri, S. Sonnino, A. Prinetti, Sphingolipids and neuronal degeneration in lysosomal storage disorders. J Neurochem (2018).
[296] S.U. Walkley, M.T. Vanier, Secondary lipid accumulation in lysosomal disease. Biochim Biophys Acta 1793 (2009) 726-736.
[297] R. McGlynn, K. Dobrenis, S.U. Walkley, Differential subcellular localization of cholesterol, gangliosides, and glycosaminoglycans in murine models of mucopolysaccharide storage disorders. J Comp Neurol 480 (2004) 415-426.
[298] E. Cherubini, R. Miles, The CA3 region of the hippocampus: how is it? What is it for? How does it do it? Front Cell Neurosci 9 (2015) 19.
[299] F. Kubaski, R.W. Mason, A. Nakatomi, H. Shintaku, L. Xie, N.N. van Vlies, H. Church, R. Giugliani, H. Kobayashi, S. Yamaguchi, Y. Suzuki, T. Orii, T. Fukao, A.M. Montano, S. Tomatsu, Newborn screening for mucopolysaccharidoses: a pilot study of measurement of glycosaminoglycans by tandem mass spectrometry. J Inherit Metab Dis 40 (2017) 151-158.
[300] T. Okumiya, H. Sakuraba, R. Kase, T. Sugiura, Imbalanced substrate specificity of mutant β-galactosidase in patients with Morquio B disease. Molecular Genetics and Metabolism 78 (2003) 51-58.
[301] G. Venn, R.M. Mason, Absence of keratan sulphate from skeletal tissues of mouse and rat. Biochem. J. 228 (1985) 443-450.
[302] S. Chakravarti, T. Magnuson, J.H. Lass, K.J. Jepsen, C. LaMantia, H. Carroll, Lumican regulates collagen fibril assembly: skin fragility and corneal opacity in the absence of lumican. The Journal of Cell Biology 141 (1998) 1277-1286.
[303] S. Ying, A. Shiraishi, C.W.C. Kao, R.L. Converse, J.L. Funderburgh, J. Swiergiel, M.R. Rother, G.W. Conrad, W.W.Y. Kao, Characterization and expression of the mouse lumican gene. The Journal of Biological Chemistry 272 (1997) 30306-30313.
[304] M.L. Broekman, R.C. Baek, L.A. Comer, J.L. Fernandez, T.N. Seyfried, M. Sena-Esteves, Complete correction of enzymatic deficiency and neurochemistry in the GM1-gangliosidosis mouse brain by neonatal adeno-associated virus-mediated gene delivery. Mol Ther 15 (2007) 30-37.
[305] V.J. McCurdy, A.K. Johnson, H.L. Gray-Edwards, A.N. Randle, B.L. Brunson, N.E. Morrison, N. Salibi, J.A. Johnson, M. Hwang, R.J. Beyers, S.G. Leroy, S. Maitland, T.S. Denney, N.R. Cox, H.J. Baker, M. Sena-Esteves, D.R. Martin, Sustained normalization of neurological disease after intracranial gene therapy in a feline model. Science Translational Medicine 6 (2014).
[306] H.L. Gray-Edwards, X. Jiang, A.N. Randle, A.R. Taylor, T.L. Voss, A.K. Johnson, V.J. McCurdy, M. Sena-Esteves, D.S. Ory, D.R. Martin, Lipidomic evaluation of feline neurologic disease after AAV gene therapy. Molecular Therapy - Methods & Clinical Development 6 (2017) 135-142.
[307] J.B. Bell, K.M. Podetz-Pedersen, E.L. Aronovich, L.R. Belur, R.S. McIvor, P.B. Hackett, Preferential delivery of the Sleeping Beauty transposon system to livers of mice by hydrodynamic injection. Nat Protoc 2 (2007) 3153-3165.

[308] E.L. Aronovich, B.C. Hall, J.B. Bell, R.S. McIvor, P.B. Hackett, Quantitative analysis of alpha-L-iduronidase expression in immunocompetent mice treated with the Sleeping Beauty transposon system. PLoS One 8 (2013) e78161.
[309] J.T. Busher, Serum albumin and globulin, in: H.K. Walker, W.D. Hall, J.W. Hurst (Eds.), Clinical Methods: The History, Physical, and Laboratory Examinations, Butterworths, Boston, MA, 1990.
[310] L. Ou, T. Herzog, B.L. Koniar, R. Gunther, C.B. Whitley, High-dose enzyme replacement therapy in murine Hurler syndrome. Mol Genet Metab 111 (2014) 116-122.
[311] M.D. Lambourne, M.A. Potter, Murine beta-galactosidase stability is not dependent on temperature or protective protein/cathepsin A. Mol Genet Metab 104 (2011) 620-626.
[312] U.H. Schueler, T. Kolter, C.R. Kaneski, G.C. Zirzow, K. Sandhoff, R.O. Brady, Correlation between enzyme activity and substrate storage in a cell culture model system for Gaucher disease. Journal of Inherited Metabolic Diseases 27 (2004) 649-658.
[313] R.J. Boado, Y. Zhang, Y. Zhang, C.F. Xia, Y. Wang, W.M. Pardridge, Genetic engineering of a lysosomal enzyme fusion protein for targeted delivery across the human blood-brain barrier. Biotechnol Bioeng 99 (2008) 475-484.
[314] T. Nishioka, S. Tomatsu, M.A. Gutierrez, K. Miyamoto, G.G. Trandafirescu, P.L. Lopez, J.H. Grubb, R. Kanai, H. Kobayashi, S. Yamaguchi, G.S. Gottesman, R. Cahill, A. Noguchi, W.S. Sly, Enhancement of drug delivery to bone: characterization of human tissue-nonspecific alkaline phosphatase tagged with an acidic oligopeptide. Mol Genet Metab 88 (2006) 244-255.
[315] A.M. Montano, H. Oikawa, S. Tomatsu, T. Nishioka, C. Vogler, M.A. Gutierrez, T. Oguma, Y. Tan, J.H. Grubb, V.C. Dung, A. Ohashi, K. Miyamoto, T. Orii, Y. Yoneda, W.S. Sly, Acidic amino acid tag enhances response to enzyme replacement in mucopolysaccharidosis type VII mice. Mol Genet Metab 94 (2008) 178-189.
[316] S. Tomatsu, A.M. Montano, V.C. Dung, A. Ohashi, H. Oikawa, T. Oguma, T. Orii, L. Barrera, W.S. Sly, Enhancement of drug delivery: enzyme-replacement therapy for murine Morquio A syndrome. Mol Ther 18 (2010) 1094-1102.
[317] Z. Yu, A.R. Sawkar, J.W. Kelly, Pharmacologic chaperoning as a strategy to treat Gaucher disease. FEBS J 274 (2007) 4944-4950.
[318] G.H.B. Maegawa, M. Tropak, J. Butner, T. Stockley, F. Kok, J.T.R. Clarke, D.J. Mahuran, Pyrimethamine as a potential pharmacological chaperone for late-onset forms of GM2 gangliosidosis. The Journal of Biological Chemistry 282 (2007) 9150-9161.
[319] M.B. Tropak, S.P. Reid, M. Guiral, S.G. Withers, D. Mahuran, Pharmacological enhancement of beta-hexosaminidase activity in fibroblasts from adult Tay-Sachs and Sandhoff patients. J Biol Chem 279 (2004) 13478-13487.
[320] T. Okumiya, M.A. Kroos, L.V. Vliet, H. Takeuchi, A.T. Van der Ploeg, A.J. Reuser, Chemical chaperones improve transport and enhance stability of mutant

alpha-glucosidases in glycogen storage disease type II. Mol Genet Metab 90 (2007) 49-57.
[321] G. Parenti, A. Zuppaldi, M. Gabriela Pittis, M. Rosaria Tuzzi, I. Annunziata, G. Meroni, C. Porto, F. Donaudy, B. Rossi, M. Rossi, M. Filocamo, A. Donati, B. Bembi, A. Ballabio, G. Andria, Pharmacological enhancement of mutated α-glucosidase activity in fibroblasts from patients with Pompe disease. Molecular Therapy 15 (2007) 508-514.
[322] T. Kudoh, K. Kikuchi, F. Nakamura, S. Yokoyama, K. Karube, S. Tsugawa, R. Minami, T. Nakao, Prenatal diagnosis of GM1-gangliosidosis: biochemical manifestations in fetal tissues. Human Genetics 44 (1978) 287-293.
[323] M.-J. Tasso, A. Martinez-Gutierrez, C. Carrascosa, S. Vazquez, R. Tebar, GM1-gangliosidosis presenting as nonimmune hydrops fetalis: a case report. Journal of Perinatal Medicine 24 (1996) 445-449.
[324] M.T. Sinelli, M. Motta, D. Cattarelli, M.L. Cardone, G. Chirico, Fetal hydrops in GM(1) gangliosidosis: a case report. Acta Paediatr 94 (2005) 1847-1849.
[325] C. Lutzko, F. Omori, A.C.G. Abrams-Ogg, R. Shull, L. Li, K. Lau, C. Ruedy, S. Nanji, C. Gartley, H. Dobson, R. Foster, S. Kruth, I.D. Dube, Gene therapy for canine α-L-iduronidase deficiency: in utero adoptive transfer of genetically corrected hematopoietic progenitors results in engraftment but not amelioration of disease. Human Gene Therapy 10 (1999) 1521-1532.
[326] B.A. Karolewski, J.H. Wolfe, Genetic correction of the fetal brain increases the lifespan of mice with the severe multisystemic disease mucopolysaccharidosis type VII. Mol Ther 14 (2006) 14-24.
[327] G. Massaro, C.N.Z. Mattar, A.M.S. Wong, E. Sirka, S.M.K. Buckley, B.R. Herbert, S. Karlsson, D.P. Perocheau, D. Burke, S. Heales, A. Richard-Londt, S. Brandner, M. Huebecker, D.A. Priestman, F.M. Platt, K. Mills, A. Biswas, J.D. Cooper, J.K.Y. Chan, S.H. Cheng, S.N. Waddington, A.A. Rahim, Fetal gene therapy for neurodegenerative disease of infants. Nat Med 24 (2018) 1317-1323.

Appendix

Copyright Clearance

Chapters II, III, and IV contain portions of text, full figures, and tables from a manuscript that was accepted for publication and is currently in press at *Molecular Genetics and Metabolism*. This manuscript is available under the terms of the Creative Commons Attribution License (https://creativecommons.org/licenses/by/4.0/). A full reference to this publication is listed below. Sections from this manuscript were adapted for publication in this dissertation. These changes were made at the sole discretion of the author of this dissertation and are not endorsed by Elsevier.

M. J. Przybilla, L. Ou, A.-F. Tăbăran, X. Jiang, R. Sidhu, P.J. Kell, D.S. Ory, M.G. O'Sullivan, C.B. Whitley. Comprehensive behavioral and biochemical outcomes of novel murine models of GM1-gangliosidosis and Morquio syndrome type B. Mol Genet. Metab. https://doi.org/10.1016/j.ymgme.2018.11.002.